

PREPARATION OF POLYETHYLENE GLYCOL COATED MAGNETIC
NANOPARTICLES FOR TARGETING OF CANCER CELLS

A THESIS SUBMITTED TO
THE GRADUATE SCHOOL OF NATURAL AND APPLIED SCIENCES
OF
MIDDLE EAST TECHNICAL UNIVERSITY

BY

TUĞBA KESKİN

IN PARTIAL FULFILLMENT OF THE REQUIREMENTS
FOR
THE DEGREE OF MASTER OF SCIENCE
IN
BIOLOGY

FEBRUARY 2012

Approval of the thesis:

**PREPARATION OF POLYETHYLENE GLYCOL COATED MAGNETIC
NANOPARTICLES FOR TARGETING OF CANCER CELLS**

submitted by **TUĞBA KESKİN** in partial fulfillment of the requirements for the degree of **Master of Science in Biology Department, Middle East Technical University** by,

Prof. Dr. Canan Özgen
Dean, Graduate School of **Natural and Applied Sciences**

Prof. Dr. Musa Doğan
Head of Department, **Biology**

Prof. Dr. Ufuk Gündüz
Supervisor, **Biology, METU**

Examining Committee Members:

Assoc. Prof. Dr. Aşen Tezcaner
Engineering Sciences Dept., METU

Prof. Dr. Ufuk Gündüz
Biology Dept., METU

Assist. Prof. Dr. Sreeparna Banerjee
Biology Dept., METU

Assist. Prof. Dr. Çağdaş Devrim Son
Biology Dept., METU

Assist. Prof. Dr. Arzu Yakar
Chemical Engineering Dept.,
Afyon Kocatepe University

Date: 10.02.2012

I hereby declare that all information in this document has been obtained and presented in accordance with academic rules and ethical conduct. I also declare that, as required by these rules and conduct, I have fully cited and referenced all material and results that are not original to this work.

Name, Last name: TUĞBA KESKİN

Signature:

ABSTRACT

PREPARATION OF POLYETHYLENE GLYCOL COATED MAGNETIC NANOPARTICLES FOR TARGETING OF CANCER CELLS

Keskin, Tuğba

M.Sc., Department of Biology

Supervisor : Prof. Dr. Ufuk Gündüz

February 2012, 119 pages

Conventional cancer chemotherapies cannot differentiate between healthy and cancer cells, and lead to severe side effects and systemic toxicity. In the last decades, different kinds of controlled drug delivery systems have been developed to overcome these shortcomings of chemotherapeutics. Magnetic nanoparticles (MNP) are potentially important in cancer treatment since they can be targeted to tumor site by an externally applied magnetic field.

In this study, it is aimed to synthesize folic acid conjugated; polyethylene glycol (PEG) coated magnetic nanoparticles with appropriate size, surface chemistry, magnetization and biocompatibility to be used in biomedical applications. First MNP were synthesized, then covered with oleic and PEG; and finally conjugated with folic acid. A detailed characterization of synthesized nanoparticles was done by TEM, XRD, FTIR, VSM and XTT analyses.

MNP synthesized by the rapid addition of ammonium hydroxide exhibited more spherical nanoparticles with a narrower size distribution. Agglomeration tendency of naked nanoparticles was prevented by oleic acid addition during the synthesis. Both naked and surface treated MNP have been found to exhibit superparamagnetic behavior both at room temperature (23°C) and body temperature (37°C). Cytotoxic effects of naked MNP, oleic acid coated MNP, PEG coated MNP and folic acid functionalized MNP were investigated on MCF-7/S breast cancer cell lines. They did not exhibit severe toxicity in the concentration range of 0 – 250 µg/ml. Cell proliferation profiles of drug resistant cell lines MCF-7/Dox, MCF-7/Pac and MCF-7/Zol were examined for folic acid conjugated MNP and a serious cytotoxicity was not observed. Endocytosis of MNP was illustrated by light microscopy images.

The synthesized nanoparticles have been found to be suitable in terms of size, shape, magnetic and cytotoxic properties for drug targeting or other biomedical applications.

Keywords: Cancer, MCF-7, drug targeting, magnetic nanoparticle

ÖZ

MANYETİK NANOPARÇACIKLARIN ANTİKANSER İLAÇ SALIMI VE HEDEFLENMESİ AMACIYLA KULLANIMI

Keskin, Tuğba

Yüksek Lisans, Biyoloji Bölümü

Tez Yöneticisi : Prof. Dr. Ufuk Gündüz

Şubat 2012, 119 sayfa

Kanser kemoterapisinde kullanılan ilaçlar, kanserli ve sağlıklı hücreleri ayırt edemedikleri için ciddi yan etkilere ve sistemik toksisiteye neden olmaktadır. Son yıllarda, mevcut anti-kanser ilaçların yan etkilerini azaltmak amacıyla kontrollü ilaç salım sistemleri geliştirilmiştir. Manyetik nanoparçacıklar (MNP) dışarıdan manyetik alan uygulanarak tümöre yönlendirilebildikleri için kanser tedavisi çalışmalarında önem kazanmışlardır.

Bu çalışmada, biyomedikal uygulamalarda kullanılmak üzere uygun boyut, şekil, manyetik, kimyasal ve sitotoksik özelliklere sahip folik asit bağlanmış, polietilen glikol (PEG) kaplı manyetik nanoparçacıkların sentezlenmesi amaçlanmaktadır. Öncelikle MNP'ler sentezlenmiş, oleik asit ve PEG kaplandıktan sonra folik asit bağlanmışlardır. Sentezlenen MNP'lerin TEM, XRD, FTIR, VSM ve XTT analizleriyle karakterizasyonları yapılmıştır.

Kaplanmamış MNP sentezinde, amonyum hidroksit çözeltisinin sisteme hızlı eklenmesi ile daha yuvarlak ve dar boyut dağılımına sahip nanaoparçacıklar elde edilebilmiştir. Bu MNP'lerin kümeleşme eğilimi, nanoparçacıkların sentezi sırasında oleik asidin eklenmesi ile engellenmiştir. Gerek kaplanmamış, gerekse işlem görmüş nanaoparçacıklar oda (23°C) ve vücut sıcaklığında (37°C) süperparamanyetik özellik sergilemişlerdir. Oleik asit kaplı ve PEG kaplı MNP'lerin sitotoksik etkileri, MCF-7/S meme kanseri hücre hattında incelenmiştir. 0–250 µg/ml derişim aralığında, nanoparçacıklara ait ciddi bir toksik etki gözlenmemiştir. Ayrıca, folik asit kaplı MNP'lerle muamele edilmiş ilaca dirençli MCF-7/Dox, MCF-7/Pac ve MCF-7/Zol hücre hatları üzerinde ciddi bir sitotoksik etki ile karşılaşılmasıdır. MNP'lerin hücre içine alımı ışık mikroskobu kullanılarak görüntülenmiştir.

Sentezlenen nanoparçacıklar boyut,şekil, manyetik ve sitotoksik özellikleriyle ilaç hedefleme ve diğer biyomedikal uygulamalar için uygun görülmektedir.

Anahtar kelimeler: Kanser, MCF-7, ilaç hedeflemesi, manyetik nanoparçacık.

To My Family

ACKNOWLEDGEMENTS

It is difficult to overstate my sincere appreciation to my supervisor and my mentor, Prof. Dr. Ufuk Gündüz. This project became possible with her academic guidance, encouragement and suggestions throughout my master studies.

I am deeply thankful to Assist. Prof. Dr. Arzu Yakar for her endless support and guidance throughout this study. I would like to acknowledge Prof. Dr. Güngör Gündüz, Assist. Prof. Dr. Bora Maviş and Research Associate Cengiz Tan for their scientific support and help.

Special thanks to my precious friends Burcu Özsoy, Gülistan Tansık and Zelha Nil. When we were all passing through tough times, I always felt the importance of their invaluable friendship. I enjoyed my time in lab and my life with their precious friendship.

I am grateful to Özlem İşeri, Yaprak Dönmez, Esra Güç, Gülşah Pekgöz, Petek Şen and Esra Kaplan for sharing their experiences and advices. Also special thanks to Lab 206 Team for their support and friendship: Çağrı Urfalı, Ahu İzgi, Rouhollah Khodadust, Gözde Ünsoy, Çiğdem Şener, Aktan Alpsoy, Neşe Çakmak, Okan Tezcan and Murat Erdem.

My times in Ankara became meaningful thanks to several invaluable friendships. I would like to express my gratitude to Handan Acar who supported me throughout my project. Since 2003, I have felt the support, closest camaraderie and cheerfulness of my best friend, Hande Acar beside me. I also would like to acknowledge Ersan Eren whose priceless friendship accompanied me in Ankara. Although he was not in Ankara, I also felt the support of my friend Can Mergin with me.

I was lucky to share my house life with my flatmates Aslı Yılmaz and Ebru Üner. Thanks to them, I will commemorate our home in Ankara as a “scientific fun house”. I also would like to thank to Edith and Joy for being always nice and cheerful to me during our short but meaningful times.

I owe my deepest gratitude to Burak Toygar Halistoprak whose companionship makes my life a sunny day. His trust, endless support, encouragement and care made this thesis possible.

Last but not least, I would like to thank to my family, my parents Mualla and Kemal, my brother Murat, my sister-in-law Deniz and my little nephews Demir and Ateş, for their endless support, love and patience.

This study was supported by The Scientific and Technical Research Council of Turkey (TUBITAK) as a part of the project “Idarubicin Loaded Magnetic Nanoparticles and Their application to MCF-7 Cell Line” under the grant number 109T949.

TABLE OF CONTENTS

ABSTRACT	iv
ÖZ.....	vi
ACKNOWLEDGEMENTS	ix
TABLE OF CONTENTS	xi
LIST OF TABLES	xv
LIST OF FIGURES.....	xvi
LIST OF ABBREVIATIONS	xix
CHAPTERS	
1 INTRODUCTION	1
1.1 Biology of Cancer	1
1.1.1 Progression of Cancer.....	2
1.2 Breast Cancer	3
1.2.1 Treatment of Breast Cancer	4
1.2.1.1 Surgery.....	5
1.2.1.2 Radiation Therapy.....	6
1.2.1.3 Hormonal Therapy	6
1.2.1.4 Chemotherapy	7
1.2.1.4.1 Side effects of Chemotherapy	8
1.2.1.5 Targeted Therapy	10

1.3 Drug Delivery Systems	10
1.3.1 Nanoparticles and Microparticles used in Tumor Targeted Therapies	13
1.4 Magnetic Nanoparticles.....	18
1.4.1 General Usage of Magnetic Nanoparticles in Biomedicine	18
1.4.2 Drug Delivery Applications of Magnetic Nanoparticles	19
1.4.3 Structure of Magnetic Nanoparticles	21
1.4.3.1 Role of Polyethylene Glycol (PEG) in Drug Delivery	23
1.4.3.2 Role of Folic Acid in Targeted Drug Delivery	24
1.4.4 Synthesis Methods of Magnetic Nanoparticles	27
1.4.5 Magnetic properties of nanoparticles.....	29
1.5 Aim of the Study	31
2 MATERIALS AND METHODS.....	32
2.1 MATERIALS	32
2.1.1 Materials for Magnetic Nanoparticle Synthesis	32
2.1.2 Materials for Cell Culture Studies	33
2.2 METHODS.....	34
2.2.1 Synthesis of Magnetic Nanoparticles (MNP).....	34
2.2.2 Preparation of Oleic Acid Coated Magnetic Nanoparticles	36
2.2.3 Functionalization of Magnetic Nanoparticles with Polyethylene Glycol	37
2.2.4 Modification of Magnetic Nanoparticles with Folic Acid.....	38
2.2.5 Chemical Characterization.....	39
2.2.5.1 X-Ray Diffraction (XRD)	39

2.2.5.2 Fourier Transform Infrared (FTIR) Spectroscopy	40
2.2.5.3 Transmission Electron Microscopy (TEM)	40
2.2.5.4 Vibrating Sample Magnetometer (VSM).....	40
2.2.6 Cell Culture.....	41
2.2.6.1 Cell Line and Culture Conditions	41
2.2.6.2 Passaging Cell Cultures	41
2.2.6.3 Freezing Cells and Thawing Frozen Cells	42
2.2.6.4 Viable Cell Count.....	42
2.2.6.5 Cell Proliferation Assay with XTT Reagent	43
2.2.6.6 Light Microscopy Observation of MNP Treated Cells	45
2.2.6.7 Statistical Analysis	45
3 RESULTS AND DISCUSSION	46
3.1 Chemical Characterization	46
3.1.1 Transmission Electron Microscopy (TEM)	46
3.1.1.1 TEM Characterization of Naked MNP	46
3.1.1.2 TEM Characterization of Oleic Acid Coated MNP	49
3.1.1.3 TEM Characterization of PEG Coated MNP	51
3.1.1.4 TEM Characterization of Folic Acid Functionalized MNP	54
3.1.2 X-ray Diffraction (XRD)	56
3.1.3 Fourier Transform Infrared (FTIR) Spectroscopy	59
3.1.3.1 FTIR Analysis of Naked MNP	59
3.1.3.2 FTIR Analysis of Oleic Acid Coated MNP	60
3.1.3.3 FTIR Analysis of PEG coated MNP	65

3.1.3.4 FTIR Analysis of Folic Acid Functionalized MNP	67
3.1.4 Thermogravimetric Analysis (TGA)	70
3.1.5 Vibrating Sample Magnetometer (VSM)	73
3.2.1 Cytotoxicity Studies of Magnetic Nanoparticles	77
3.2.1.1 Cytotoxicity of Naked MNP	78
3.2.1.2 Cytotoxicity of Oleic Acid Coated MNP	79
3.2.1.3 Cytotoxicity of PEG Coated MNP	81
3.2.1.4 Cytotoxicity of Folic Acid Functionalized MNP	82
3.2.1.4.1 Cytotoxicity of Folic Acid Functionalized MNP on Drug Resistant Cells	84
3.2.2 Light Microscopy Images	90
4 CONCLUSION	92
REFERENCES	96
A. ATR AND FTIR SPECTRA	112
B. HYSTERESIS LOOP CURVES	115

LIST OF TABLES

TABLES

Table 1.1 Comparison of MNP synthesis methods (Gupta 2005)*	28
Table B.1 Magnetic Properties of N-MNP ₃	116
Table B.2 Magnetic Properties of OA- MNP ₂	116
Table B.3 Magnetic Properties of PEG-MNP ₂	117
Table B.4 Magnetic Properties of FA-MNP ₁	118
Table B.5 Magnetic Properties of FA-MNP ₂	119

LIST OF FIGURES

FIGURES

Figure 1.1 Targeting of nanoparticles to tumor site passively by EPR effect or by active targeting in tumor tissue	13
Figure 1.2 Different types of nanocarriers used in cancer therapy.	14
Figure 1.3 Biomedical Applications of MNP.....	19
Figure 1.4 Schematic representation of manipulation of MNP by external magnetic field.....	20
Figure 1.5 General structural design of MNP used in biomedical applications	22
Figure 1.6 Chemical structure of PEG with the molecular formula.....	23
Figure 1.7 Chemical Structure of Folic Acid acid.....	24
Figure 1.8 Schematic representation of receptor mediated endocytosis of drug carriers.....	26
Figure 1.9 Schematic representation of magnetization graphs of diamagnetic, paramagnetic, ferromagnetic and superparamagnetic materials	30
Figure 2.1 Design of experimental setup for MNP synthesis.....	35
Figure 2.2 Schematic representation of XTT cell proliferation design on 96 well plate.	44
Figure 3.1 TEM images of a) N-MNP ₁ b) N-MNP ₂ and c) N-MNP ₃	47
Figure 3.2 TEMs images of OA-MNP ₁	49
Figure 3.3 TEM images of OA-MNP ₂	50
Figure 3.4 TEM images of PEG-MNP ₁	52
Figure 3.5 TEM images of PEG-MNP ₂	53
Figure 3.6 TEM images of PEG-MNP ₃	54

Figure 3.7 TEM images of FA-MNP ₁	55
Figure 3.8 TEM images of FA-MNP ₂	55
Figure 3.9 XRD patterns of a) N-MNP ₁ , b) N-MNP ₂ and c) N-MNP ₃	56
Figure 3.10 XRD patterns of a) NMNP ₃ , b) OA-MNP ₂ and c) PEG-MNP ₂ .	58
Figure 3.11 FTIR spectrum of N-MNP ₃	60
Figure 3.12 FTIR spectra of a) pure oleic acid and b) OA-MNP ₁	61
Figure 3.13 FTIR spectra of a) pure oleic acid, b) OA-MNP ₂ ^W and c) OA-MNP ₂ ^E	63
Figure 3.14 Schematic representation of a) bilayer Oleic acid coated Fe ₃ O ₄ and b) monolayer Oleic acid coated Fe ₃ O ₄	64
Figure 3.15 FTIR Spectra of a) Polyethylene glycol monooleate, b) PEG-MNP ₁ , c) PEG-MNP ₂ and d) PEG-MNP ₃	66
Figure 3.16 FTIR Spectra of a) pure folic acid and b) FA-MNP ₁ and c) FA-MNP ₂	68
Figure 3.17 FTIR Spectra of a) OA-MNP ₂ , b) PEG-MNP ₂ c) FA-MNP ₁ and d) FA-MNP ₂	69
Figure 3.18 TGA curves of N-MNP ₃ , OA-MNP ₂ ^W , OA-MNP ₂ ^E , PEG-MNP ₂ and PEG-MNP.....	72
Figure 3.19 Hysteresis loops of N-MNP ₃ , OA-MNP ₂ , PEG-MNP ₂ , FA-MNP ₁ and FA-MNP ₂ at 23 °C.	74
Figure 3.20 Hysteresis loops of N-MNP ₃ , OA-MNP ₂ , PEG-MNP ₂ , FA-MNP ₁ and FA-MNP ₂ at 37 °C.	76
Figure 3.21 Cell proliferation profile of MCF-7/S cells treated with N-MNP ₃ for 72 hr.	78
Figure 3.22 Cell proliferation profile of MCF-7/S breast cancer cells treated with OA-MNP ₂ for 72 hr.	80
Figure 3.23 Cell proliferation profile of MCF-7/S breast cancer cells treated with PEG-MNP ₂ for 72 hr.	81

Figure 3.24 Cell proliferation profile of MCF-7/S cancer cells treated FA-MNP ₁ for 72 hr..	82
Figure 3.25 Cell proliferation profile of MCF-7/S breast cancer cells treated with a)N-MNP ₃ , b) OA-MNP ₂ , c) PEG-MNP ₂ and d) FA-MNP ₁ for 72 hr.	83
Figure 3.26 Cell proliferation profile of MCF-7/Dox cells treated with FA-MNP ₁ for 72 hr.	85
Figure 3.27 Cell proliferation profile of MCF-7/Pac cells treated with FA-MNP ₁ for 72 hr at 37°C.	86
Figure 3.28 Cell proliferation profile of MCF-7/Zol treated with FA-MNP ₁ for 72 hr at 37°C.	87
Figure 3.29 Cell proliferation profile of a)MCF-7/S, b)MCF-7/Dox, c)MCF-7/Pac and d)MCF-7/Zol breast cancer cells treated with FA-MNP ₁ for 72 hr.	88
Figure 3.30 Light microscopy images of a) untreated control MCF-7/S cells, and MCF-7/S cells treated with 250 µg/ml of b)N-MNP ₁ , c) PEG-MNP ₂ and d) FA-MNP ₁ for 48 hr (400X magnification)	90
Figure A.1 ATR spectra of a) pure oleic acid and b) Polyethylene glycol monooleate.	112
Figure A.2 FTIR Spectrum of pure folic acid	113
Figure B.1 Magnetization curve of N-MNP ₃ at 23 °C and 37 °C	115
Figure B.2 Magnetization curve of OA- MNP ₂	116
Figure B.3 Magnetization curve of PEG-MNP ₂	117
Figure B.4 Magnetization curve of FA-MNP ₁	118
Figure B.5 Magnetization curve of FA-MNP ₂	119

LIST OF ABBREVIATIONS

BCRP	Breast Cancer Resistance Protein
FA-MNP ₁	Folic Acid conjugated magnetic nanoparticles - 1
FA-MNP ₂	Folic Acid conjugated magnetic nanoparticles - 2
FeCl ₂ .4H ₂ O	Iron (II) chloride tetrahydrate
FeCl ₃ .6H ₂ O	Iron (III) chloride hexahydrate
DCC	Dicyclohexyl carbodiimide
DMSO	Dimethylsulfoxide
MCF-7/DOX	Doxorubicin Resistant MCF-7 Subline
MCF-7/PaC	Paclitaxel Resistant MCF-7 Subline
MCF-7/S	Sensitive MCF-7 breast cancer cell line
MCF-7/Zol	Zoledronic acid Resistant MCF-7 Subline
MDR1	P-glycoprotein
NH ₄ OH	Ammonium hydroxide
N-MNP ₁	Naked Magnetic Nanoparticles - 1
N-MNP ₂	Naked Magnetic Nanoparticles - 2
N-MNP ₃	Naked Magnetic Nanoparticles - 3
OA	Oleic acid
OA-MNP ₁	Oleic Acid coated Magnetic Nanoparticles - 1
OA-MNP ₂	Oleic Acid coated Magnetic Nanoparticles - 2
OA-MNP ₂ ^W	Oleic Acid coated Magnetic Nanoparticles - 1 washed with dH ₂ O
OA-MNP ₂ ^E	Oleic Acid coated Magnetic Nanoparticles - 2 washed with ethanol
PEG	Polyethylene glycol
PEG-MNP ₁	PEG coated Magnetic Nanoparticles - 1.

PEG-MNP₂

PEG coated Magnetic Nanoparticles - 2

PEG-MNP₃

PEG coated Magnetic Nanoparticles - 3

CHAPTER 1

INTRODUCTION

1.1 Biology of Cancer

Cancer is a genetic disease in which cells exhibit abnormal cell proliferation. Cancer cells are different than their healthy origins in a way that they lose their control over cell division and increase in number at an inappropriate rate while they are becoming able to invade neighboring tissues and spread to distant parts of the body through blood and lymph systems (Purves *et al.* 2004, <http://www.cancer.gov/cancertopics/cancerlibrary/what-is-cancer>)

Cancer is group of genetic diseases arising from defects in cellular mechanisms such as DNA repair, cell cycle, apoptosis and differentiation. Cancer is not a disease mostly inherited. Only about 1 % of the cancer cases bases on hereditary history (Klug *et al.* 2006). Genetic alterations leading to cancer develop in the genome of somatic cells of patients during their life span (Karp 2004). This is also why most of the cancer incidents occur in old ages, because of the accumulation of gene mutations. External and internal risk factors increasing the chance of developing cancer can be listed as ageing,

consumption of tobacco and alcohol, exposure to sun light, ionizing radiation, certain chemicals, infectious agents like some viruses and bacteria, poor diet, lack of physical activity and family history (<http://cancer.gov/cancertopics/wyntk/cancer/page3>).

In 2008, 7.6 million cases of cancer death were recorded and accounted for 13% of all deaths in worldwide. Major types of cancer leading to death were reported as lung, stomach, liver, colorectal and breast cancer. (<http://www.who.int/mediacentre/factsheets/fs297/en/>). 20.7% of all deaths cases in Turkey were due to cancer in 2009 (TUIK 2009).

1.1.1 Progression of Cancer

Progression of cancer is an evolutionary process requiring primarily genetic changes. Accumulation of these genetic changes results in loss of control over cell division which can result in abnormal cell proliferation. Moreover, by these changes or mutations cancer cells become able to bypass apoptosis and survive under conditions that they should die. Additionally, they are not affected by telomere degradation (O'Morgan 2007). Aberrant cell proliferation results in multilayer cell clumps called benign tumors. Benign tumors do not exhibit a normal cell growth pattern but unable to invade and spread to other tissues (Karp 2004). While solid tumors are growing, the lack of enough oxygen and nutrients drive a natural selection among cancer leading to selection of most adapted cells for tumor growth (O'Morgan 2007).

Acquisition of the ability of secreting angiogenic factors promote angiogenesis, after which cells can enter bloodstream and invade distant tissues by a process called metastasis. Metastatic tumors are called malignant tumors which are very aggressive and able to spread through the body (Klug *et al.* 2006).

Genetic instability accelerates this process. Especially mutations of oncogenes and tumor suppressor genes are key factors in the development of cancer. Following the mutation of proto-oncogenes, they gain function and called oncogenes which are able to promote cell division. Tumor suppressor genes normally restrain cell proliferation. A mutation in tumor suppressor genes causes a loss of function and promotion of tumorigenesis (O'Morgan 2007).

Tumor cells are named according to tissue they have originated. Benign tumors derived from epithelial tissues are called adenoma, while malignant ones are called carcinoma. Malignant tumors originated from connective tissue or muscles are classified as sarcoma (O'Morgan 2007).

1.2 Breast Cancer

According to World Health Organization, 12.66 million new cancer cases recorded in worldwide in 2008. Among all types of cancer cases, breast cancer was the most secondly seen cancer type with the percentage of 10.9% after

lung cancer (12.7%) (http://globocan.iarc.fr/pie_pop.asp?selection=221900&title=World&sex=0&type=0&window=1&join=1&submit=%A0Execute%A0). It ranks as the most frequent cancer among women with the percentage of 23% (http://globocan.iarc.fr/pie_pop.asp?selection=221900&title=World&sex=2&type=0&window=1&join=1&submit=%A0Execute%A0). It was even more widespread in Turkey; 25.6% of all cancer cases were breast cancer among women in 2008 (http://globocan.iarc.fr/pie_pop.asp?selection=99792&title=Turkey&sex=2&type=0&window=1&join=1&submit=%A0Execute%A0).

Breast tissue mainly consists of milk producing glands which are called lobules, ducts carrying milk from lobules to nipple and stroma which is composed of surrounding fatty tissue and connective tissue. Mostly, breast cancer develops in cells lining through ducts. Some cases start in lobules. It begins in stroma very rarely. If cancer cells gain ability of invasion and enter into lymph nodes, they could metastatize to distant tissues in the body (American Cancer Society, 2011-2012)

1.2.1 Treatment of Breast Cancer

Treatment of breast cancer involves systemic and local therapies. Hormone therapy, chemotherapy and targeted therapy are examples of systemic therapy which allow travel of drugs throughout the whole body in blood stream to find cancer cells. Surgery and radiation therapy are local therapies aiming to treat

only tumor site and do not affect whole body (American Cancer Society, 2011-12).

1.2.1.1 Surgery

The oldest treatment way of cancer is surgery. It helps to diagnose and understand the stage of cancer. Breast cancer surgeries are divided into two classes based on the removal of the whole breast or just part of it. Mastectomy operations remove whole breast even sometimes with the surrounding tissues. Breast conserving surgeries are usually called lumpectomy involving the removal of only affected breast tissue.

Before or after surgery, patients can get extra therapies which are called neo-adjuvant and adjuvant therapies, respectively. Patients can undergo chemotherapy or hormone therapy to shrink tumor size before operation. After surgery, patients can be treated with systemic therapies or radiation therapy as adjuvant therapy (<http://www.cancer.org/Cancer/BreastCancer/DetailedGuide/breast-cancer-pdf23>).

1.2.1.2 Radiation Therapy

Radiation therapy is usually given to breast cancer patients after surgery to kill the any remnant cancer cells. It destroys cancer cells by high energy rays or particles leading to damage at DNA level. Gamma ray, X-ray and charged particles are being used in radiation therapy.

Radiation therapy can be applied to body either from outside, called external beam radiation therapy, or inside, called brachytherapy, in which a radioactive material is put near by the tumor site in breast tissue. (<http://www.cancer.gov/cancertopics/factsheet/Therapy/radiation>).

1.2.1.3 Hormonal Therapy

Hormone therapy is a systemic therapy which can be given to patients after or before surgery as an adjuvant or a neo-adjuvant therapy. Only hormone receptor positive breast cancers can be treated by hormone therapy, either preventing estrogen binding to receptors on cancer cells or by decreasing estrogen levels in the body (<http://www.breastcancer.org/treatment/hormonal/>).

Tamoxifen and toremifene are common medicines used in hormonal therapy aiming to block estrogen receptors. Aromatase inhibitors like letrozole, anastrozole and exemestane stop estrogen production in the body. Fulvestrant

is another class of drug which downregulates estrogen receptor on cells (<http://www.cancer.org/Cancer/BreastCancer/DetailedGuide/breast-cancer-pdf23>).

1.2.1.4 Chemotherapy

In chemotherapy, certain drugs are used to kill cancer cells. Chemotherapeutic drugs target cells which grow and proliferate quickly. This therapy is usually given to patients as neoadjuvant or adjuvant therapy along with radiotherapy. Sometimes it can even be selected as the principle form of treatment. Chemotherapy aims to kill cancer cells resulting in shrinkage of tumors and prevention of metastasis ([http://www.cancer.gov/cancertopics/coping/chemotherapy-and-you /page2](http://www.cancer.gov/cancertopics/coping/chemotherapy-and-you/page2)).

Chemotherapy drugs can be directly given into blood stream, taken orally or applied on skin. Chemotherapeutic agents are classified as alkylating agents, antimetabolites, antitumor antibiotics, topoisomerase inhibitors, mitotic inhibitors and corticosteroids.

The mechanism of alkylating agents bases on aberrant crosslinking of DNA strands which results in anomalous base pairing and cessation of cell proliferation. Long term treatment with these agents may lead to acute leukemia. Antimetabolites are drugs which put a halt in DNA and RNA synthesis, affecting cells at S phase of cell division. Moreover, antitumor

antibiotics are actually anthracyclines which influence the DNA replication. However, it was reported that they can damage heart muscle tissue as a side effect (<http://www.mesotheliomaweb.org/mesothelioma/treatment/chemo-therapeutic-agents/>). Further, Topoisomerase inhibitors prevent DNA supercoiling by inhibition of topoisomerase enzyme. They may also cause acute leukemia in long term treatment. Mitotic inhibitors are usually plant alkaloids which can stop mitosis. Corticosteroids are hormones that are usually used in treatment of leukemia and lymphoma.

In chemotherapy treatment of breast cancer, using different combinations of drugs gives most effective results. Doxorubicin, cyclophosphamide, methotrexate, 5-fluorouracil, paclitaxel and zoledronic acid are among the drugs that are used in combination to treat breast cancer. Doxorubicin and cyclophosphamide are alkylating agents while methotrexate and 5-fluorouracil are in the family of antimetabolites. On the other hand, Paclitaxel is a mitotic inhibitor (<http://www.cancer.org/acs/groups/cid/documents/webcontent/002995-pdf.pdf>).

1.2.1.4.1 Side effects of Chemotherapy

The trick behind the mechanism of chemotherapeutic drugs relies on the growing and proliferation ability of cells, which means those drugs target dividing cells. The failure of chemo drugs is resulted from the fact that they cannot differentiate between healthy and cancer cells. This situation results in several side effects of the treatment. Since there are healthy cells which are

also dividing as a normal procedure like cells in bone marrow, hair follicle, in gastrointestinal track and reproductive track, severe side effects are seen in those organs or tissues (<http://www.cancer.org/acs/groups/cid/documents/webcontent/002995-pdf.pdf>).

Side effects of chemotherapy can be divided into two groups; namely, short term and long term effects. Severity of side effects is related to type and dose of the drugs, period of the treatment and genetic background of individuals. Loss of hair, mouth sores, changes in taste sense and body weight, nausea and vomiting, decreasing number of blood cells and platelets resulting in easy bruising and bleeding, fatigue and poor immunity against infectious disease can be listed as the short term drawbacks. Menstrual changes harm to nerves other than in brain and spinal cord, hearth damage and leukemia are the mostly seen long term effects of chemotherapy (American Breast Cancer, 2011-2012).

Moreover, chemotherapy may cause to drug resistance at molecular level. Unresponsiveness to chemotherapy could be intrinsic but it is often acquired after chemotherapy. Resistance to chemotherapy could be related to increased expression of drug efflux pumps, decreased drug uptake into cell, alterations in drug targets, increased repair systems and inhibition of apoptosis. Also simultaneous resistance to different drugs could be seen in metastatic breast cancers, which is known as multidrug resistance (Gottesman 2002).

1.2.1.5 Targeted Therapy

In order to prevent the side effects of chemotherapeutic drugs, new drugs have been found with ability of targeting growth of cancer cells. Trastuzumab and labatinip are the mostly used drugs in targeted therapy of HER2/neu (Human Epidermal Growth Factor Receptor 2) positive breast cancer patients . Trastuzumab (Herceptin) is a man-made monoclonal antibody that selectively binds to HER2/neu which is a receptor on cell surface promoting cell growth and proliferation. Attachment of trastuzumab to HER2 receptors on cancer cells slows down cell division rate. It is usually given to patients as adjuvant therapy. It may cause lighter short term side effects like fever, weakness, headache and nausea. In addition to Ttastuzumab, Labatinip is another drug targeting HER2/neu. By binding to tyrosine kinase domain of receptors, it inhibits signal transduction required for cell growth (<http://www.cancer.org/Cancer/BreastCancer/DetailedGuide/breast-cancer-treating-targeted-therapy>).

1.3 Drug Delivery Systems

Chemotherapy is a systemic therapy using free drugs with poor biodistribution and targeting. Since conventional chemotherapeutics target only dividing cells without the ability of differentiating between cancer and healthy cells, their success is still questionable (Vlerken 2006). Targeted therapy agents have been developed to overcome the severe side effects of traditional chemo drugs

on healthy cells. However, acquisition of drug resistance has become a significant obstacle in targeted therapy, too (Cho *et al.* 2008).

Drug delivery systems (DDS) have been designed to enhance the pharmaceutical properties and eliminate the side effects of conventional agents. DDS are drug carriers which are usually made up of lipid and/or polymers. DDS can be small scale and larger scale systems. Drug releasing implants are used as larger scale systems. Small scale DDS can be nanoparticles and microparticles used as drug reservoir in parenteral drug administration (Allen 2004).

DDS systems are designed to overcome the failures and drawbacks of conventional chemotherapy drugs. They can present both hydrophilic and hydrophobic environment to enhance drug solubility. Since DDS are like drug reservoirs, they can prevent unwanted rapid drug metabolism and also rapid clearance of drugs by kidney. Most importantly with an efficient design, DDS enable targeted drug delivery to kill cancer cells preferentially (Allen 2004, Peer *et al.* 2007).

In the treatment of solid tumors nanoparticles are very successful. Tumor environment has a different vascular architecture compared to healthy tissues (Figure 1.1). In tumor site, leaky blood vessels are formed due to rapid and defective angiogenesis (Peer *et al.* 2007). Nanoparticles can escape to tumor site through these gaps. Poor lymphatic drainage in tumor site enables gathering of these nanoparticles in tumor environment resulting in release of drug in that site. The biology of tumor with leaky blood vessels and ineffective

lymph drainage leading to accumulation of nanoparticles in tumor is called enhanced permeability and retention (EPR) effect. EPR effect enables passive targeting of nanoparticles to tumor site instead of healthy tissues (Peer *et al.* 2007, Ferrari 2005, Vlerken 2006, Cho *et al.* 2008). Kaul *et al.* (2002) stated that nanoparticles could enhance drug delivery to tumor site 10 to 100 fold compared to free drug administration.

Although by passive targeting small scale DDS can accumulate primarily in tumor site, there are still some limitations to overcome. Some tumors may not possess effective EPR effect and some may exhibit drug resistance. Therefore, a detailed design of drug carriers and its characterization is critical to achieve an effective therapy.

Nanoparticles and microparticles can be tailored with small molecules which are able to recognize uniquely cancer cells. For active targeting of nano/microcarriers different molecules can be used such as folic acid, thiamine, lectine and some antibodies like HER2/7neu. Actively targeted carriers can release their cargo near to tumor site (Figure 1.1-i). Besides this, They can bind to cell surface and either leave drug extracellularly (Figure 1.1-ii) or be endocytosed and enable intracellular drug release (Figure 1.1-iii) (Vlerken 2006).

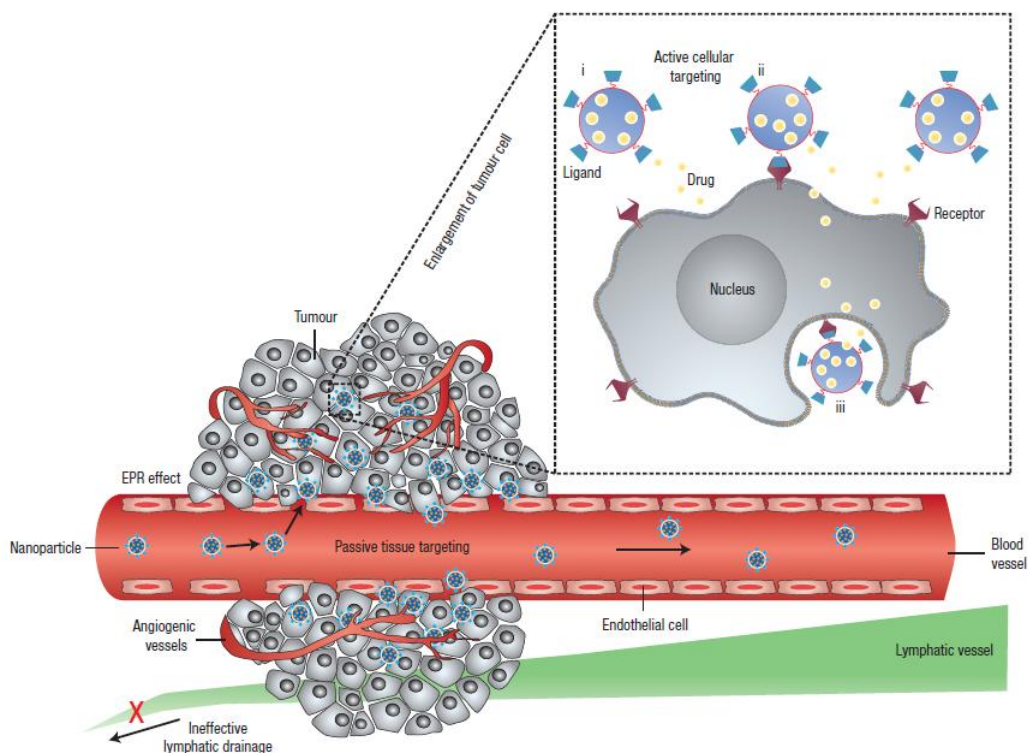


Figure 1.1 Targeting of nanoparticles to tumor site passively by EPR effect or by active targeting in tumor tissue (Peer *et al.* 2007).

1.3.1 Nanoparticles and Microparticles used in Tumor Targeted Therapies

The idea of nano scale drug delivery systems firstly discussed in 1970s while in 1980s clinical studies started. Up to now many advanced nano-scale products have been developed (Hoffman 2008). In drug delivery studies, different size particles are being used. Generally, particles smaller than 1 μm are called nanoparticles while microparticles are the ones with size range of 1 – 1000 μm (Orive *et al.* 2005).

Current nanoparticle systems used in cancer therapy studies are dendrimers, micelles, liposomes, polymeric nanoparticles such as nanospheres and nanocapsules, carbon nanotubes, ceramic nanoparticles, solid lipid nanoparticles and magnetic nanoparticles (Vlerken 2006, Orive *et al.* 2005, and Byrne *et al.* 2008). Some of them are given in Figure 1.2 representatively.

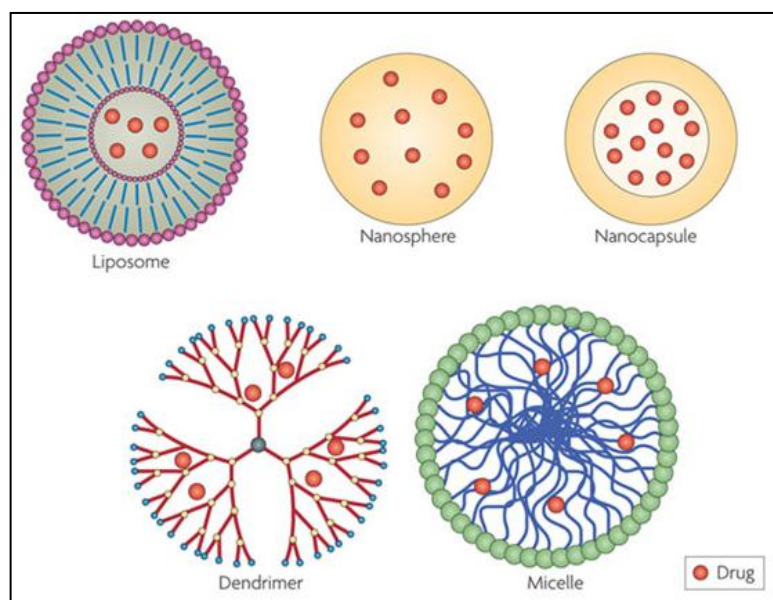


Figure 1.2 Different types of nanocarriers used in cancer therapy (Orive *et al.* 2009).

Currently available nanocarriers have different properties and characteristics depending on their size, chemistry and structural architecture.

Dendrimers have an inner core which is surrounded by repetitive branches of monomer polymers. They may have more than 100 terminal groups which enable their easy functionalization (Orive *et al.* 2009).

Micelles are particles composed of amphiphilic polymers resulting in an architecture of hydrophobic core and hydrophilic shell. They are appropriate for administration of hydrophobic drugs (Cho *et al.* 2008).

Liposomes constitute from an aqueous core covered by lipid bilayer (Orive *et al.* 2005). They are mostly studied drug systems. Liposomes with anticancer agent doxorubicin was clinically approved in 1995 (Orive *et al.* 2005, Hoffman 2008).

Nanospheres and nanocapsules are small scale DDS. The drug in nanospheres is dispersed uniformly in a polymer matrix system while in nanocapsules it is covered by a polymer shell (Orive *et al.* 2005).

Carbon nanotubes are hollow cylinders made up of benzene rings. They are normally insoluble in all solvents. However, with a surface treatment, they can be made water soluble and functionalized with different targeting agents (Cho *et al.* 2008).

Ceramic nanoparticles are composed of inorganic compounds. They are not affected by pH or temperature changes. Therefore, they can protect encapsulated drugs very effectively (Sahoo 2003).

Solid lipid nanoparticles are composed of a solid lipid core covered by surfactants and they are mostly effective in hydrophobic drug administration (Mühlen *et al.*1998).

Magnetic nanoparticles have a core composed of magnetic compounds and a polymeric cover. They can be targeted to a site with an applied magnetic field (McBain *et al.* 2008).

Nanoparticles employed in cancer drug delivery studies are efficient in differentiating cancer cells from healthy cells by passive and active targeting. They are successful to prevent severe side effects of conventional therapy. By conjugating to specific agents, they can be taken up into cell by receptor mediated endocytosis which makes them effective in drug delivery to drug resistant cells. However, there are still some limitations regarding to their toxicity, stability in circulation and effective tissue distribution (Cho *et al.* 2008).

To achieve a successful drug targeting by nanoparticles, firstly they should not be filtered from blood stream very quickly. Size and surface chemistry of nanoparticles are important characteristics influencing their circulating half life. Nanoparticles should be small enough to escape from endocytosis of

macrophages in reticuloendothelial system (RES) and also to extravasate to tumor site through leaky blood vessels. Gaps between endothelial cells of blood vessel lining have size range of 100 – 600 nm (Yuan *et al.* 1995). Nanoparticles larger than 200 nm can be recognized by RES easily (Cho *et al.* 2008, Gupta 2004). Particles smaller than 10 nm can be cleared by kidney very quickly (Alexis *et al.* 2008, Choi *et al.* 2007). Hence, optimum size range for nanoparticles used in drug delivery is considered between 10 and 100 nm (Gupta 2004, Byrne *et al.* 2008, Cho *et al.* 2008).

Additionally, surface chemistry of nanoparticles plays a significant role on blood circulation time. Hydrophobic surfaces are recognized by RES more easily. On the other hand, Hydrophilic surfaces reduce opsonization, plasma protein adsorption process, on nanoparticles. If plasma proteins are adsorbed on nanoparticles, drug carriers are rapidly eliminated by macrophages and Kupffer cells in the liver (Gupta 2005, Peer *et al.* 2007).

Apart from drug delivery, nanoparticles due to their accumulation ability in tumor site have been started to be studied in magnetic resonance imaging (MRI) of tumor area, guided hyperthermia and radiotherapy. Especially, nanoparticles with a metallic core or shell are considered for these purposes (Vlerken 2006).

1.4 Magnetic Nanoparticles

The research of magnetic micro and nanoparticles with the aim of drug delivery has been started in 1970s (Senyei 1978, Widder 1978, McBain *et al.* 2008). Within last 40 years, magnetic nanoparticles have been studied in detail and their structural architecture has been improved. They have become important and been started to used widely in cancer treatment and clinical diagnostic.

1.4.1 General Usage of Magnetic Nanoparticles in Biomedicine

Magnetic nanoparticles (MNP) were firstly developed as MRI contrast agents. Owing to their characteristics; nontoxicity, biocompatibility, small size, easy targeting to a place with external magnetic field, they have been started to be considered for targeted drug delivery and hyperthermia treatments in cancer researches (Dobson 2006, Caruntu *et al.* 2007).

Additionally, MNP are very efficiently used in several biomedical applications. which can be classified as therapeutic and diagnostic applications (Figure 1.4).

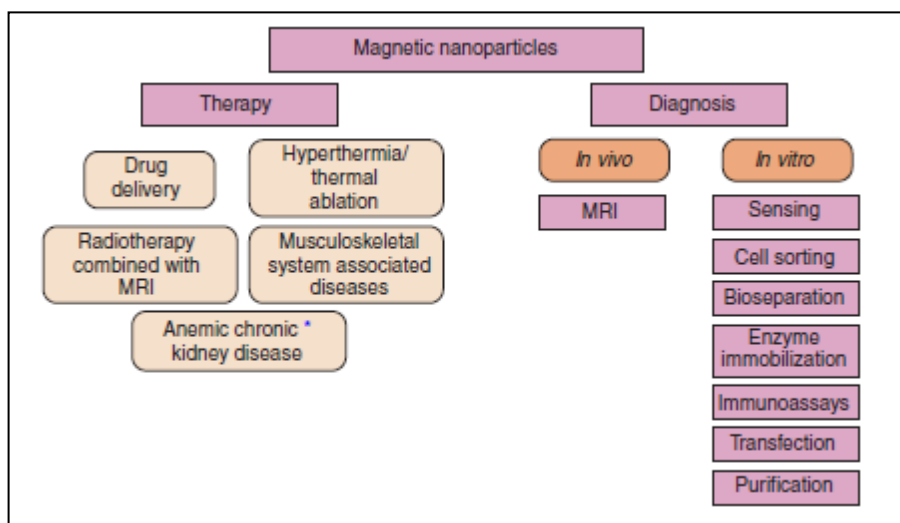


Figure 1.3 Biomedical Applications of MNP (Arruebo *et al.* 2007).

In addition to drug delivery, hyperthermia and MRI usage, MNP were widely preferred nanoparticles for sensing, cell sorting, cell targeting, enzyme immobilization, immunoassays, and gene transfection systems (Arruebo *et al.* 2007).

1.4.2 Drug Delivery Applications of Magnetic Nanoparticles

The idea behind using MNP in targeted drug delivery is that they can be easily guided by an external magnetic field to the targeted area, such as tumor tissue. Besides, cytotoxic drugs, therapeutic DNA, different targeting agents or permeation enhancers can be conjugated to them (Sun *et al.* 2008). First

clinical research of drug loaded magnetic nanoparticles was study of epirubicine loaded starch coated magnetic nanoparticles (Lubbe *et al.* 1996). In another study, Wilson *et al.* (2004) studied success of doxorubicin loaded MNP on hepatocellular carcinoma patients and stated efficient shrinkage of tumor.

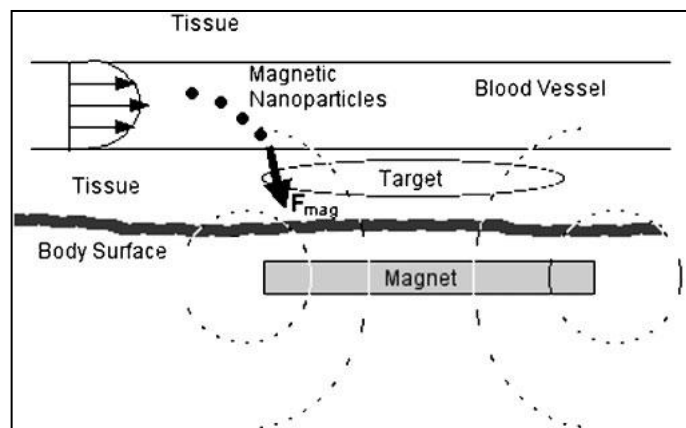


Figure 1.4 Schematic representation of manipulation of MNP by external magnetic field (Dobson 2006).

MNP can be

- manipulated to a site by a magnetic field,
- employed for hyperthermia purposes,
- functionalized with different kinds of chemotherapy agents,
- visualized and used in MRI (Arruebo *et al.* 2007).

These characteristics of MNP give rise to the idea of all-in-one multifunctional nanoparticles with tumor targeted imaging and drug delivery abilities. However, proper synthesis and design of magnetic particles play significant roles in effective therapeutic and diagnostic applications of MNPs. Kohler *et al.* (2005) synthesized methotrexate, a chemotherapy agent able to bind to folic acid receptors, loaded MNP with the aim of multifunctional nanoparticles (Kohler *et al.* 2005, McBain *et al.* 2008).

1.4.3 Structure of Magnetic Nanoparticles

General structure of MNP is composed of an inner magnetic core and outer polymeric shell (Figure 1.4). Magnetic core is usually a magnetite (Fe_3O_4) or maghemite (Fe_2O_3). It is covered with a polymeric shell which renders MNP biocompatible, prevents their agglomeration and functions as drug reservoir (McBain *et al.* 2008).

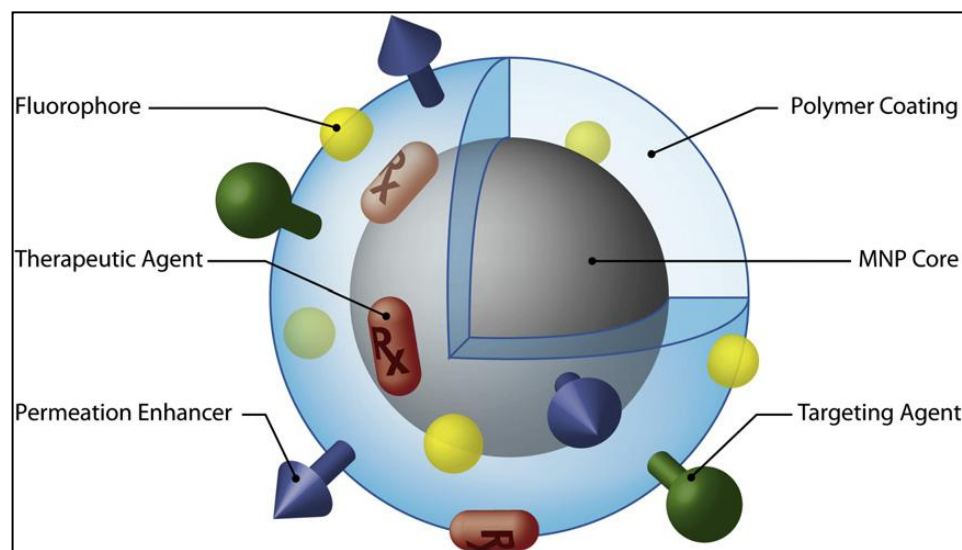


Figure 1.5 General structural design of MNP used in biomedical applications (Sun *et al.* 2008).

Different types of polymers and molecules are used for covering surfaces of naked magnetic nanoparticles to stabilize them and for further biological applications. Starch, dextran, polyethylene glycol, fatty acids, polyvinyl alcohol, polyacrylic acid, poly lactides, gelatin and chitosan are some of the examples of widely used coating material with different purposes (Gupta 2005).

According to the aim of the use, unique targeting agents can be tailored to surface of MNP. Transferrin, lactoferrin, elastin, albumin, Tat peptide, RGD peptide and folic acid are remarkable targeting ligands which are able to target cell surface receptors (Gupta 2005).

1.4.3.1 Role of Polyethylene Glycol (PEG) in Drug Delivery

MNP have high surface to volume ratio, leading to an intense surface electrostatic charge. Hence, they tend to agglomerate. Moreover, uncoated nanoparticles can be covered with plasma proteins by opsonization process, which triggers clearance of MNP by macrophages. Surface covering of nanoparticles helps to prevent this agglomeration problem by producing a steric barrier and to increase the circulation time of MNP by reducing opsonization (Sun *et al.* 2008).

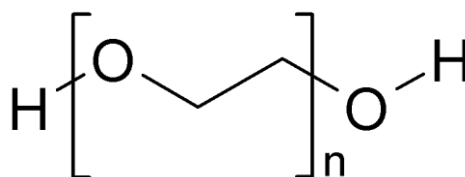


Figure 1.6 Chemical structure of PEG with the molecular formula $C_{2n}H_{4n+2}O_{n+1}$ (http://www.sigmaaldrich.com/catalog/ProductDetail.do?D7=0&N5=SEARCH_CONCAT_PNO%7CBRAND_KEY&N4=P5413%7CSIAL&N25=0&QS=O_N&F=SPEC).

PEG is one of the mostly used synthetic polymers to cover MNP. It gives MNP a hydrophilic surface and minimizes agglomeration. Thus, PEG coating enhances the circulation time of MNP by reducing their phagocytosis by macrophages (Sun *et al.* 2008). Besides, PEG is nonimmunogenic, nonantigenic and can be easily excreted through the kidney (Gupta 2004). Only limitation of PEG shell is that it is hard to further functionalize, since it

has only end groups available for this aim (McBain *et al.* 2008). However, different methods have investigated to link PEG on MNPs, such as silane grafting to oxide surfaces, polymerization at the surface of MNP and sol–gel approaches (Sun *et al.* 2008).

1.4.3.2 Role of Folic Acid in Targeted Drug Delivery

Folic acid is a kind of vitamin B. It is important in synthesis of purines, pyrimidines and DNA. It helps cell division and growth, especially has significant roles in both pregnancy and infant development (<http://ods.od.nih.gov/factsheets/folate/>).

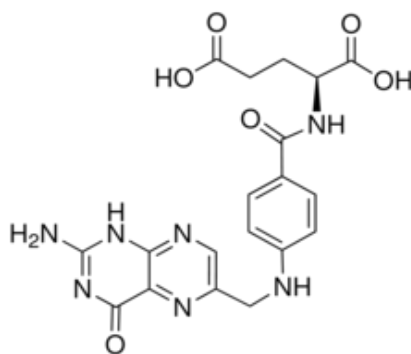


Figure 1.7 Chemical Structure of Folic Acid (<http://www.sigmaaldrich.com/medium/structureimages/05/mfcd00079305.png>)

Folic acid can be taken up into cell by folic acid receptors (FR) and reduced folate carriers (Spinella *et al.* 1995). FR are found to be overexpressed on different types of cancer cells such as ovarian, brain, kidney, lung, head and neck, breast and colorectal cancers (Byrne *et al.* 2008). Lu *et al.* (2003) stated that 32% of breast cancer cases in USA were recorded as FR positive in 2002. Normal cells do not express FR or it locates on apical surface of polarized epithelia where drugs cannot reach (Lu *et al.* 2002). Besides, while only reduced folate can be transported in healthy cells, cancer cells are able to transport folate conjugates by FR via receptor mediated endocytosis. In this process, after folic acid ligand of targeting agents binds to FR on cell surface, they are internalized into an endosome. The release of drug cargo in nanoparticles becomes easier as pH value decreases in the endosome resulting in entry of drug into cytoplasm. By this mechanism, folic acid covered nanoparticles can overcome drug resistance caused by P-glycoprotein efflux pumps (Cho *et al.* 2008) (Figure 1.7).

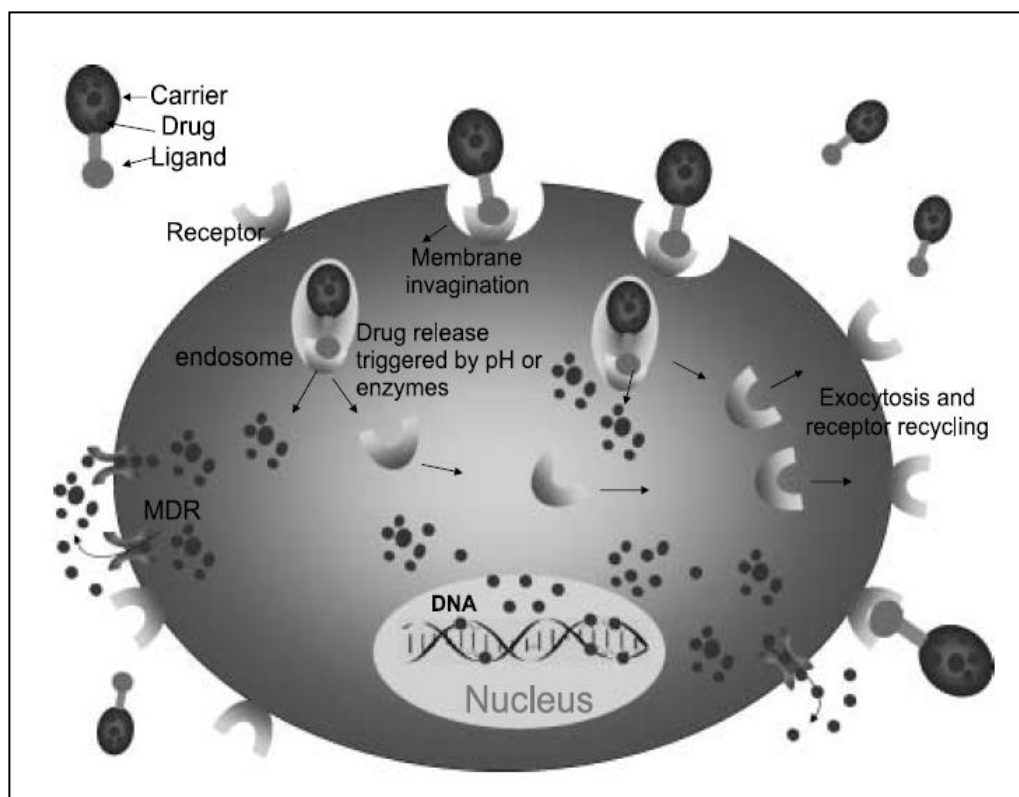


Figure 1.8 Schematic representation of receptor mediated endocytosis of drug carriers. (Cho *et al.* 2008)

Folate ligands are not expensive, toxic or immunogenic. Also they can be easily attached to drug carriers and bind to FR with high affinity. They keep their stable form in storage and in circulation for long time (Byrne *et al.* 2008).

These natural characteristics of folic acid and folic acid receptors on cancer cells make them very efficient agents for drug targeting, immunotherapy and tumor imaging (Lu 2002). Since cancer cells overexpress FR and folic acid conjugated agents are primarily taken up into cancer cells, folic acid coated agents can ameliorate the severe side effects of free drugs and overcome drug resistance.

Reddy et al. (1998) investigated that folic acid conjugated nanoparticles exhibited significant uptake and accumulation in breast cancer tissue. Zang *et al.* (2004) stated that targeted drug release increased in FR positive cervical cancer and colon cancer cells by folic acid conjugated liposomes. In another study, it was found that folate attached liposomes were efficient in bypassing P-glycoprotein associated drug efflux mechanism in drug resistant acute myelogenous leukemia cells (Ratman *et al.* 2003).

1.4.4 Synthesis Methods of Magnetic Nanoparticles

Different synthesis methods of MNP have been investigated to synthesize nanoparticles with the desired characteristics of size and shape. Aerosol/ vapor (pyrolysis), gas deposition, bulk solution (co-precipitation), sol-gel and microemulsion are the methods through which MNP can be synthesized (Gupta 2005, McBain *et al.* 2008). According to intended purpose, an appropriate synthesis method can be followed, since each method has different advantages and disadvantages, which are given in Table 1.1.

Table 1.1 Comparison of MNP synthesis methods (Gupta 2005)*

Methods →	Aerosol/ vapor (pyrolysis) method	Gas Deposition	Bulk solution (co-precipitation) method	Sol-Gel method	Microemulsion method
Characteristics ↓					
Size and Distribution	5 - 60 nm Broad distribution	5 - 60 nm Narrow distribution	10-50 nm Broad distribution	20-200 nm Broad distribution	4- 15 nm Narrow size distribution
Magnetization Values	10 – 50 emu/g with desired magnetic property	> 20 emu/g	20-50 emu/g with superparamagnetic behavior	10-40 emu/g with paramagnetic behavior	> 30 emu/g with superparamagnetic behavior
Advantages	High production Rate	Useful for protective coating and thin film deposition	Large quantities can be synthesized	Useful in hybrid nanoparticle synthesis	Uniform properties and also size of the nanoparticles can be modulated
Disadvantages	Formation of large aggregates	Require very high temperatures	Diamagnetite contribution	Products usually contains sol-gel matrix components at their surfaces	Surfactants are difficult to remove, only small quantities can be obtained synthesized

*Adapted from Gupta AK, Gupta M. 2005. Synthesis and surface engineering of iron oxide nanoparticles for biomedical applications. Biomaterials. 26 (18): 3995-4021

1.4.5 Magnetic properties of nanoparticles

In addition to size and surface chemistry of MNP, magnetic property is very important. Since their magnetic ability is central in drug delivery to targeted tissues, their response to externally applied magnetic field should be determined. MNP with superparamagnetic characteristics are desired for biomedical applications.

Magnetic materials can be diamagnetic, paramagnetic, ferromagnetic and superparamagnetic based on their magnetization behavior toward magnetic field (Spaldin 2011). In atomic levels, electrons are usually found in pairs and spin in opposite directions resulting in zero net magnetic field. However, materials with unpaired electrons exhibit magnetic characteristics. Diamagnetic materials do not have any unpaired electrons and so they do not show any magnetization upon the externally applied magnetic field. On the other hand, paramagnetic materials have some unpaired electrons. Although they are magnetized under magnetic field, they do not exhibit magnetic property with the canceling of field. Conversely, ferromagnetic materials have their own net magnetization due to the unpaired electrons. After the removal of applied field, they are persistent to keep permanent magnetization (<http://www.ndt-ed.org/EducationResources/CommunityCollege/MagParticle/Physics/MagneticMatls.html>). Since single atoms cannot show ferromagnetism, it is a concept of materials with multiple atoms. Besides, superparamagnetism is related to size of particles. Ferromagnetic particles, 6-15nm in size, have superparamagnetic characteristics while the same particle in micrometer size exhibits ferromagnetism. In nanoscale, each particle behaves as a single domain (Gupta 2005). Superparamagnetic materials exhibit high magnetization

under external magnetic field like ferromagnetics and do not show any magnetization like paramagnetic materials when field is removed (Arruebo *et al.* 2007). Magnetic characteristic of materials can be understood from hysteresis loop graphs which is plotting magnetization of material, M , against applied magnetic field, B (Figure 1.8).

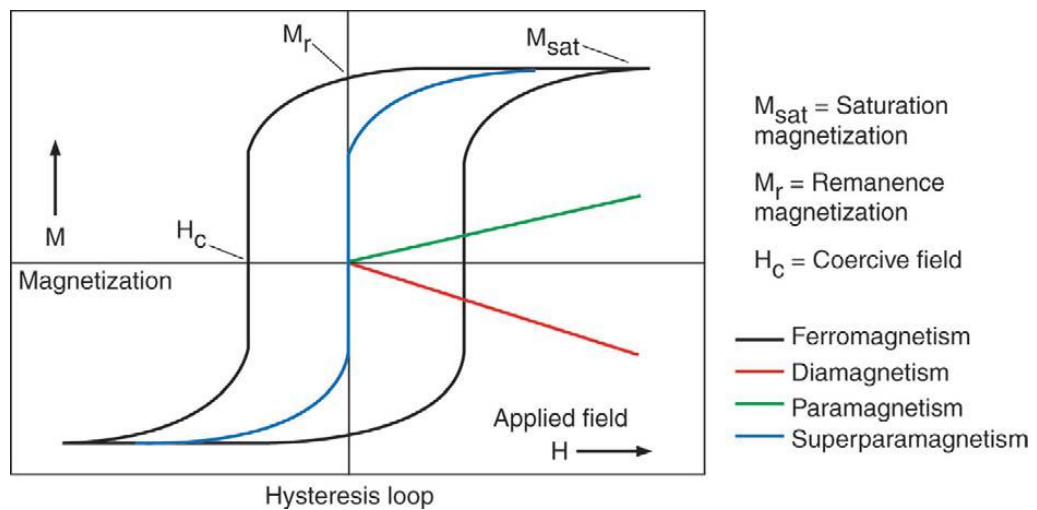


Figure 1.9 Schematic representation of magnetization graphs of diamagnetic, paramagnetic, ferromagnetic and superparamagnetic materials. (M_{sat} is the point where almost all magnetic domains of material aligned in same directions. M_r is the point shows remnant magnetization of material even though field is removed. H_c indicates the required applied field to cancel out remanence magnetization) (Arruebo *et al.* 2007).

Superparamagnetism is a required specification for MNP, especially in drug delivery. MNP are considered to be manipulated by an external magnetic field to targeted tumor area. Therefore, they are sought to possess high

magnetization. However, when applied field is removed, they are supposed to not to hold magnetization which means negligible remanence and coercivity values. If magnetization becomes permanent after the removal of magnetic field, they may agglomerate, which might lead to embolization of capillary vessels (Arruebo *et al.* 2007).

1.5 Aim of the Study

The aim of this research is synthesis and characterization of folic acid conjugated, PEG coated magnetic nanoparticles and their *in vitro* application to MCF-7 breast cancer cells. The objectives of this study can be summarized as follows:

- To synthesize Fe_3O_4 magnetic nanoparticles by co-precipitation method.
- To cover MNP with oleic acid.
- To modify surface of synthesized MNP by Polyethylene Glycol (PEG) monooleate.
- To attach Folic Acid to PEG modified MNP.
- To characterize the synthesized naked and coated MNP.
- To investigate whether synthesized MNP have toxic effects on sensitive and drug resistant lines of MCF-7 breast cancer cells.

CHAPTER 2

MATERIALS AND METHODS

2.1 MATERIALS

2.1.1 Materials for Magnetic Nanoparticle Synthesis

Iron (II) chloride tetrahydrate ($\text{FeCl}_2 \cdot 4\text{H}_2\text{O}$), iron (III) chloride hexahydrate ($\text{FeCl}_3 \cdot 6\text{H}_2\text{O}$), oleic Acid, polyethylene monooleate, folic acid, dicyclohexyl carbodiimide (DCC) and dimethylsulfoxide (DMSO) were purchased from Sigma-Aldrich (U.S.A). Ammonium hydroxide solution (NH_4OH) was obtained from Merck (Germany). Dimethylsulfoxide (cell culture grade) was obtained from Applichem (Germany). Nitrogen gas was provided from Asya Gaz (Turkey).

2.1.2 Materials for Cell Culture Studies

MCF-7 monolayer type human epithelial breast adenocarcinoma cell line was provided from Food and Mouth Diseases Institute (Ankara). 1 μ M Doxorubicin, 400 nM paclitaxel and 8 μ M zoledronic acid resistant cell lines, namely; MCF-7/Dox, MCF-7/Pac and MCF-7/Zol were developed from MCF-7 (MCF-7/S) previously in our laboratory by continuous drug application (İşeri 2009, Kars 2007, Kars 2008)

RPMI 1640 medium [(1x), 2.0g/l NaHCO₃ stable glutamine], fetal bovine serum (tested for mycoplasma) were obtained from Biochrom Ag. (Germany).

Trypsin-EDTA solution (0.25% Trypsin&EDTA), gentamycin sulphate (50mg/ml as base), tryphan blue solution (0.5%), cell proliferation kit (XTT assay) were obtained from Biological Industries, Kibbutz Beit Haemek (Israel).

2.2 METHODS

2.2.1 Synthesis of Magnetic Nanoparticles (MNP)

In the literature, different methods are employed to synthesize magnetic nanoparticles; such as: microemulsion, co-precipitation, laser pyrolysis, sol-gel, thermal decomposition (Gupta 2005).

In this study, magnetic nanoparticles were synthesized by co-precipitation method (Liu *et al.* 2006, Yallapu *et al.* 2010). Generally, nanoparticles synthesized by this method possess 10-50 nm particle size distribution which is in the optimal size range of nanoparticles used in biomedical applications. They are spherical in shape and the yield of the experiment is excess in amount.

In this method, particles are usually obtained by addition of a base such as alkali metal hydroxides into aqueous solution of Fe (II) and Fe (III) salts. The chemical reaction of Fe₃O₄ precipitation is given below (Equation 2.1).



In this study, magnetic nanoparticles were synthesized in a 5 necked glass bottle. Experimental setup of the MNP synthesis is given in Figure 2.1. System was placed on a heater and reaction was started in a reflux system, with the help of the mechanical stirrer (Heildolf RZR 2021, Germany). Solution was stirred under nitrogen gas, as the ammonium hydroxide given into system drop by drop by a peristaltic pump.

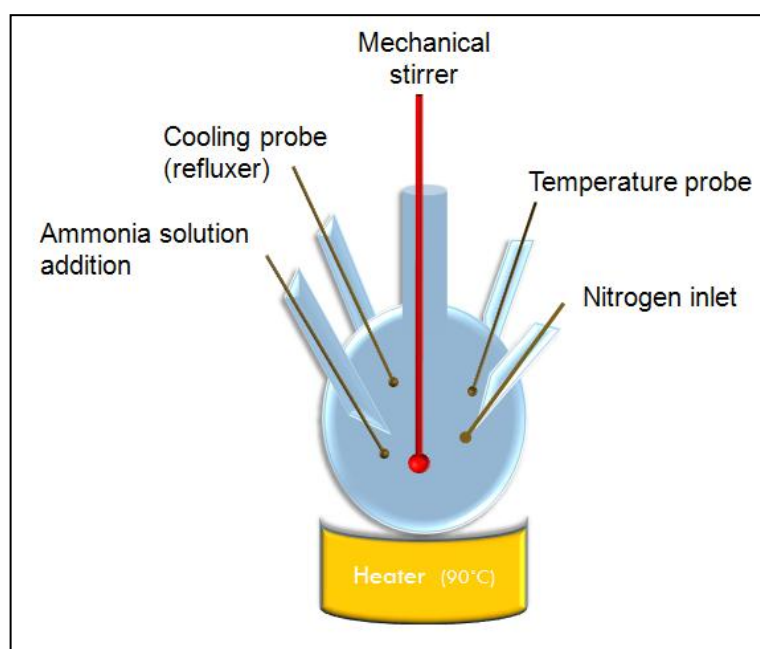


Figure 2.1 Design of experimental setup for MNP synthesis

Firstly, $\text{FeCl}_3 \cdot 6\text{H}_2\text{O}$ and $\text{FeCl}_2 \cdot 4\text{H}_2\text{O}$ salts were dissolved in water. Then, ammonium hydroxide was added to system with the help of the peristaltic pump.

Black precipitate of MNP were gathered by magnetic decantation. Black precipitate was washed until the pH of the solution fell down to 9.

For the optimization of synthesis step, three different synthesis experiments were performed. In two of them, 25 ml and 35 ml ammonium hydroxide were used. Speed of peristaltic pump was adjusted to 0.2. Those nanoparticles were named as N-MNP₁ and N-MNP₂ respectively. In the third experimental setup, 25 ml ammonium hydroxide was added in to system in a shorter time and yield of the sample was labeled as N-MNP₃.

2.2.2 Preparation of Oleic Acid Coated Magnetic Nanoparticles

One of the significant problems of MNP synthesis is agglomeration of the nanoparticles. Since they have large surface area to volume ratio, MNP tend to agglomerate (Gupta 2004). In order to prevent agglomeration, surfactants are needed.

In this study, oleic acid was used as surfactant to prevent agglomeration. Oleic acid coated MNP were synthesized in two different methods. In first method, after MNP were synthesized and washed, oleic acid was added on MNP solution and stirred for 1 hour by mechanical stirrer (Yan *et al.* 2009). Particles were washed with ethanol 3 times to get rid of excess amount of oleic acid and labeled as OA-MNP₁.

In second way, oleic acid was directly added into synthesis system. After black precipitate was obtained, temperature was decreased to 80°C and oleic acid was added into system. Stirring proceeded for 24 hours (Yallapu *et al.* 2010). Sample was labeled as OA-MNP₂.

2.2.3 Functionalization of Magnetic Nanoparticles with Polyethylene Glycol

When nanoparticles tend to agglomerate, they absorb plasma proteins on their surfaces and quickly cleared by macrophages which reduce their blood circulation time. Nanoparticles modified with hydrophilic polymeric surfactants do not prone to protein adsorption which increases their blood circulation time.

In this research, oleic acid conjugated polyethylene glycol (Polyethylene glycol monooleate) was used as polymeric surfactant. It was hypothesized that the oleate part of PEG monooleate would adsorb on to oleic acid coating on the iron-oxide core. Hence, PEG could form an exterior surface layer that renders MNP hydrophilicity.

PEG coated MNP were prepared by two different methods. PEG-MNP₁ nanoparticles were synthesized by mixing oleic acid coated nanoparticles (OA-

MNP₁ samples were used) with PEG monooleate in aqueous environment for 24 hr.

In second method, after the synthesis of oleic acid coated MNP, the temperature of the system was decreased to room temperature, and the aqueous solution of PEG monooleate was added to system and the stirring was continued for an additional 24 h at room temperature. PEG coated MNP obtained by this method was labeled as PEG-MNP₂.

In the synthesis of PEG-MNP₃, after washing oleic acid coated MNP with ethanol, (OA-MNP₂ particles were used) they were mixed with aqueous solution of PEG monooleate for 24 hr.

2.2.4 Modification of Magnetic Nanoparticles with Folic Acid

Folic acid needs the activation of its carboxyl group with dicyclohexyl carbodiimide (DCC) to conjugate to surface polymer (Zhang *et al.* 2008). Folic acid and DCC with 1:1 ratio were added in dimethyl sulfoxide (DMSO) and stirred for 2 h. PEG-coated PEG-MNP₂ sample was added into system and continuously stirred for either 2 h or 24 h under a nitrogen atmosphere. After washing of the nanoparticles with dH₂O, they were freeze-dried for one night. The sample stirred for 2 hr or 24 h labeled as FA-MNP₁ and FA-MNP₂, respectively.

2.2.5 Chemical Characterization

Chemical characterizations using X-Ray Diffraction, Vibrating Sample Magnetometer were carried in METU Central Laboratory. The Fourier Transform Infrared Spectroscopy analyses were carried in Hacettepe University. Transmission Electron Microscopy analysis was performed either in UNAM, Bilkent University or METU Central Laboratory.

2.2.5.1 X-Ray Diffraction (XRD)

X-ray powder diffraction (XRD) is an analytical technique used for phase identification of a crystalline material and can provide information on unit cell dimensions. It reveals information about the crystallographic structure, chemical composition, and physical properties of materials. It is based on observing the scattered intensity of an X-ray beam hitting a sample as a function of incident and scattered angle, polarization, and wavelength or energy (<http://mit.edu/cmse/facilities/techniques.shtml>). XRD was used to understand crystal structure of the synthesized Fe₃O₄ nanoparticles. Rigaku Ultima-IV X-Ray Diffractometer instrument was used for analysis.

2.2.5.2 Fourier Transform Infrared (FTIR) Spectroscopy

FTIR spectra were used to understand the chemical composition of the naked MNP, oleic acid coated MNP, PEG coated MNP, folic acid and folic acid functionalized MNP samples. 0.1 g sample was pelleted with 0.19 g KBr. FTIR instrument with the brand Thermo Scientific and the model Nicolet 6700 was used for analysis.

2.2.5.3 Transmission Electron Microscopy (TEM)

To visualize shape of MNP and to learn their size TEM was used. Naked MNP, OA coated MNP, PEG coated MNP and FA functionalized MNP were visualized by TEM. FEI - Tecnai G2 F30 TEM and FEI - 120kV HCTEM instruments were used for analysis.

2.2.5.4 Vibrating Sample Magnetometer (VSM)

Magnetic properties of naked MNP, OA coated MNP, PEG coated MNP and FA functionalized MNP were studied by VSM (EV/9, ADE Magnetics).

2.2.6 Cell Culture

2.2.6.1 Cell Line and Culture Conditions

MCF-7 human breast cancer adenocarcinoma cell line was used in cell culture studies. Cell cultures were maintained in 1640 RPMI medium (Biochrom AG, Berlin) with 10% (v/v) fetal bovine serum (FBS) (Biochrom AG, Berlin) and 10% (w/v) gentamicin (Biological Industries, Israel). Incubation of cell cultures was maintained in incubator (Heraeus, Germany) at 37 °C in a humidified atmosphere with 5% CO₂. Under sterile laminar flow (BioAir, Italy) cell culture experiments were performed.

2.2.6.2 Passaging Cell Cultures

When cell growth reached 80% confluency, cells were passaged. While subculturing, cell to cell and cell to substrate interactions are dissociated by trypsinization. Old medium from culture flasks was discarded. Cells were washed with PBS to remove the traces of serum which inactivates trypsin. Trypsin-EDTA was added on cells. After dispersed suspension of detached cells was obtained, fresh medium was added on cells and required amount of cell suspension was passaged to culture flask.

2.2.6.3 Freezing Cells and Thawing Frozen Cells

To freeze cells, firstly they should be trypsinized. After suspension of detached cells was centrifuged, supernatant was removed and pellet was redispersed in PBS. PBS solution containing cells was centrifuged again at 800 rpm for 5 min. Supernatant was discarded, cells were redispersed in 1 mL of cold freezing medium (90% (v/v) FBS and 10% (v/v)). After transferring cells in freezing medium into the cryovials, they were incubated at -20 °C for 3-4 hours before they were put into -80 °C for short term storage. For long term, they were stored in liquid nitrogen tank.

To thaw cells, frozen cell cryovials taken from -80 °C or nitrogen tank were kept at 37 °C until they thawed completely. After thawing, cell suspension was transferred to sterile falcon tubes and centrifuged to discard supernatant. Fresh medium containing serum was added on cells. Homogenized cell suspension was transferred to new cell culture flask.

2.2.6.4 Viable Cell Count

For cell proliferation assay, number of cells should be determined. In cell counting studies, Trypan Blue dye was used. Since dead cells have impaired membrane, they are stained into blue, while live cells have intact membrane, they can exclude dye (Strober *et al.* 2007).

Trypsinized MCF-7 cell suspension was stained with Trypan Blue solution. Cells were counted on Neubauer hemacytometer under light microscopy (Olympus, USA). There are 16 large squares on hemocytometer each of which consists 16 small squares. Volume of one small squares is 0.00025 mm^3 . The number of the cells in 1 mL of cell suspension was calculated by the formula given below (Equation 2.2):

$$\text{Cell number/mL} = \text{Average count per square} \times \text{Dilution factor} \times 4.10^6 \quad (2.2)$$

2.2.6.5 Cell Proliferation Assay with XTT Reagent

To understand whether synthesized MNP has an effect on proliferation of MCF-7 cells, XTT Cell Proliferation Kit was used. The kit based on the idea that metabolically active cells can reduce XTT (2, 3-bis (2-methoxy-4-nitro-5-sulfophenyl)-2H-tetrazolium-5-carboxanilide) tetrazolium salt to orange colored, water soluble formazan products by mitochondrial enzymes which are inactivated after cell death. The intensity of formazan compound is proportional to number of living cells in the sample and it can be spectrophotometrically measured (Biological Industries, 2002).

In this study 96 well plates were used and 10,000 cell/well were seeded into plate starting from the 2nd column (Figure 2.2). Highest concentration of synthesized MNP was applied to 3rd column (Figure 2.2) and it was diluted horizontally. First and second columns were used as medium control and cell

control columns. 3rd to 12th columns contain cells, medium and ½ diluted concentrations of MNP. To prevent the absorbance interference of MNP and to formazan absorbance, the bottom and top rows, containing only medium and defined concentration of MNP were used as control of MNP. Cell seeded plates were incubated at 37 °C in a humidified atmosphere with 5% CO₂ for 72 hours. After 72 hours, XTT and activator reagents were applied to each of three plates. The optical density of soluble product was measured at 496 nm by microplate reader (Anthos 2010, England).

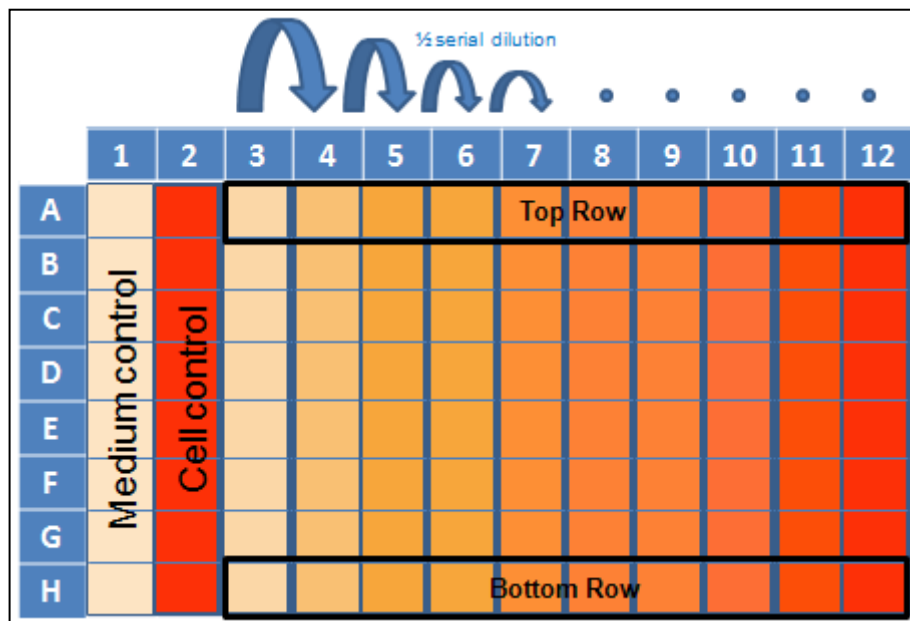


Figure 2.2 Schematic representation of XTT cell proliferation design on 96 well plate.

By converting dye intensity into percent viability, cell proliferation curves were constructed. The average dye intensity of the cell control column (2nd column) indicates the 100% cell proliferation. For every cell column exposed

to different concentrations of MNP, average dye intensity was calculated by considering average of the top and bottom rows.

2.2.6.6 Light Microscopy Observation of MNP Treated Cells

To investigate and observe the response of cells to nanoparticles *in vitro* conditions, MCF-7/S cells were seeded in 6 well plate (25,000 cell/well) and incubated with 500 $\mu\text{g/ml}$ of N-MNP₁, PEG-MNP₂ and FA-MNP₁. After 48 hr of incubation, cells were observed under light microscopy and images were taken.

2.2.6. Statistical Analysis

All data representative of three independent experiments, each run in triplicates and expressed as mean \pm standard error of means (SEM). GraphPad Prism 5 Demo Software (USA) was used to determine significant differences between mean of the groups ($\alpha=0.05$). One-way ANOVA, two-way ANOVA, Tukey and bonferroni post tests were carried out.

CHAPTER 3

RESULTS AND DISCUSSION

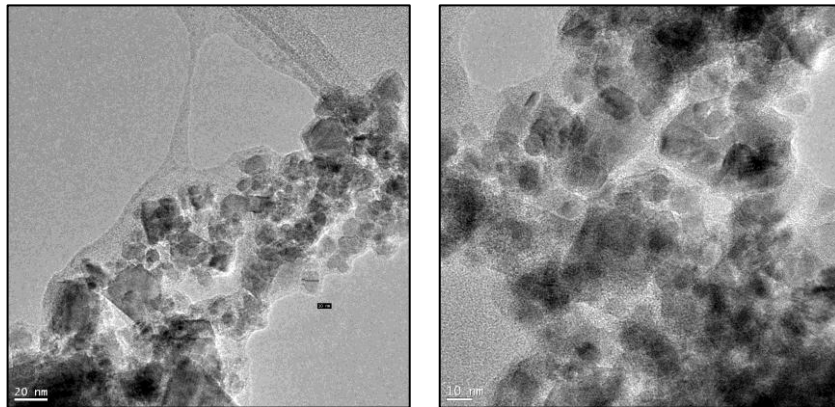
3.1 Chemical Characterization

3.1.1 Transmission Electron Microscopy (TEM)

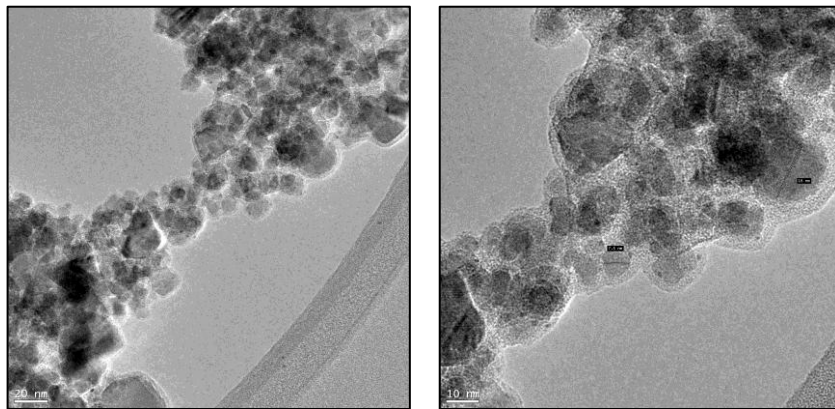
Shapes and sizes of naked, oleic acid, PEG coated and folic acid functionalized nanoparticles were analyzed by TEM.

3.1.1.1 TEM Characterization of Naked MNP

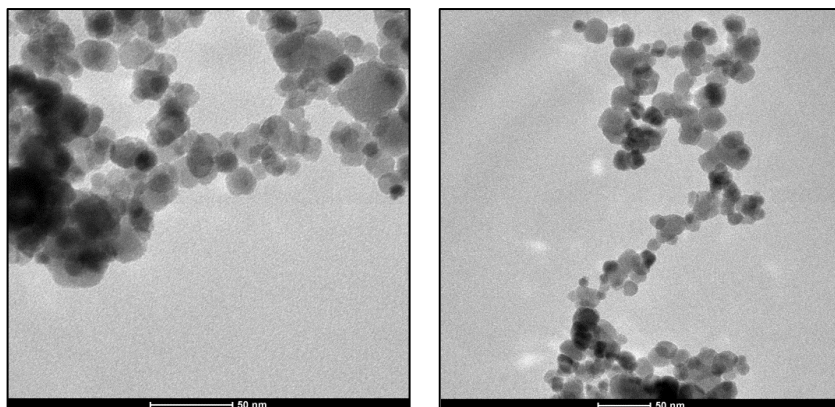
In Figure 3.1, TEM images of N-MNP₁, N-MNP₂ and N-MNP₃ samples are shown. Sizes of naked magnetic nanoparticles seemed to be approximately between 10 to 60 nm. In images of all three samples, agglomeration of MNP was observed.



a)



b)



c)

Figure 3.1 TEM images of a) N-MNP₁ b) N-MNP₂ and c) N-MNP₃

When images of N-MNP₁ and N-MNP₂ samples were compared, particle sizes were found to be similar. TEM image of N-MNP₃ sample exhibited more spherical nanoparticles with similar morphologies compared to N-MNP₁ and N-MNP₂ particles. N-MNP₃ sample seemed to have a narrower size distribution and it can be confirmed with dynamic light scattering (DLS) analysis.

Yield is high in co-precipitation method; however, synthesized particles usually have broad size distribution between 10-50 nm (Gupta 2005). In this method, during synthesis pH is important and has a role on particle size and morphology (McBain *et al.* 2008). During synthesis of N-MNP₁ and N-MNP₂ samples, addition of ammonium hydroxide solution to system took 3 to 4 hours by a peristaltic pump. Within this time period, pH of the system was continuously increasing and leading to precipitation reaction at different pH values. Increase in pH during the reaction may lead to synthesis of particles with irregular morphologies and broad size distribution. On the other hand, during the synthesis of N-MNP₃ particles, ammonium hydroxide solution was given into system in 15 minutes at a higher speed. Hence, pH value of the system increased and fixed in a shorter time. This may cause the reaction to take place in a narrower pH value range which probably resulted in narrower size distribution and similar morphologies.

3.1.1.2 TEM Characterization of Oleic Acid Coated MNP

In Figure 3.1 it is observed that magnetic nanoparticles made clusters. Since naked nanoparticles have high surface area to volume ratio, attractive forces between naked nanoparticles are strong. This attraction results in agglomeration of particles (Gupta 2005). In this study, oleic acid was used as surfactant to prevent agglomeration of nanoparticles.

Oleic acid coated MNP were synthesized in two different methods. In the first method (M_1), after MNP were synthesized and washed, oleic acid was added. Figure 3.2 displays TEM images of OA-MNP₁ synthesized by this method. Size distribution of OA-MNP₁ was found to be between 10-60 nm. Agglomeration of nanoparticles was still observed.

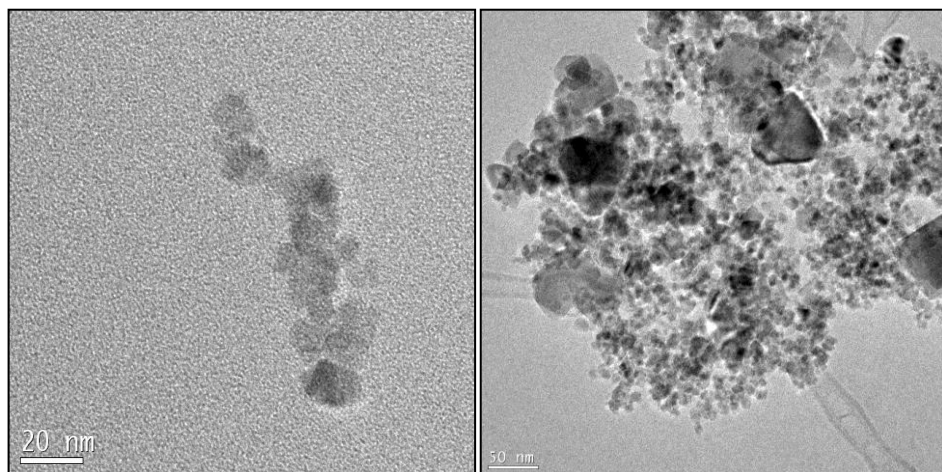


Figure 3.2 TEMs images of OA-MNP₁

In second way (M_2), oleic acid was directly added into system during Fe_3O_4 synthesis. After black precipitate was obtained, oleic acid was added into system at $80^\circ C$. Figure 3.3 displays TEM images of OA-MNP₂ synthesized by this second method (M_2). Sizes of MNP were found approximately between 10-15 nm. Agglomeration of nanoparticles was prevented to some extent.

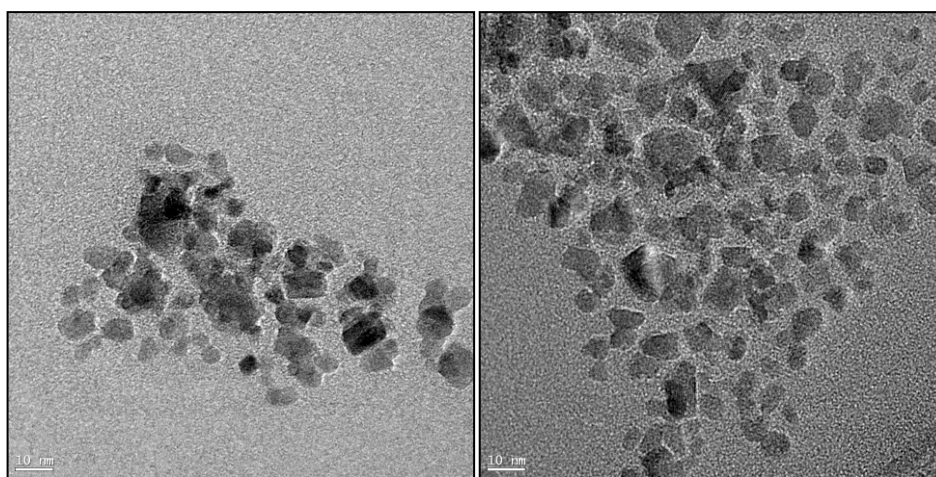


Figure 3.3 TEM images of OA-MNP₂

When Figures 3.2 and 3.3 are examined, it is observed that particles of OA-MNP₁ sample were tend to agglomerate more compared to OA-MNP₂ particles. This could be explained by interaction of oleic acid with the surface of nanoparticles. MNP has Fe-OH hydroxyl groups on their surfaces. Oleic acid interacts with the surface of naked MNP by its $-COOH$ carboxyl group (Boyer *et al.* 2010). When oleic acid was added during synthesis, pH of the system was basic since there was still ammonium hydroxide in the system. Interaction between Fe-OH hydroxyl groups of naked MNP and $-COOH$

carboxyl group of oleic acid is easier at high pHs. When oleic acid was added after synthesis, naked MNP were washed before oleic acid addition until pH 8. After washing, oleic acid and MNP were mixed at room temperature. Both low pH and higher temperature (80 °C) could affect the interaction of oleic acid with the surfaces of naked MNP. Poor coating of oleic acid layer in OA-MNP₁ sample may result in higher agglomeration. Meanwhile, shapes of OA-MNP₂ nanoparticles are more regular compared to OA-MNP₁ nanoparticles. The naked MNP which were used in OA-MNP₁ synthesis were belonging to N-MNP₂ samples which have irregular shapes and broad size distribution (Figure 3.1.b). In the literature similar results have been reported. Yan *et al.* (2009) synthesized oleic acid coated Fe₃O₄ nanoparticles and added oleic acid after synthesis of particles. In their study agglomeration tendency of oleic acid coated nanoparticles was observed. On the other hand, Liu *et al.* (2006) prepared oleic acid coated nanoparticles by addition of oleic acid to system during the synthesis. Their oleic acid coated Fe₃O₄ particles seemed to prevent agglomeration.

3.1.1.3 TEM Characterization of PEG Coated MNP

Polyethylene glycol coated nanoparticles were synthesized by three different methods and labeled as PEG-MNP₁, PEG-MNP₂ and PEG-MNP₃. During preparation of PEG-MNP₁ nanoparticles, PEG was not added into system during synthesis. Firstly, naked MNPs were synthesized and washed. After they were coated with oleic acid, PEG coating step was performed. PEG-MNP₂ nanoparticles were synthesized by *in situ* addition of both oleic acid and PEG during synthesis. PEG-MNP₃ nanoparticles were coated with PEG after

washing of oleic acid coated MNP which were synthesized by *in situ* addition of oleic acid. TEM images of PEG-MNP₁, PEG-MNP₂ and PEG-MNP₃ are given in Figures 3.4, 3.5 and 3.6, respectively.

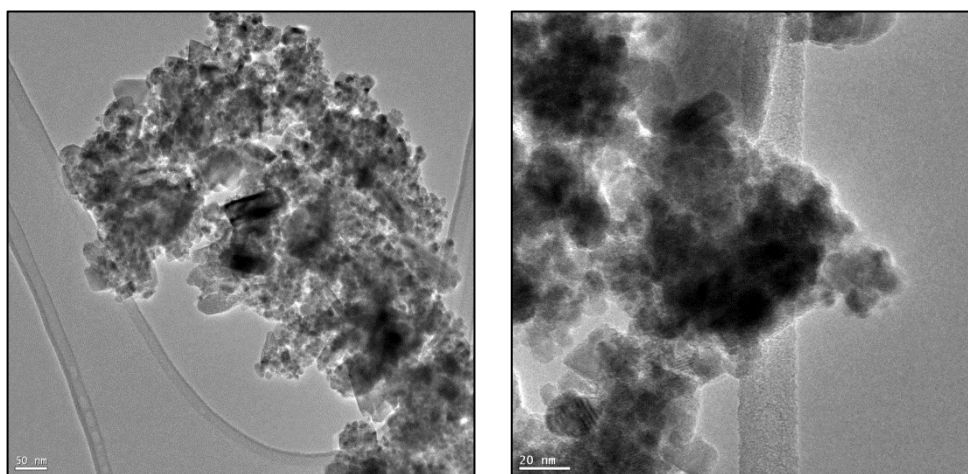


Figure 3.4 TEM images of PEG-MNP₁

In Figure 3.4, it is observed that PEG-MNP₁ samples tend to agglomerate. Their morphology was irregular with a broad size distribution. When TEM images of OA-MNP₁ and PEG-MNP₁ are compared, they seem similar in shape and size (Figures 3.2 and 3.4).

In Figure 3.5, shape and morphology of PEG-MNP₂ nanoparticles are seen more regular and spherical. Their size distribution seemed to be narrower. Their sizes were found to be around 10 nm according to TEM examination.

PEG-MNP₂ nanoparticles did not make clusters as much as naked MNP (Figure 3.1). They seemed agglomerate less compared to PEG-MNP₁ nanoparticles (Figure 3.4).

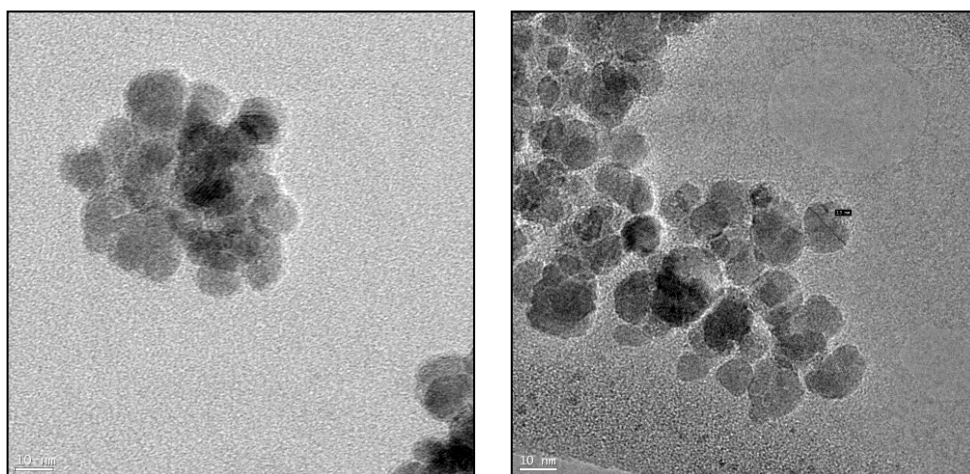


Figure 3.5 TEM images of PEG-MNP₂

In Figure 3.6, TEM images of PEG-MNP₃ were observed. Nanoparticles were spherical in shape and sized between approximately 10 to 40 nm. Agglomeration of nanoparticles seemed to be prevented better compared to naked nanoparticles (Figure 3.1).

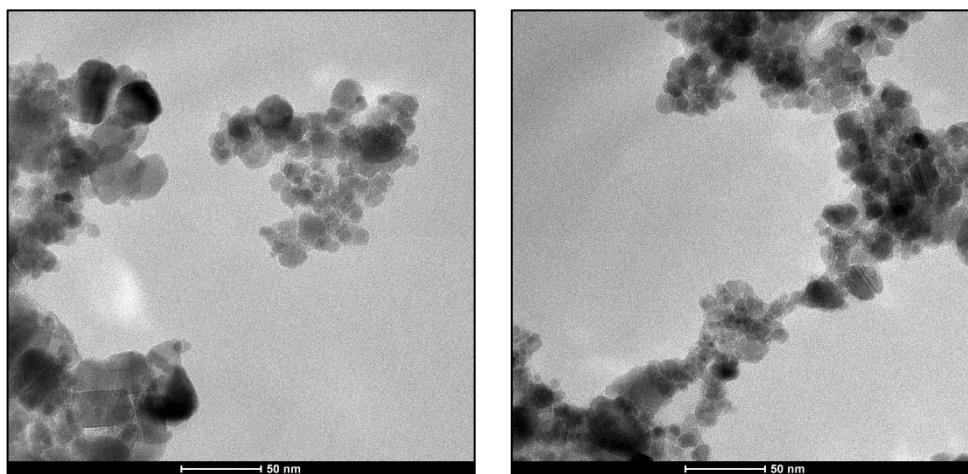


Figure 3.6 TEM images of PEG-MNP₃

3.1.1.4 TEM Characterization of Folic Acid Functionalized MNP

Folic acid can be used as targeting agent in biomedical applications of cancer therapies (Sonvico *et al.* 2005). In this study, magnetic nanoparticles were functionalized with folic acid after covering with PEG. During folic acid functionalization, reaction time was one of the parameters. Conjugation of folic acid to surface of PEG coated MNP was performed either for 2 hr or for 24 hr and the yields were labeled as FA-MNP₁ and FA-MNP₂, respectively. TEM images of FA-MNP₁ and FA-MNP₂ samples are given in Figures 3.7 and 3.8.

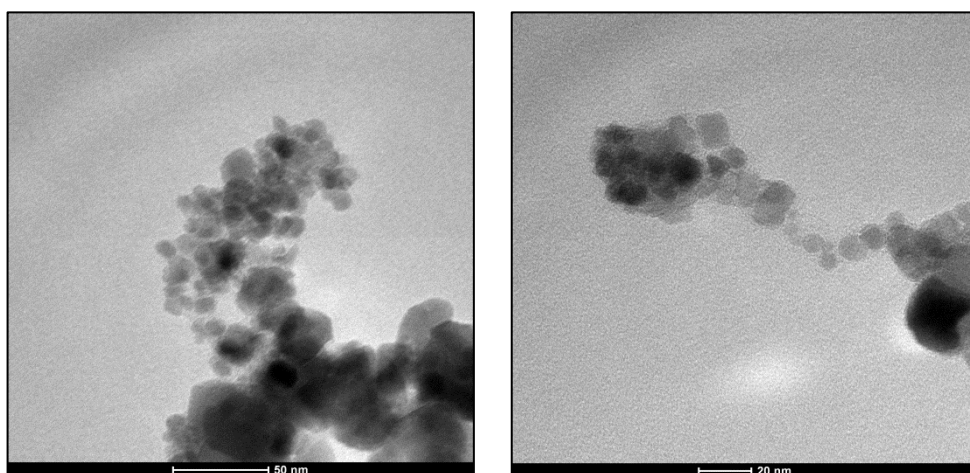


Figure 3.7 TEM images of FA-MNP₁

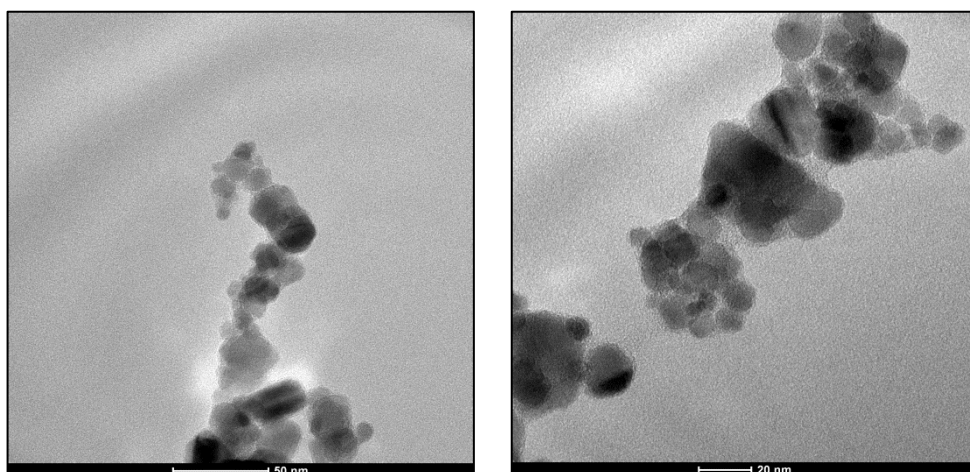


Figure 3.8 TEM images of FA-MNP₂

Shape and morphology of FA-MNP₁ and FA-MNP₂ nanoparticles were similar. The sizes were between 10-40 nm approximately. They exhibited some degree of agglomeration.

3.1.2 X-ray Diffraction (XRD)

Naked MNP, oleic acid coated MNP and PEG coated MNP were analyzed with XRD to study their crystal structure.

Figure 3.9 shows XRD patterns of N-MNP₋₁, N-MNP₋₂ and N-MNP₋₃

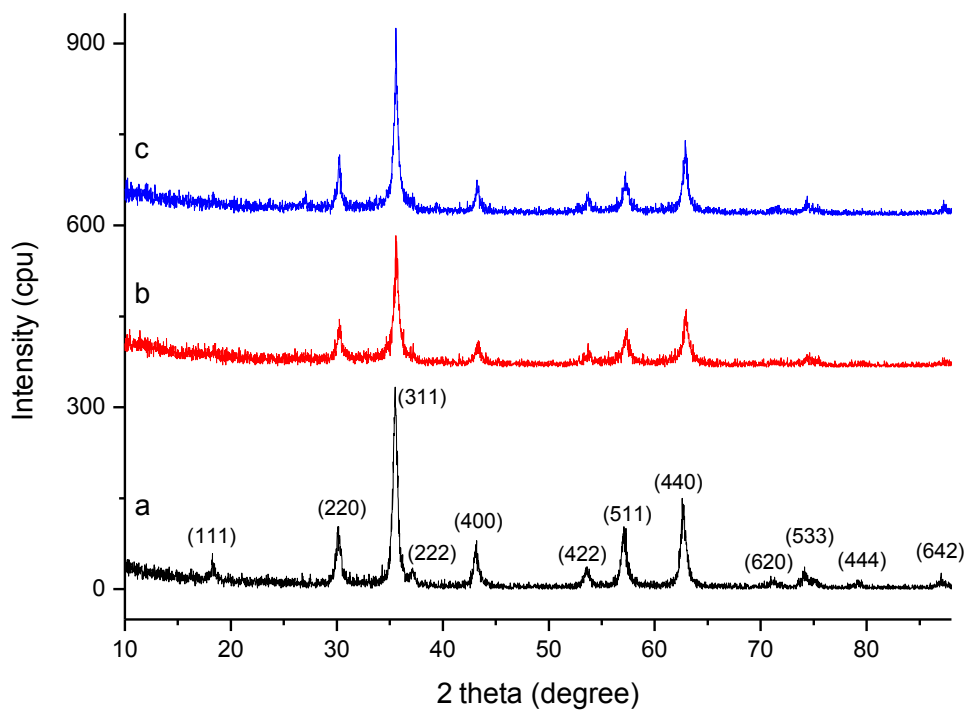


Figure 3.9 XRD patterns of a) N-MNP₋₁, b) N-MNP₋₂ and c) N-MNP₋₃

XRD patterns of all synthesized naked MNP were examined by comparing to peaks of standard magnetite in JCPDS file (PDF no: 01-071-6337). Standard Fe_3O_4 gives major peaks at 30.22, 35.60, 43.27, 53.68, 57.23, 62.85 2θ (degrees) which are corresponding to specific diffractive plane indexes (220), (311), (400), (422), (511), (440), respectively. N-MNP₁, N-MNP² and N-MNP₃ nanoparticles had exactly same peaks with standard magnetite which indicates that all synthesized naked nanoparticle samples had cubic spinal structure (Finger 1986). N-MNP₃ sample even exhibited minor peaks of standard Fe_3O_4 with corresponding plane indexes (111), (222), (620), (533), (444), (642) and (731) at 18.37, 35.60, 71.31, 74.36, 79.36, 87.21, 90.13 2θ (degrees), respectively. Besides, no additional peaks were observed indicating that there were not any impurities in the samples. These results are in parallel with the literature (Caruntu *et al.* 2004, Sun *et al.* 2006).

During the coating steps, both oleic acid and PEG were added into system during synthesis without any washing. XRD analysis of OA-MNP₂ and PEG-MNP₂ were also done to investigate whether this influenced the crystal structure of core nanoparticles (Figure 3.10).

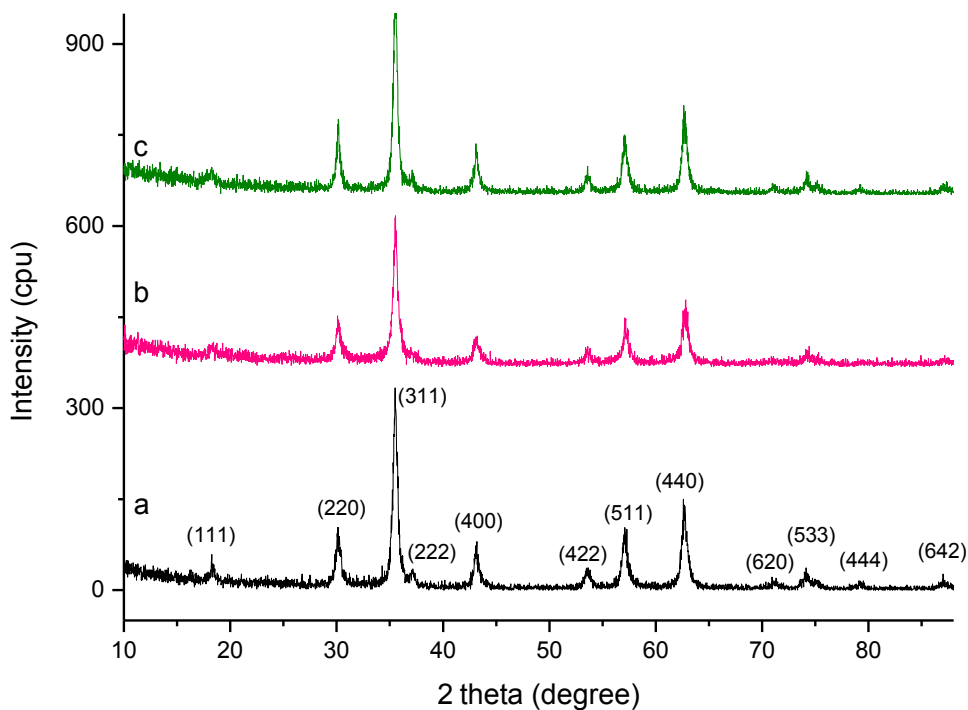


Figure 3.10 XRD patterns of a) NMNP₃, b) OA-MNP₂ and c) PEG-MNP₂

In Figure 3.10, XRD patterns of PEG-MNP₂ and OA-MNP₂ were compared to N-MNP₃. Major diffraction peaks with corresponding plane indexes (220), (311), (400), (422), (511), (440) and minor peaks with (111), (620), (533), (642), (731) plane indexes of core magnetite were also observed in PEG-MNP₂ and OA-MNP₂ samples which identify that those samples kept their cubic spinel structure after the coating process.

3.1.3 Fourier Transform Infrared (FTIR) Spectroscopy

Naked MNP, oleic acid coated MNP, PEG coated MNP and folic acid functionalized MNP were characterized with FTIR spectroscopy.

3.1.3.1 FTIR Analysis of Naked MNP

FTIR spectrum of N-MNP₃ is given in Figure 3.11. The band with the wavelength 580 cm^{-1} belongs to vibrations of the Fe-O bond of magnetite (Yan 2009). This result is in agreement with XRD pattern of N-MNP₃ (Figure 3.9) which indicates that synthesized N-MNP₃ sample nanoparticles were magnetite.

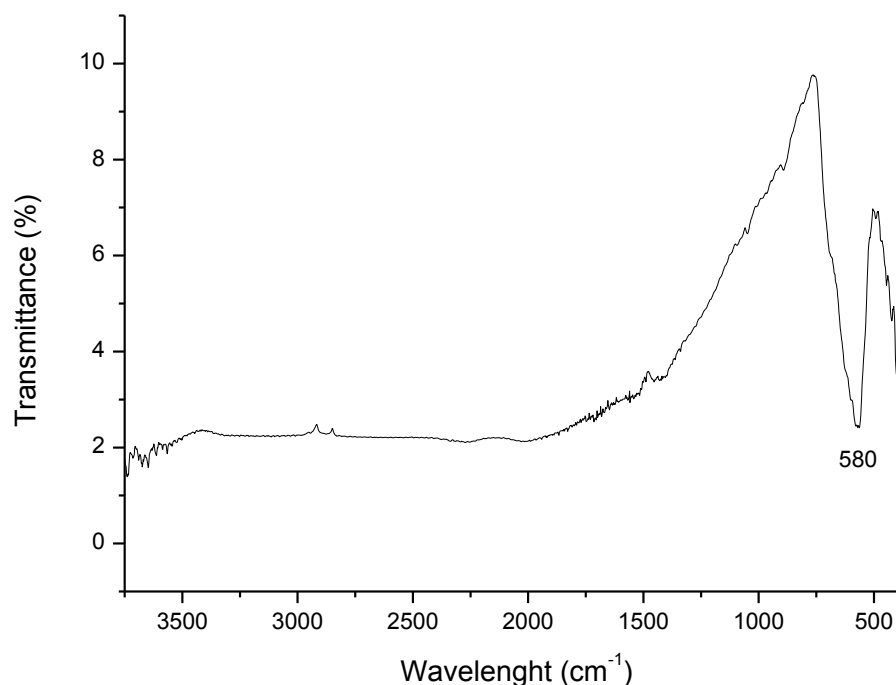


Figure 3.11 FTIR spectrum of N-MNP₃

3.1.3.2 FTIR Analysis of Oleic Acid Coated MNP

FTIR spectra of pure oleic acid and OA-MNP₁ sample are given together in Figure 3.12. As explained earlier, OA-MNP₁ sample was prepared by addition of oleic acid after synthesis step (Section 2.2.2). Before FTIR characterization, nanoparticles were first washed with ethanol. Pure oleic acid gave strong peaks at 2924 cm⁻¹ and 2854 cm⁻¹ belonging to asymmetric and symmetric CH₂ stretch, respectively. Peak at 3005 cm⁻¹ was attributed to C-H bond in C=C-H. Vibration of C=O stretch of carboxyl group exhibited an intense band at 1710 cm⁻¹. Peaks at 1462 cm⁻¹ and 937 cm⁻¹ were derived from the O-H in-plane

and out-of-plane stretch, respectively. The peak appeared at 1285 cm^{-1} exhibited the presence of the C-O stretch (Albuquerque *et al.* 2003, Wu *et al.* 2004 and Zhang *et al.* 2006).

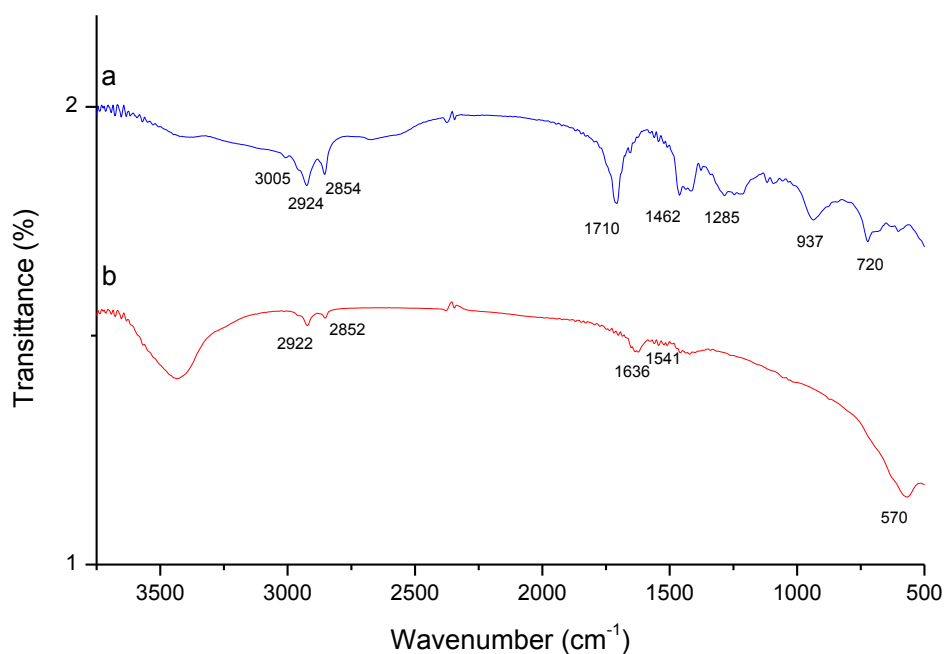


Figure 3.12 FTIR spectra of a) pure oleic acid and b) OA-MNP₁

OA-MNP₁ sample exhibited broad band around 3500 cm^{-1} corresponding to surface -OH groups. Asymmetric and symmetric CH_2 stretching bands at 2924 cm^{-1} and 2854 cm^{-1} of pure oleic acid, shifted to 2922 cm^{-1} and 2852 cm^{-1} in OA-MNP₁ sample (Figure 3.12-b). A similar shift was reported in the literature (Lan *et al.* 2007 and Yan *et al.* 2009). This shift was attributed to adsorption of oleic acid onto surface of magnetite nanoparticles. When surfactant is attached to a surface, it is exposed to the field of solid surface

which leads to shifting of bands (Wu *et al.* 2004, Zhang *et al.* 2006). In the same manner, while pure oleic acid had a strong peak at 1710 cm^{-1} derived from C=O stretch of carboxyl group, OA-MNP¹ sample exhibited band of symmetric and asymmetric vibration of COO⁻ stretch at 1636 cm^{-1} and 1541 cm^{-1} , respectively. The reason of this shift was due to the interaction state of oleic acid with solid surface. When oleic acid is chemisorbed onto a surface as carboxylate, COO⁻ gives C=O stretching peak around 1639 cm^{-1} (Zhang *et al.* 2006, Lan *et al.* 2007). Those shifts of bands in the FTIR spectrum revealed that oleic acid was chemisorbed on to magnetic nanoparticles and formed a monolayer corona around the MNP (Figure 3.14). Any bands regarding physisorbed OA layer was not observed on FTIR spectrum of OA-MNP₁ sample. Since sample was washed with ethanol before FTIR characterization, excess oleic acid which could form second layer by making hydrophobic interactions with chemisorbed layer on surface of MNP was probably prevented. Intense band of Fe-O stretching was seen at 570 cm^{-1} .

Oleic acid coating of OA-MNP₂ sample was performed by addition of oleic acid during synthesis step. This sample gave better size distribution and nanoparticle morphology comparing to OA-MNP₁ sample (Figure 3.2-3.3). The agglomeration of nanoparticles was also prevented in this sample. Figure 3.13 shows FTIR spectrum of OA-MNP₂ samples which were washed either with dH₂O or ethanol before FTIR characterization. OA-MNP₂ samples washing with dH₂O or ethanol were labeled as OA-MNP₂^W and OA-MNP₂^E, respectively.

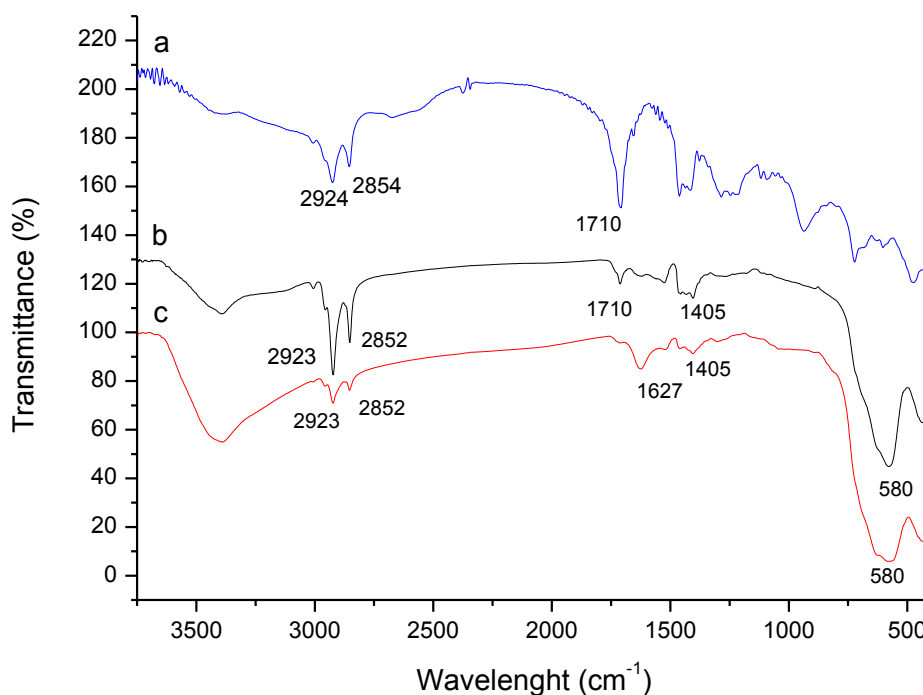


Figure 3.13 FTIR spectra of a) pure oleic acid, b) OA-MNP₂^W and c) OA-MNP₂^E (OA-MNP₂^W: oleic acid coated MNP washed with dH₂O, OA-MNP₂^E: oleic acid coated MNP washed with ethanol).

Broad band around 3250-3500 cm⁻¹ corresponding to surface -OH groups was seen in FTIR spectra of both OA-MNP₂^W and OA-MNP₂^E (Wu *et al.* 2004). Intense peaks of CH₂ at 2923 cm⁻¹ and 2852 cm⁻¹ were attributed to asymmetric and symmetric C-H vibrating, respectively. Both OA-MNP₂^W and OA-MNP₂^E exhibited those peaks indicating presence of oleic acid (Figure 3.13). C-H bending of CH₂ gave a peak at 1405 cm⁻¹ (Lan *et al.* 2007). Fe-O stretching of Fe₃O₄ exhibited a strong peak at 580 cm⁻¹ in both samples. C=O stretching of COOH of oleic acid layer gave a intense band at 1710 cm⁻¹ in the FTIR spectrum of OA-MNP₂^W, while this peak shift left to 1627 cm⁻¹ in the

FTIR spectrum of OA-MNP₂^E. A slight peak at 1627 cm⁻¹ was also seen in the curve of OA-MNP₂^W. Strong peak of C=O stretching at 1627 cm⁻¹ revealed that carboxyl group was in the form of carboxylate which indicating that oleic acid was chemisorbed on MNP surface. Since OA-MNP₂^W sample was washed with only dH₂O, excess of oleic acid remained and formed physically absorbed oleic acid layer on the surfaces of nanoparticles. This physical layer and chemisorbed layer of oleic acid were in hydrophobic interaction and formed a bilayer on MNP. Intense peak at 1710 cm⁻¹ in the FTIR spectrum of OA-MNP₂^W was derived from the C=O stretching of carboxyl group of physically absorbed oleic acid layer. Since oleic acid is soluble in ethanol, excess oleic acid was washed with ethanol, and probably did not form a secondary layer on OA-MNP₂^E nanoparticles. Hence, a peak at 1710 cm⁻¹ was not observed in the FTIR curve of OA-MNP₂^E. A similar situation was reported by Yan *et al.* (Yan 2009) and Liu *et al.* (2006).

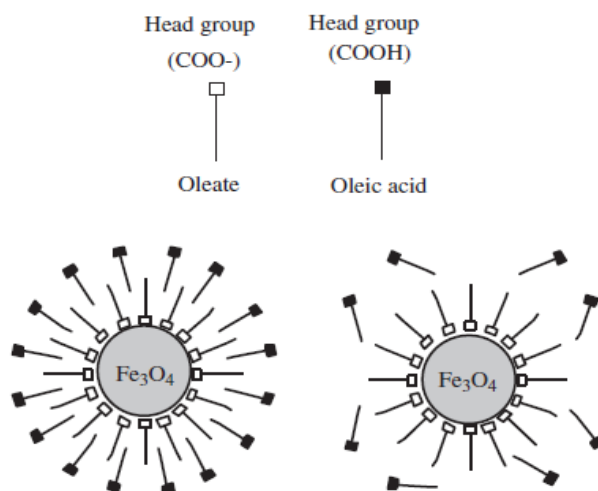


Figure 3.14 Schematic representation of a) bilayer Oleic acid coated Fe₃O₄ and b) monolayer Oleic acid coated Fe₃O₄ (Liu *et al.* 2006)

3.1.3.3 FTIR Analysis of PEG coated MNP

In this study, PEG was used as coating material. The type of used PEG was polyethylene glycol monooleate. It includes oleic acid which conjugates through its carboxylate to PEG. ATR spectra of pure oleic acid and PEG monooleate was given in Appendix A.

FTIR spectra of Polyethylene glycol monooleate, PEG-MNP₁, PEG-MNP₂ and PEG-MNP₃ are displayed in Figure 3.15. Adsorption spectra of PEG coated samples exhibited a similar pattern with spectrum of Polyethylene glycol monooleate. Characteristic vibrations of Fe-O bands of Fe₃O₄ were seen at 578 cm⁻¹. Broad peak around 3500-3250 cm⁻¹ were due to -OH groups (Yallapu *et al.* 2010). Strong bands appeared at 2923 and 2852 cm⁻¹ were due to -CH₂ asymmetric/ symmetric stretching while broad band at 1465 cm⁻¹ belonged to bending vibrations of -CH₂. At 1735 cm⁻¹ stretching vibration of the C=O was observed (Xiong *et al.* 2006). Symmetric stretching of C-O-C at 1109 cm⁻¹ indicating the presence of PEG was seen clearly in the FTIR spectra of PEG-MNP₂ and PEG-MNP₃ while a mild peak was observed in the FTIR spectra PEG-MNP₁. However, peak at 945 cm⁻¹ derived from out of plane bending vibrations of the C-H of PEG was observed only in the adsorption spectra of PEG-MNP₂ and PEG-MNP₃ (Li *et al.* 2008, Zhang *et al.* 2008).

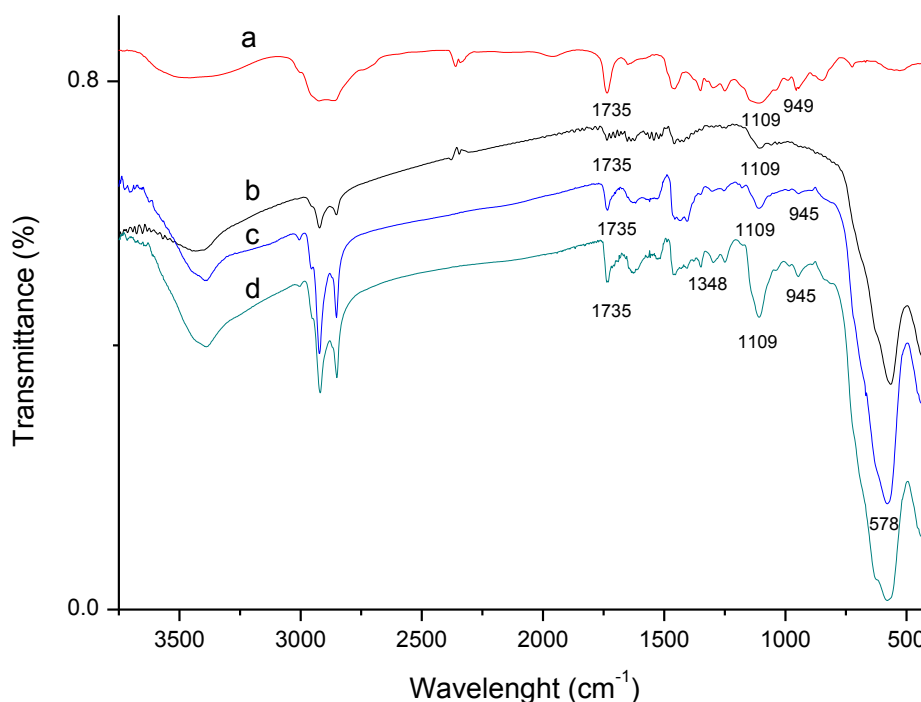


Figure 3.15 FTIR spectra of a) Polyethylene glycol monooleate, b) PEG-MNP₁, c) PEG-MNP₂ and d) PEG-MNP₃

Peak of symmetric stretching vibration of C-O-C at 1109 cm⁻¹ became a very sharp in the spectrum of PEG-MNP₃ (In Figure 3.15-d). Out of plane bending vibration of C-H of PEG at 944 cm⁻¹ was also more intense. More importantly additional peak at 1348 cm⁻¹ derived from asymmetric stretching of C-O-C of PEG was observed.

PEG-MNP₂ nanoparticles were synthesized by *in situ* addition of both oleic acid and PEG during synthesis. There was not any washing step of oleic acid before PEG addition. When oleic acid coated nanoparticles were prepared by *in*

situ oleic acid addition and washed after coating step, there was a second oleic acid layer on nanoparticles. This layer was due to the excess of oleic acid and could be prevented by washing of nanoparticles with ethanol (Figure 3.13). PEG-MNP₃ were coated with PEG after purifying of oleic acid coated MNP which were synthesized by *in situ* addition of oleic acid. Since oleic acid coated nanoparticles lost their second layer by ethanol washing step, there may not be any excess oleic acid competing with polyethylene glycol monooleate to interact with chemisorbed oleic acid layer of PEG-MNP₃. Hence, more polyethylene glycol monooleate could be attached to the surface in this case. This could explain stronger peaks at 1109 and 944 cm⁻¹ and the extra peak at 1348 cm⁻¹.

3.1.3.4 FTIR Analysis of Folic Acid Functionalized MNP

Pure folic acid and folic acid functionalized MNP were analyzed by FTIR. In Appendix A, FTIR spectrum of pure folic acid was given.

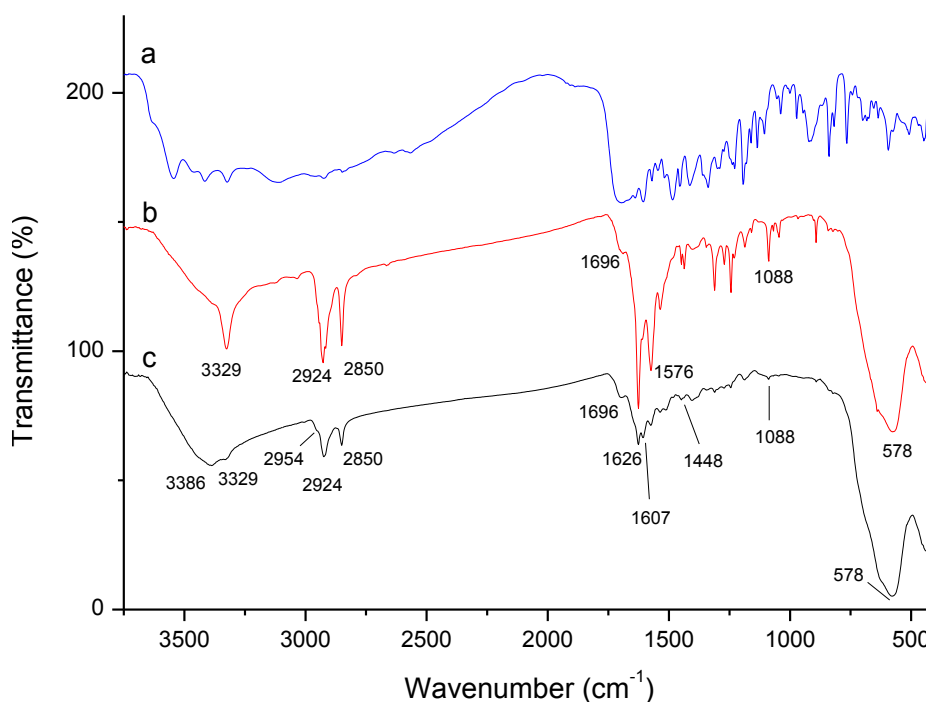


Figure 3.16 FTIR Spectra of a) pure folic acid and b) FA-MNP₁ and c) FA-MNP₂

Figure 3.16 shows FTIR spectra of pure folic acid, FA-MNP₁ and FA-MNP₂. Both, FA-MNP₁ and FA-MNP₂ samples revealed parallel peak patterns with pure folic acid. Vibration of NH stretching at 3329 cm⁻¹ was seen in curve of both FA-MNP₁ and FA-MNP₂, indicating presence of folic acid. The peak seen at 3386 cm⁻¹ was due to the terminal OH group in PEG (Li *et al.* 2008). Asymmetric and symmetric C-H stretching of CH₂ group, seen at 2954, 2924 and 2850 cm⁻¹ in both samples were corresponded to oleic acid and PEG. The band at 1696 cm⁻¹ was derived from C=O stretching of -COOH of folic acid and PEG. The intense peak at 1627 cm⁻¹ was characteristic band of folic acid, shifted from 1639 cm⁻¹, corresponding to vibration of C=O of -CONH₂ which

identify the presence of folic acid. Peak at 1607 and 1448 cm^{-1} were corresponded to NH_2 bending vibration and phenyl ring of folic acid. Peak at 1088 cm^{-1} indicated C-O-C ether stretching of PEG, while vibration band at 578 was derived from Fe-O stretching of Fe_3O_4 (Zhang *et al.* 2008, Mohapatra *et al.* 2007).

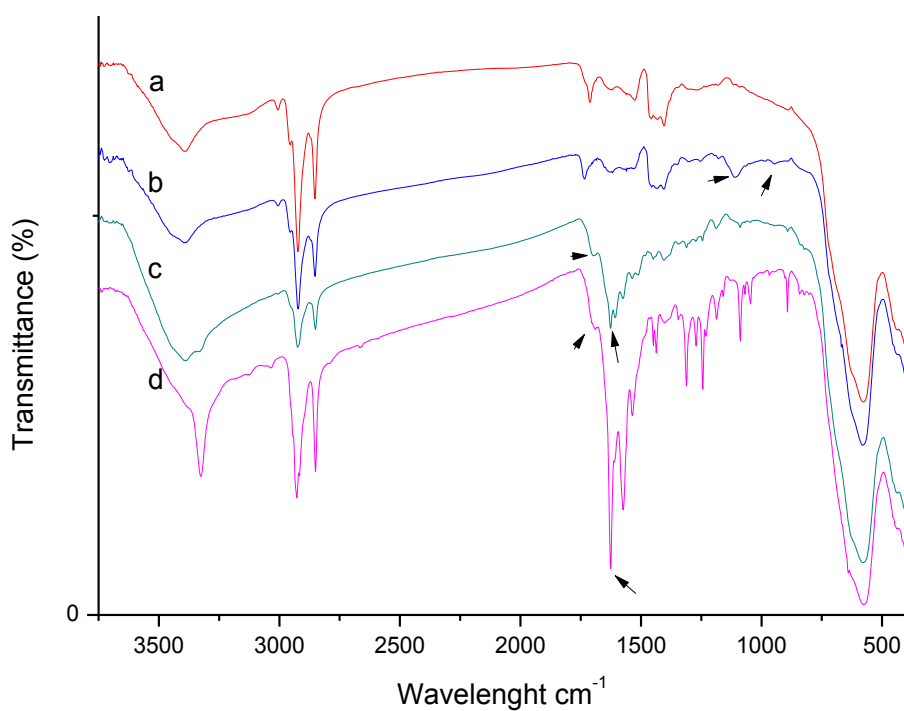


Figure 3.17 FTIR Spectra of a) OA-MNP₂, b) PEG-MNP₂ c) FA-MNP₁ and d) FA-MNP₂

In Figure 3.17 different and similar peaks OA-MNP₂, PEG-MNP₂, FA-MNP₁ and FA-MNP₂ are seen. All four curves revealed the characteristic peaks of

oleic acid around 2924 cm^{-1} , 2854 cm^{-1} and 3005 cm^{-1} belonging to asymmetric, symmetric CH_2 stretching and C-H stretching bond in C=C-H. Additionally, Fe-O stretching of Fe_3O_4 was observed around 580 cm^{-1} in the curves of all samples. Important different peaks indicating the presence of PEG or folic acid were indicated with arrow. Compared to OA-MNP₂, additional peaks around 1109 and 945 cm^{-1} were observed in the curve of PEG-MNP₂, FA-MNP₁ and FA-MNP₂ attributed to C-O-C stretching and bending of C-H of polyethylene glycol. In the adsorption spectra of FA-MNP₁ and FA-MNP₂, new peaks at 1696 cm^{-1} and 1627 cm^{-1} were derived from mainly folic acid.

3.1.4 Thermogravimetric Analysis (TGA)

Uncoated MNP, oleic acid coated MNP and PEG coated MNP were analyzed thermogravimetrically in order to find the amount of oleic acid or PEG polymer on the magnetite nanoparticles.

Figure 3.18 shows TGA curves of N-MNP₃, OA-MNP₂^W, OA-MNP₂^E, PEG-MNP₂ and PEG-MNP₃. When TGA curve of N-MNP₃ was examined, up to 130°C there was a 2% weight loss which was derived from desorption of water molecules from surface of magnetic nanoparticles. OA-MNP₂^W sample revealed two step weight loss; one was between 200 and 300°C attributed to loss of physically absorbed oleic acid layer on nanoparticles. Second one was between 330 and 500°C attributed to chemisorbed oleic acid layer on nanoparticles. Since OA-MNP₂^W sample was with dH_2O before analysis,

second layer of oleic acid was probably not removed. The two step mass loss of OA-MNP₂^W indicating bilayer oleic acid layer confirmed FTIR result of OA-MNP₂^W further (Figure 3.13). Total weight loss was 13% indicating that 13% of OA-MNP₂^W nanoparticles were oleic acid by weight.

OA-MNP₂^E were washed with ethanol before TGA analysis. One step mass loss between 330 and 500 °C was observed in TGA curve of OA-MNP₂^E, indicating presence of only chemisorbed oleic acid layer. Since oleic acid was removed by ethanol, a second mass loss step was not observed. This result was in agreement with FTIR spectra of OA-MNP₂^E (Figure 3.13-c). Total weight loss was 9%. This result revealed that 9% of OA-MNP₂^E nanoparticles were corresponding to chemisorbed oleic acid layer on nanoparticles by weight. Two step and one step mass loss TGA results were also reported in literature (Lan *et al.* 2007, Yan *et al.* 2009).

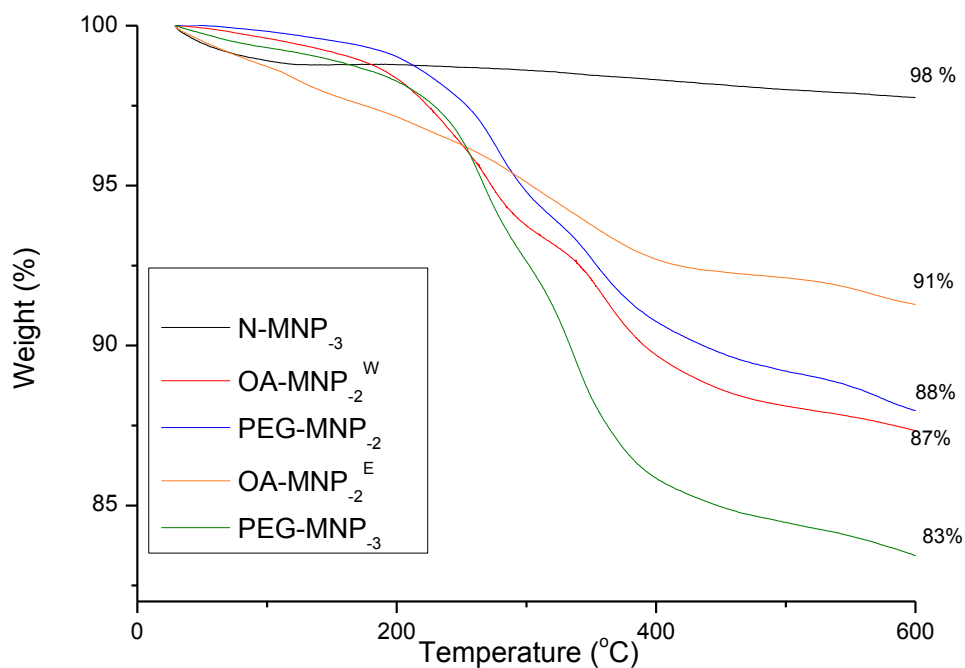


Figure 3.18 TGA curves of N-MNP₋₃, OA-MNP₋₂^W, OA-MNP₋₂^E, PEG-MNP₋₂ and PEG-MNP.

While weight loss of OA-MNP₋₂^W was 13%, it was 12% for PEG-MNP₋₂ nanoparticles (Figure 3.18). This 12% weight loss was both due to oleic acid and PEG cover. Since during PEG-MNP₋₂ synthesis, PEG polymer was added into system without any oleic acid washing step, oleic acid molecules and PEG were competing with each other to be absorbed on MNP. Hence, there was not a big weight loss difference between OA-MNP₋₂^W and for PEG-MNP₋₂ nanoparticles.

On the other hand, PEG-MNP₃ nanoparticles revealed 17% weight loss while it was 9% for OA-MNP₂^E nanoparticles. Excess oleic acid was removed by ethanol washing before PEG addition for PEG-MNP₃ sample. Hence, most probably there was not physically absorbed oleic acid competing with PEG polymer which led to an enhanced degree of PEG coverage. Here it could be argued that, since 9% of OA-MNP₂^E nanoparticles were only oleic acid by weight, 8% (17-9 = 8) of PEG-MNP₃ nanoparticles were only PEG by weight. In the literature, Yallapu *et al.* found weight % of PEG on MNP around 4.56 % using the same procedure without washing step (Yallapu *et al.* 2010). It is important to notice that washing step is central for increasing the amount of absorbed PEG polymer on oleic acid coated nanoparticles.

3.1.5 Vibrating Sample Magnetometer (VSM)

Magnetization characteristics of naked, oleic acid coated, PEG coated and folic acid functionalized MNP were analyzed by VSM at room temperature (23 °C). Additionally, since cell culture experiments were carried out at body temperature, VSM analyses were also performed at 37 °C for all samples.

Hysteresis loops of N-MNP₃, OA-MNP₂, PEG-MNP₂, FA-MNP₁ and FA-MNP₂ samples are given in Appendix B separately with their corresponding Ms (saturation magnetization), Mr (remanent magnetization) and Hc (coercivity) values.

3.1.5.1 VSM Analysis at 23 °C

In Figure 3.19, comparative magnetization curves of N-MNP₃, OA-MNP₂, PEG-MNP₂, FA-MNP₁ and FA-MNP₂ at 23 °C are given.

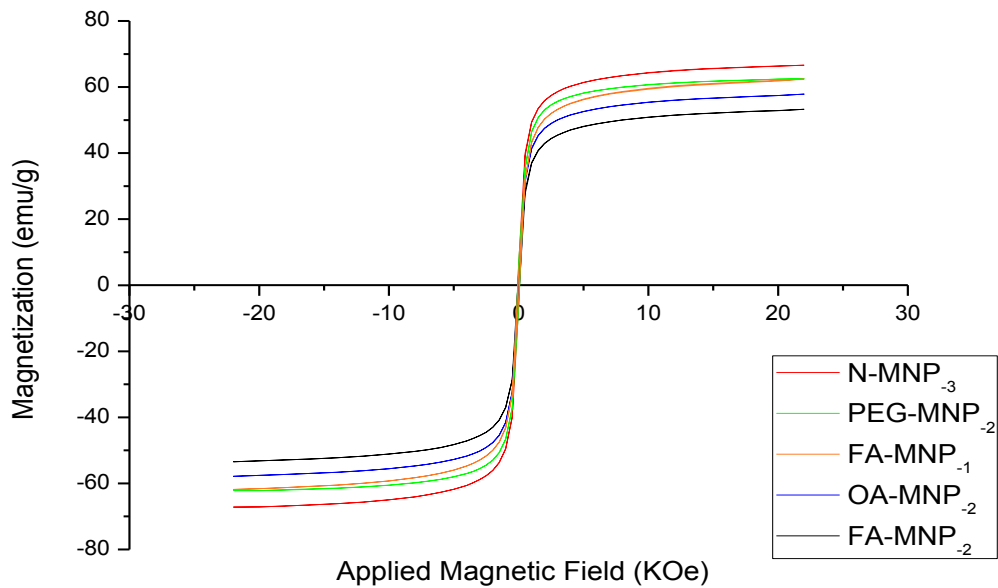


Figure 3.19 Hysteresis loops of N-MNP₃, OA-MNP₂, PEG-MNP₂, FA-MNP₁ and FA-MNP₂ at 23 °C.

Magnetization curves of N-MNP₃, OA-MNP₂, PEG-MNP₂, FA-MNP₁ and FA-MNP₂ nanoparticles exhibited very similar curves. They had negligible coercivity and remanent magnetization with high saturation magnetization

values at 23 °C (Appendix B). It could be stated that they exhibited magnetic characteristics similar to superparamagnetism. Compared to N-MNP₃, a general decrease in saturation magnetization values of OA-MNP₂, PEG-MNP₂, FA-MNP₁ and FA-MNP₂ nanoparticles have been observed. This drop was attributed to diamagnetic coating materials on the surface of nanoparticles (Mohapatra *et al.* 2007, Gang *et al.* 2007, Arias *et al.* 2008, Gupta 2005).

When Ms values of N-MNP₃ and OA-MNP₂ were compared, for both temperatures a decrease in Ms values of OA-Fe₃O₄* was observed. Oleic acid is a diamagnetic material. Thus, it decreases the Ms value of N-MNP₃ from 66.89 (emu/g) to 57.87 (emu/g) at 23°C. A drop of 13.5% in Ms was recorded. Additionally, according to TGA results 13% of the analyzed sample was oleic acid by weight (Figure 3.17). VSM and TGA results are consistent. The same phenomenon was recorded in the literature. Liu *et al.* found the Ms values of 58 (emu/g) and 46 (emu/g) for the bare magnetite and oleic acid coated magnetite nanoparticles at room temperature, respectively. They calculated oleic acid layer mass percentage from this data as 20%.

3.1.5.2 VSM Analysis at 37 °C

Magnetization behaviors of N-MNP₃, OA-MNP₂, PEG-MNP₂, FA- MNP₁ and FA- MNP₂ samples were also examined at 37 °C.

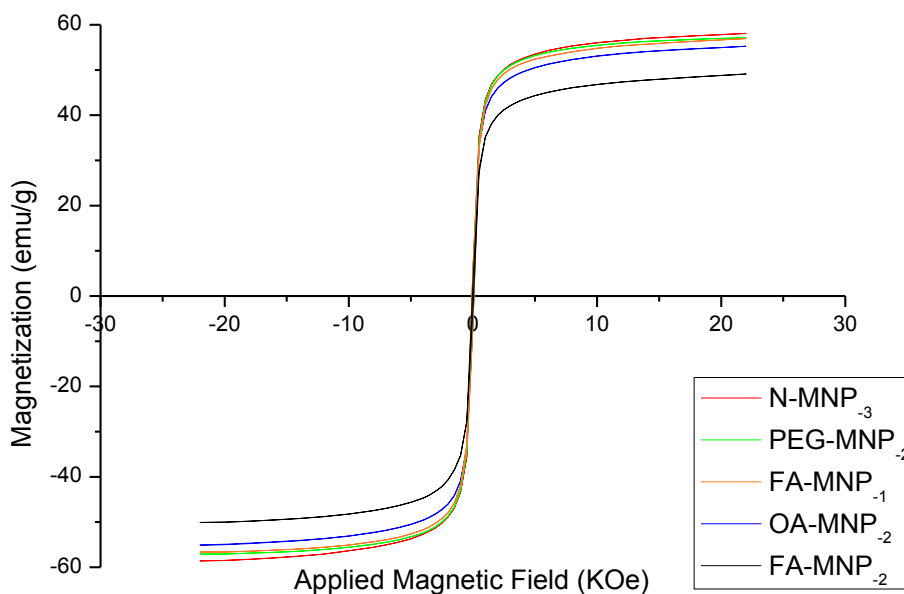


Figure 3.20 Hysteresis loops of N-MNP₋₃, OA-MNP₋₂, PEG-MNP₋₂, FA-MNP₋₁ and FA- MNP₋₂ at 37 °C.

Figure 3.20 demonstrates magnetization curves of N-MNP₋₃, OA-MNP₋₂, PEG-MNP₋₂, FA- MNP₋₁ and FA- MNP₋₂ at 37 °C comparatively. A general decrease in M_s values was observed. They exhibited negligible coercivity and remanent magnetization. It could be concluded that at 37°C, N-MNP₋₃, OA-MNP₋₂, PEG-MNP₋₂, FA- MNP₋₁ and FA- MNP₋₂ retains their superparamagnetic characteristic.

Superparamagnetic materials do not show any coercivity in magnetization curve. Besides, their magnetization versus applied magnetic field graphs at different temperatures show similar pattern (Varadan *et al.* 2008, pg: 48). To illustrate, N-MNP₋₃ nanoparticles exhibited very similar magnetization curves

at 23 °C and 37 °C with the M_s values of 66.89 and 59.34 (emu/g), respectively (Appendix B). The slight decrease in M_s by increasing temperature was also stated in the literature. Bean and Jacops (1956) studied magnetization of iron nanoparticles which had similar pattern of superparamagnetic magnetization curves at 77 K and 200 K with slightly lower magnetization value at 200K. This drop of M_s value is explained by the Langevin theory stating that while magnetization is proportional to applied field, it decreases by elevated temperatures (Spaldin 2003, pg: 51, 52,150). Additionally, 66.89 (emu/g) M_s value of N-MNP₃ agrees with previous studies. Hai *et al.* found saturation magnetization of 60 (emu/g) for uncoated Fe₃O₄ nanoparticles which were synthesized by co-precipitation method (Hai *et al.* 2009). Similar to N-MNP₃, each of the samples: namely; OA-MNP₂, PEG-MNP₂, FA-MNP₁ and FA-MNP₂ exhibited similar magnetization curves at 23 °C and 37 °C (Appendix B).

3.2.1 Cytotoxicity Studies of Magnetic Nanoparticles

Cytotoxicities of naked nanoparticles, oleic acid coated nanoparticles, PEG coated nanoparticles and folic acid conjugated nanoparticles were determined by using XTT assay kit. 10,000 MCF-7 cells/well were seeded to 96 well plates at 37°C. Cells that were exposed to MNP were incubated for 72 h at 37°C. Cell proliferation profiles were determined by considering control groups.

3.2.1.1 Cytotoxicity of Naked MNP

To understand biocompatibility of naked magnetite nanoparticles or whether they were toxic to MCF-7/S cells, XTT assay was performed. Figure 3.21 demonstrates cell proliferation profile of MCF-7/S cells which were incubated with different concentrations of N-MNP₃.

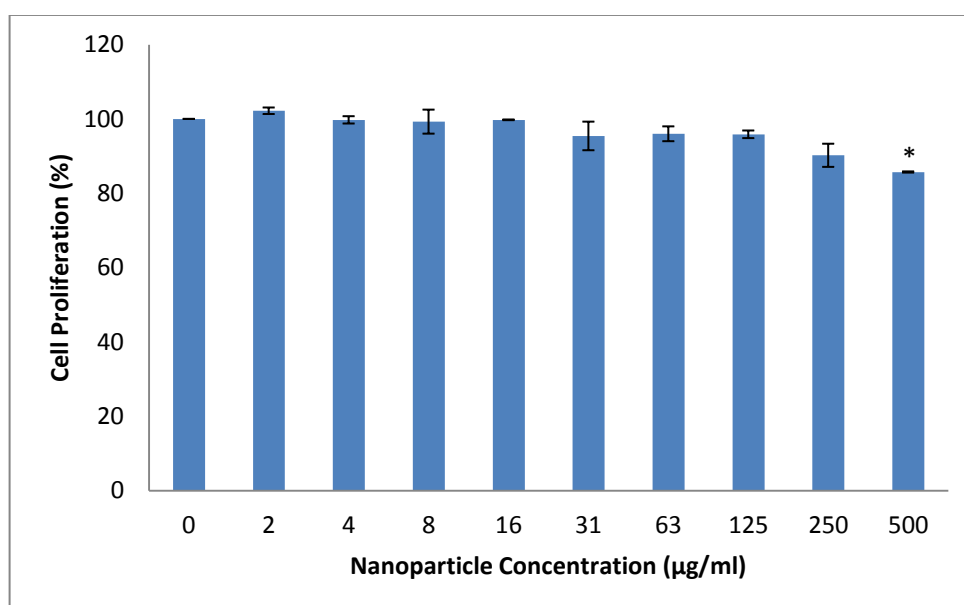


Figure 3.21 Cell proliferation profile of MCF-7/S cells treated with N-MNP₃ for 72 hr. * $p < 0.05$ compared to untreated cells exhibiting 100% proliferation. Results were given as Mean \pm SEM. All experiments were carried out in triplicates.

MCF-7 cells incubated with different concentrations of naked magnetic nanoparticles (0 - 500 µg/ml) did not exhibit a dramatic cell death. At 500

$\mu\text{g/ml}$, significant drop in cell proliferation was observed. Maximum cell death compared to untreated cells observed at $500 \mu\text{g/ml}$ was 15 %. It could be concluded that N-MNP₃ nanoparticles did not exhibit a significant toxic effect on MCF-7 cells after 72 hr incubation between the concentration range of 0 - $250 \mu\text{g/ml}$. Hence, they can be used and fabricated in further studies.

3.2.1.2 Cytotoxicity of Oleic Acid Coated MNP

Cytotoxicity of oleic acid coated OA-MNP₂ nanoparticles was determined with XTT assay. MCF-7/S breast cancer cells were incubated with OA-MNP₂ in the concentration range of 0 - $500 \mu\text{g/ml}$ for 72 hr at 37°C . Cell viability profile was given in Figure 3.22.

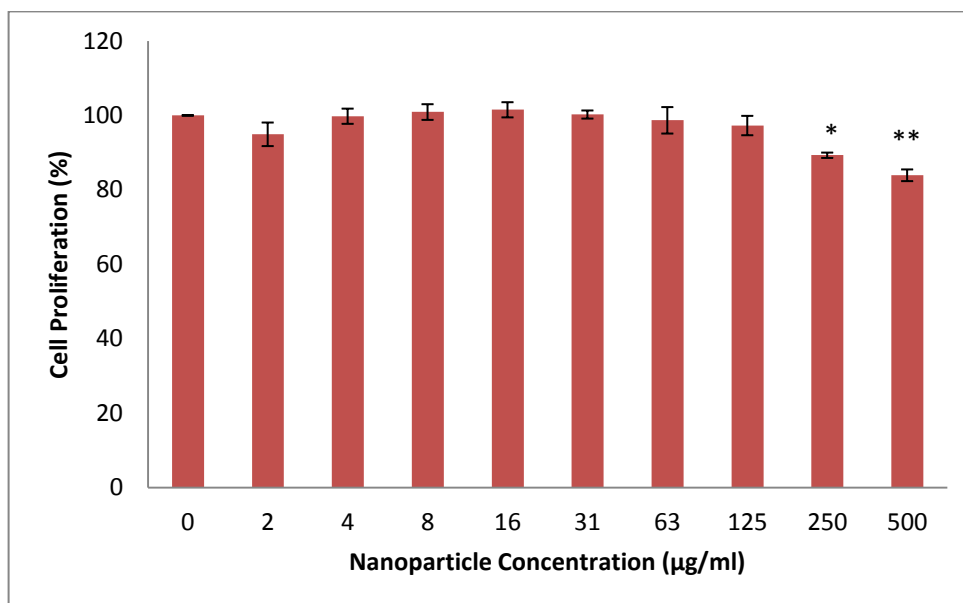


Figure 3.22 Cell proliferation profile of MCF-7/S breast cancer cells treated with OA-MNP₂ for 72 hr. *p<0.05 and **p< 0.01 relative to untreated cells exhibiting 100% proliferation. Results were given as Mean ± SEM. All experiments were carried out in triplicates.

OA-MNP₂ nanoparticles were found to be biocompatible and not toxic to MCF-7 cells in the concentration range of 0 - 125 µg/ml for 72 hr. A significant decrease in the cell proliferation relative to untreated cells was observed at the nanoparticle concentration of 250 and 500 µg/ml. Cell proliferation at 250 and 500 µg/ml was 89 and 84 %, respectively. OA-MNP₂ could be used for *in vitro* studies with the concentration of 0-125 µg/ml.

3.2.1.3 Cytotoxicity of PEG Coated MNP

PEG-MNP₂ nanoparticles have been studied to learn their toxicity profile on MCF-7/S breast cancer cells. Cells were exposed to nanoparticles for 72 hr at 37°C. Figure 3.23 shows MCF-7/S cell proliferation profile incubated with PEG-MNP₂ nanoparticles between 0 - 500 µg/ml.

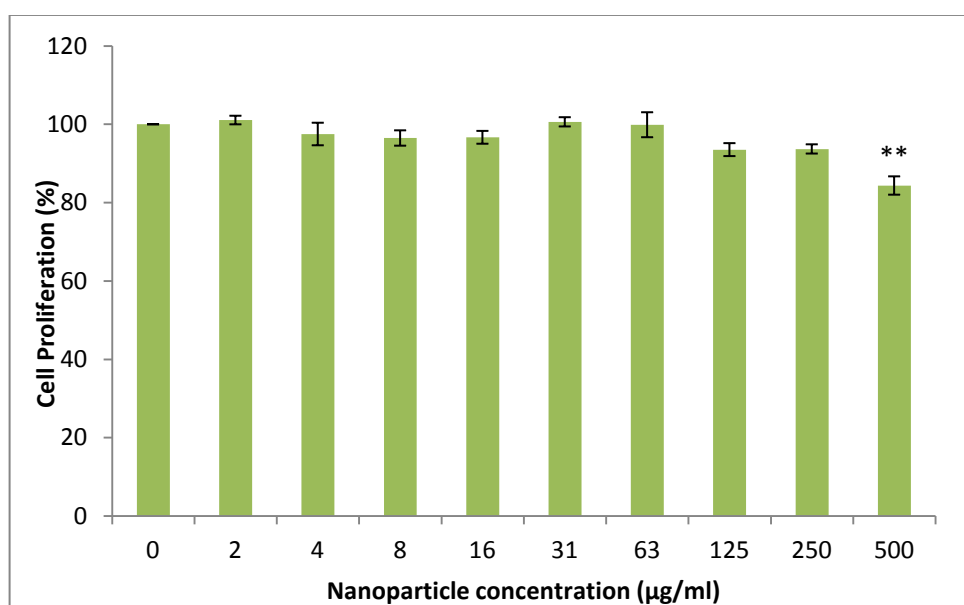


Figure 3.23 Cell proliferation profile of MCF-7/S breast cancer cells treated with PEG-MNP₂ for 72 hr. **p < 0.01 relative to nanoparticle untreated cells exhibiting 100% proliferation. Results were given as Mean ± SEM. All experiments were carried out in triplicates.

Toxicity profile of PEG-MNP₂ nanoparticles suggested that up to 500 µg/ml, significant cell toxicity was not observed. Cell proliferation of 84 % was

observed at 500 $\mu\text{g/ml}$. It could be concluded that PEG-MNP₂ revealed a very a toxicity on MCF-7 cells at 500 $\mu\text{g/ml}$ concentration compared to untreated control group.

3.2.1.4 Cytotoxicity of Folic Acid Functionalized MNP

Folic Acid functionalized FA-MNP₁ nanoparticles have been investigated on MCF-7/S breast cancer cells to determine whether they have toxic effects *in vitro*. Cell proliferation profile of MCF-7/S cells exposed to FA-MNP₁ nanoparticles in the concentration range of 500 $\mu\text{g/ml}$ was given in Figure 3.24.

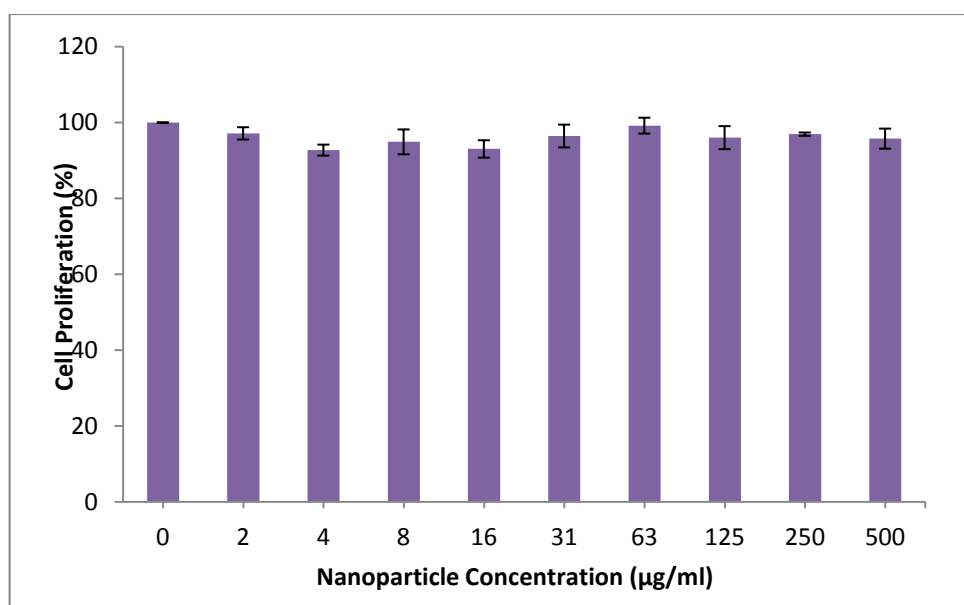


Figure 3.24 Cell proliferation profile of MCF-7/S cancer cells treated FA-MNP₁ for 72 hr. Results were given as Mean \pm SEM. All experiments were carried out in triplicates.

In the concentration range of 0 – 500 $\mu\text{g/ml}$, FA-MNP₁ nanoparticles did not have significant toxic influence on MCF-7/S cells compared to untreated cells. Folic acid is an important targeting agent, especially used in cancer chemotherapy studies. Hence, FA-MNP₁ nanoparticles could be used in further studies such as drug targeting and hyperthermia.

To understand how coating process of naked nanoparticles affect cell proliferation relative to naked nanoparticles, cell proliferation profiles of N-MNP₃, OA-MNP₂, PEG-MNP₂ and FA-MNP₁ were given comparatively in Figure 3.25. Control group of each concentration was the N-MNP₃ treated cells at this particular concentration.

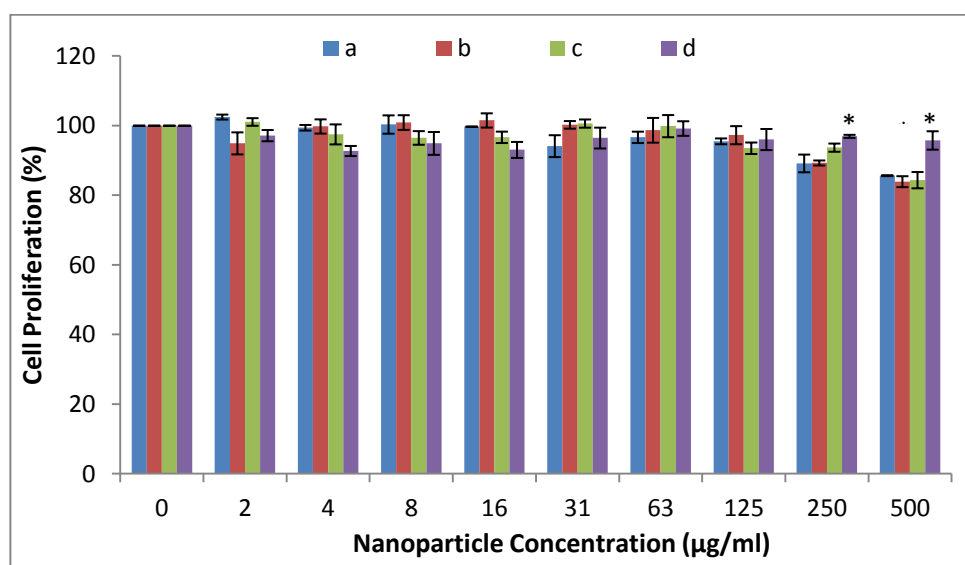


Figure 3.25 Cell proliferation profile of MCF-7/S breast cancer cells treated with a) N-MNP₃, b) OA-MNP₂, c) PEG-MNP₂ and d) FA-MNP₁ for 72 hr. * $p < 0.05$ compared to same concentration of N-MNP₃ nanoparticle treated cells. Results were given as Mean \pm SEM. All experiments were carried out in triplicates.

In Figure 3.25 it is observed that cells exposed to 250 and 500 $\mu\text{g/ml}$ FA-MNP₁ had significantly higher cell proliferation profiles compared to cells incubated with N-MNP₃ of 250 and 500 $\mu\text{g/ml}$. It could be concluded that at higher concentrations, folic acid conjugated nanoparticles influenced cell proliferation less compared to naked nanoparticles.

3.2.1.4.1 Cytotoxicity of Folic Acid Functionalized MNP on Drug Resistant Cells

FA-MNP₁ nanoparticles have been also studied to learn their toxicity profile on drug resistant MCF-7 breast cancer cell lines, namely; MCF-7/Dox (1000 nM Doxorubine resistant), MCF-7/Pac (400 nm Paclitaxel resistant) and MCF-7/Zol (8 μM Zoledronic Acid resistant). Figure 3.26, Figure 3.27 and Figure 3.28 demonstrates the cell proliferation profiles of MCF-7/Dox, MCF-7/Pac and MCF-7/Zol cells, respectively.

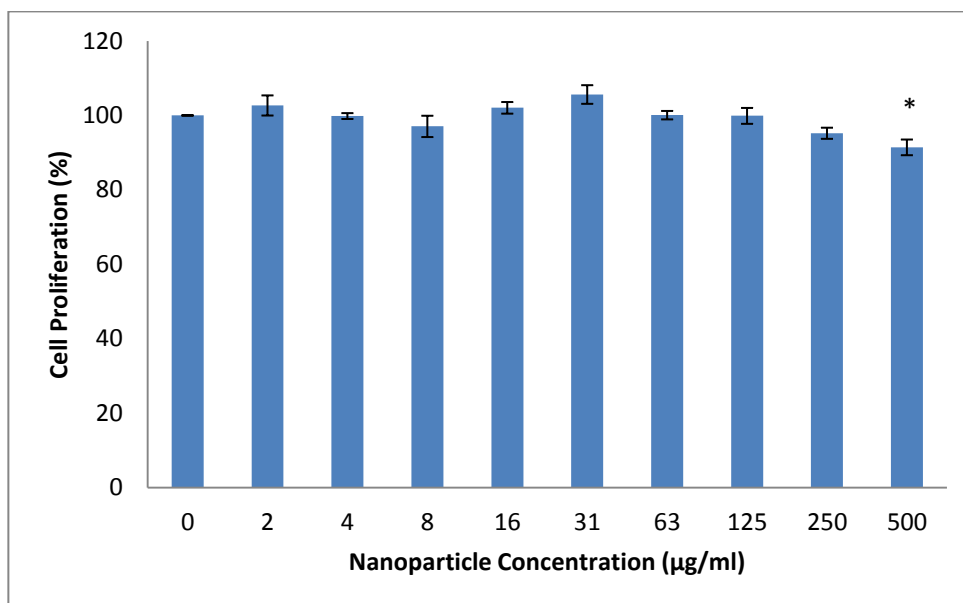


Figure 3.26 Cell proliferation profile of MCF-7/Dox cells treated with FA-MNP₁ for 72 hr at 37°C. *p<0.05 relative to nanoparticle untreated cells exhibiting 100% proliferation. Results were given as Mean ± SEM. All experiments were carried out in triplicates.

FA-MNP₁ nanoparticles were found to not to have severe toxic effects on MCF-7/Dox cells in the concentration range of 0 - 250 µg/ml. A significant decrease in the cell proliferation relative to untreated cells was observed at the nanoparticle concentration of 500 µg/ml. Cell proliferation at 500 µg/ml was 91 %.

Figure 3.27 illustrates cell proliferation profile of MCF-7/Pac cells treated with FA-MNP₁ for 72 hr at 37°C.

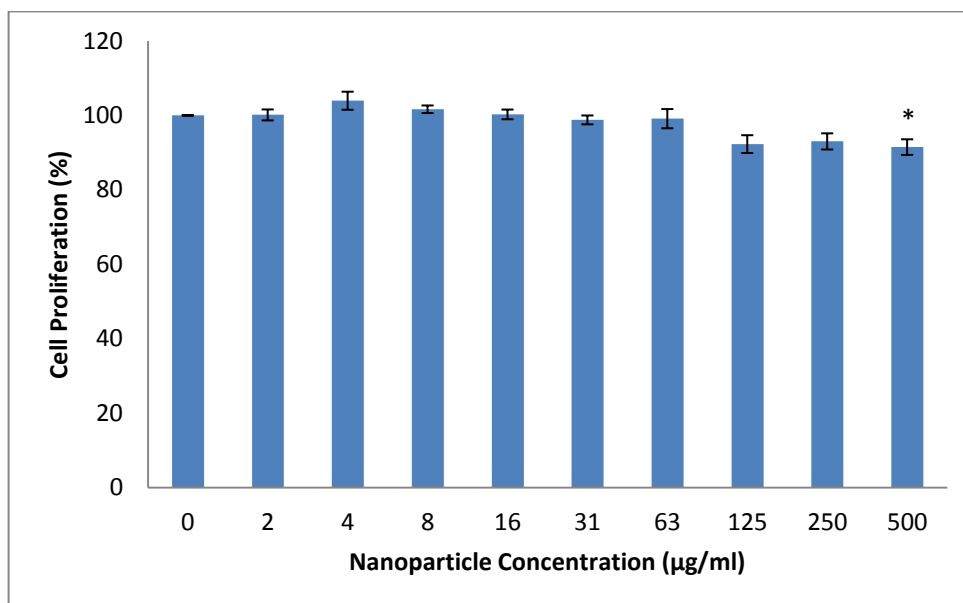


Figure 3.27 Cell proliferation profile of MCF-7/Pac cells treated with FA-MNP₁ for 72 hr at 37°C. *p< 0.05 relative to nanoparticle untreated cells exhibiting 100% proliferation. Results were given as Mean ± SEM. All experiments were carried out in triplicates.

MCF-7/Pac cells incubated with FA-MNP₁ did not exhibited a significant cell death in the concentration range of 0 – 250 µg/ml. Maximum cell death compared to untreated cells was observed at 500.00 µg/ml and found as 9 %. It could be concluded that FA-MNP₁ nanoparticles did not revealed a significant toxic effect on MCF-7/Pac cells after 72 hr incubation in the concentration range of 0 – 250 µg/ml.

Cell viability profiles of MCF-7/Zol cells are given in Figure 3.28. A significant decrease in the cell proliferation relative to untreated cells was

observed at the nanoparticle concentrations of 125, 250 and 500 $\mu\text{g/ml}$ with cell proliferation values of 88 %, 85 and 79 %, respectively.

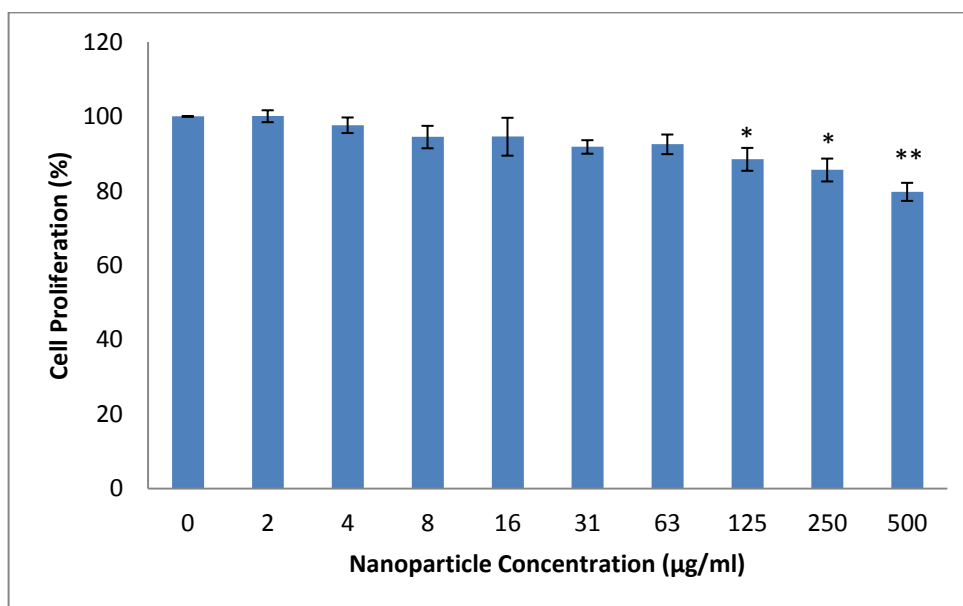


Figure 3.28 Cell proliferation profile of MCF-7/Zol treated with FA-MNP₁ for 72 hr at 37°C. * $p < 0.05$ and ** $p < 0.01$ relative to nanoparticle untreated cells exhibiting 100% proliferation. Results were given as Mean \pm SEM. All experiments were carried out in triplicates.

To investigate how different drug resistant cell lines response to treatment of FA-MNP₁ in the concentration range of 0- 500 $\mu\text{g/ml}$ for 72 hr, their cell proliferation profiles were compared to sensitive cells and given in Figure 3.29. Control group of each concentration was the FA-MNP₁ treated MCF-7/S cells at this particular concentration

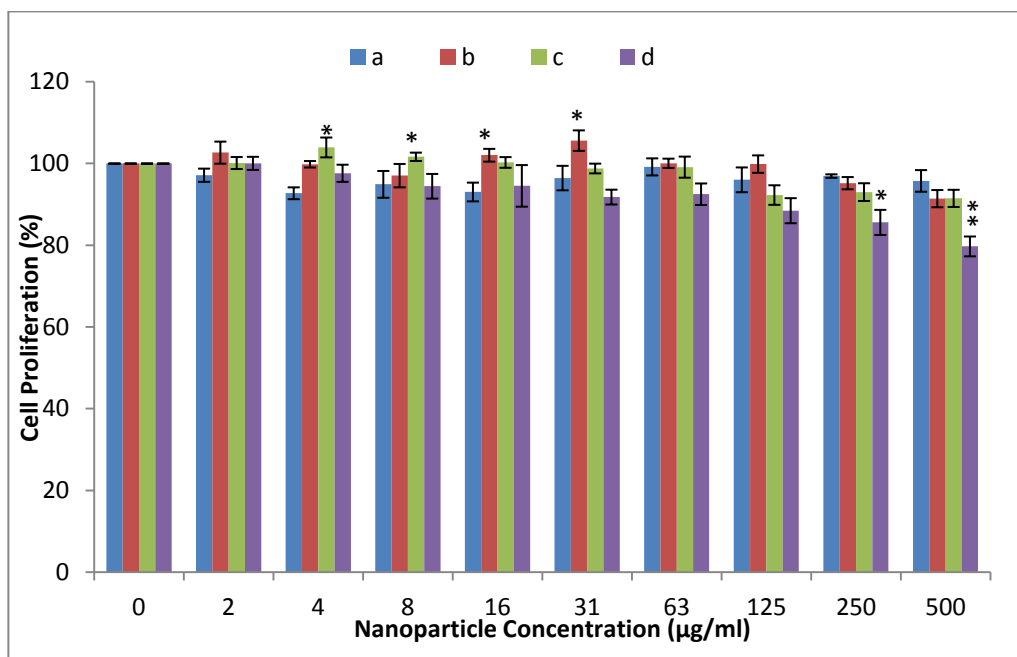


Figure 3.29 Cell proliferation profile of a)MCF-7/S, b)MCF-7/Dox, c)MCF-7/Pac and d)MCF-7/Zol breast cancer cells treated with FA-MNP₁ for 72 hr. *p<0.05 and **p< 0.01 compared to same concentration of Fe₃O₄ nanoparticle treated cells. Results were given as Mean \pm SEM. All experiments were carried out in triplicates.

In general, up to concentrations of 31 and 16 µg/ml, doxorubicin and paclitaxel resistant cell lines revealed significant increases in cell proliferation compared to same concentration treated sensitive cells. Increase in the cell proliferation was also reported in the literature (Gupta et al. 2004, Okassa *et al.* 2007, Ankamwar *et al.* 2007). The rise of cell proliferation in lower concentrations may arise from the absorption of the endocytosed MNP in cell. In the literature, the research of Li *et al.* (2011) indicated that folic acid receptor expression was upregulated in the taxol resistant nasopharyngeal carcinoma cells compared to sensitive nasopharyngeal carcinoma cells (Li *et al.* 2011). Similarly, Györfffy *et*

al. (2005) reported upregulation of folic acid receptor expression in doxorubicin resistant breast cancer tumor cells compared to sensitive ones. If there is an upregulated folic acid receptor expression in our resistant cell lines, this could lead to endocytosis of higher amounts of FA-MNP₁ leading to higher absorption values for resistant cell lines compared to sensitive cells. However, to confirm this, expressional analysis of folic acid receptor in resistant and sensitive cell lines should be performed and crosschecked with nanoparticle uptake studies. In the treatment of higher concentrations of FA-MNP₁, significant decreases in cell viability was observed. Increased levels of FA-MNP₁ endocytosis could prevent cell proliferation.

FA-MNP-1 nanoparticles did not exhibit severe toxicity neither on sensitive nor on resistant cell lines up to 125 µg/ml. Since folic acid conjugated nanoparticles are taken up into cell by folic acid mediated endocytosis, they are also successful in bypassing drug resistance derived from upregulation of efflux pumps like MDR1, MRP1 and BCRP (Peer *et al.* 2007). In previous researches, it was demonstrated that the MCF-7/Dox, MCF-7/Pac and MCF-7/Zol resistant cell lines used in this study overexpressed BCRP, MRP1 and MDR1, significantly (Kars 2007, Kars 2008, İşeri 2009). Thus, with the loading of an appropriate drug cargo, it can be used as possible drug delivery systems to resistant cell lines.

3.2.2 Light Microscopy Images

MCF-7/S cells treated with 500 $\mu\text{g/ml}$ of N-MNP₋₁, PEG-MNP₋₂ and FA-MNP₋₁ for 48 hr were examined under light microscopy. The images of observations were given in Figure 3.30.

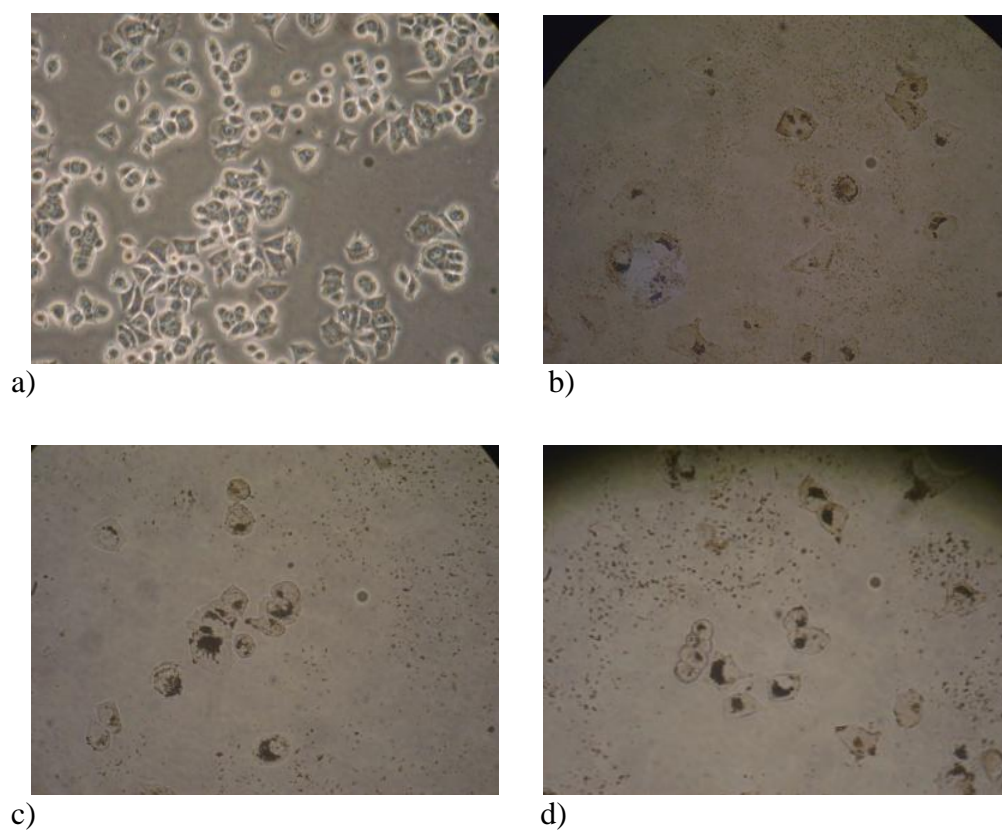


Figure 3.3030 Light microscopy images of a) untreated control MCF-7/S cells, and MCF-7/S cells treated with 500 $\mu\text{g/ml}$ of b) N-MNP₋₁, c) PEG-MNP₋₂ and d) FA-MNP₋₁ for 48 hr (400X magnification)

MCF-7/S cells exposed nanoparticles seems to tolerate incubation with particles (Figure 3.30). Compared with the control, MNP treated cells exhibited lesser proliferation. This observation was in agreement with XTT assay results (Figure 3.25). All the images were taken after PBS washing step. Thus, it can be argued that, MCF-7/S cells could take up both naked and coated nanoparticles. Figure 3.30 demonstrates that endocytosed MNP had a tendency to accumulate around nucleus inside the cell. Similar observations were reported in the literature (Zhang *et al.* 2002, Ankamwar *et al.* 2007).

CHAPTER 4

CONCLUSION

Magnetic nanoparticles, owing to their small scale size and magnetization ability are widely used in cancer treatment and imaging studies such as drug delivery, hyperthermia and MRI. In this study magnetic nanoparticles were synthesized, and they were functionalized with folic acid after being PEG covered. The detailed characterization analyses of nanoparticles revealed the potential of particles in further drug delivery researches.

- The sizes of synthesized nanoparticles seemed to be in the range of 10 – 60 nm which is appropriate for drug delivery applications.
- Among the naked nanoparticles, N-MNP₃ sample, synthesized by the rapid addition of ammonium hydroxide, exhibited more spherical nanoparticles with a narrower size distribution.
- Agglomeration tendency of naked nanoparticles was prevented by oleic acid covering to a certain degree.

- Among the oleic acid coated nanoparticles, OA-MNP₂ sample, which was synthesized by the addition of oleic acid during synthesis reaction, prevented agglomeration better than OA-MNP₁ sample, which was synthesized by the addition of oleic acid after synthesis.
- Addition of oleic acid into system during synthesis reaction produced oleic acid coated nanoparticles with better size distribution and morphology.
- Naked MNP, oleic acid coated MNP and PEG coated MNP samples were found to be magnetite with a cubic spinel structure.
- FTIR analysis of magnetic nanoparticles revealed the presence of oleic acid, PEG and folic acid.
- Depending on the type of the chemical (ethanol or dH₂O) used in washing step, monolayer or bilayer oleic acid covering on MNP was obtained.
- The weight ratio of PEG cover on MNP was enhanced 5% by washing step with ethanol.

- Naked, oleic acid coated, PEG coated and folic acid conjugated nanoparticles all exhibited magnetic properties similar to superparamagnetism both at 23°C and 37°C.
- Cytotoxicity studies of synthesized magnetic nanoparticles were performed on MCF-7 sensitive breast cancer cell line. In general, MNP did not have toxic effects on MCF-7/S in the concentration range of 0 – 250 µg/ml. Besides, toxic effects of folic acid conjugated MNP was studied on drug resistant cell lines, namely: MCF-7/Dox, MCF-7/Pac, MCF-7/Zol. Folic acid conjugated MNP did not exhibited toxic effects on drug resistant cell lines up to 125 µg/ml.
- *In vitro* examination of MCF-7/S cells by light microscopy demonstrated that both naked and coated MNP could be endocytosed by cells after 48hr incubation.

In this study, the synthesized magnetite nanoparticles were found to have appropriate size, surface chemistry, magnetization and biocompatibility properties to be used in further biomedical applications. Folic acid conjugated PEG covered magnetic nanoparticles were characterized in detailed. They have a potential to be used in biomedical studies such as drug delivery, hyperthermia and MRI. Since those particles have a hydrophobic layer covered with hydrophilic PEG corona, they have a proper design for delivery of lipophilic drugs. Besides, folic acid on MNP surface could help to receptor mediated endocytosis of nanoparticles and by this way drug resistance obstacle of convenient chemotherapy could be overcome. To illustrate receptor mediated endocytosis of nanoparticles, cells incubated with MNP can be imaged by

TEM. In the case of a fluorescent anticancer drug loading to MNP, drug accumulation in the cell can be examined by confocal microscopy. Moreover, cellular uptake assays could be performed to investigate whether PEG coating or folic acid conjugation enhance the uptake of nanoparticles by cell.

REFERENCES

Albuquerque MLS, Gluedes I, Alcantara P, Moreira SGC. 2003. Infrared absorption spectra of Buritti oil. *Vibrational Spectroscopy*. 33: 127-131.

Allen TM, Cullis PR. 2004. Drug delivery systems: Entering the mainstream. *Science*. 303 (5665): 1818-1822.

Alexis F, Pridgen E, Molnar LK, Farokhzad OC. 2008. Factors Affecting the Clearance and Biodistribution of Polymeric Nanoparticles. *Molecular Pharmaceutics*. 5 (4): 505–515

American Cancer Society. 2011-2012. *Breast Cancer Facts & Figures 2011-2012*. Atlanta: American Cancer Society; 2011.

American Cancer Society. 2012. Breast cancer, detailed guide. <<http://www.cancer.org/Cancer/BreastCancer/DetailedGuide/breast-cancer-pdf23>>. Last accessed date: 2012, January 3.

American Cancer Society. 2011. *Chemotherapy Principles: An Indepth discussion of the techniques and Its Role in Cancer Treatment*.

<<http://www.cancer.org/acs/groups/cid/documents/webcontent/002995-pdf.pdf>>. Last accessed date: 2012, January 3.

American Cancer Society. 2011. Breast Cancer; Targeted therapy. <<http://www.cancer.org/Cancer/BreastCancer/%20DetailedGuide/breast-cancer-treating-targeted-therapy>>. Last accessed date: 2012, January 3.

Ankamwar B, Lai TC, Huang JH, Hsia M, Chen CH, Hwu YK. 2007. Biocompatibility of Fe₃O₄ Nanoparticles Evaluated by in vitro Cytotoxicity Assays Using Normal, Glia and Breast Cancer Cells. *Nanotechnology*. 21 (7): 075102.

Arias JS, Ruiz A, Gallardo V, Delgado AV. 2007. Tegafur loading and release properties of magnetite / poly (alkylcyanoacrylate) (core/shell) nanoparticles. *Journal of controlled release* 125: 50- 58.

Arruebo M, Fernandez-Pacheco R, Ibarra MR, Santamaria J. 2007. Magnetic nanoparticles for drug delivery. *Nanotoday*. 2 (3): 22-32.

Bean JP, Jacops IS. 1956. Magnetic granulometry and super-paramagnetism. *Journal of Applied Physics* 27: 1448.

Biological Industries. 2002. Cell Proliferation Assay with XTT Reagent Protocol.

<<http://www.bioind.com/HTMLs/article.aspx?C2004=12557&BSP=12410>>.

Last accessed date: 2012, January 3.

Boyer C, Whittaker M, Bulmus V, Jingquan L, Davis T. 2010. The design and utility of polymer-stabilized iron oxide nanoparticles for nanomedicine applications. *NPG Asia Materials* 2 (1): 23-30.

Breastcancer.org. 2011. Hormonal Therapy.

<<http://www.breastcancer.org/treatment/hormonal/>>. Last accessed date: 2012, January 3.

Byrne JD, Betancourt T, Peppas LB. 2008. Active targeting schemes for nanoparticle systems in cancer therapeutics. *Advanced Drug Delivery Reviews* 60: 1615-1626.

Caruntu D, Caruntu G, Chen Y, O'Connor CJ, Goloverda G, Kolesnichenko VL. 2004. Synthesis of variable-size nanocrystals of Fe₃O₄ with high surface reactivity. *Chemistry of Materials*. 16: 5527-5534

Caruntu D, Caruntu G, O'Connor CJ. 2007. Magnetic Properties of variable-sized Fe₃O₄ Nanoparticles Synthesized from non-aqueous Homogenous Solutions of Polyols. *Journal of Physics*. 40: 5801-5809.

Chen TJ, Cheng TH, Hung YC, Lin KT, Liu GC. 2007. Targeted folic acid-PEG nanoparticles for noninvasive imaging of folate receptor by MRI. *Journal of Biomedical Materials Research PART A* 87 A (1): 165-175.

Cho K, Wang X, Nie S, Chen ZG, Shin DM. 2008. Therapeutic Nanoparticles for Drug Delivery in Cancer. *Clinical Cancer Researches*. 14 (5): 1310-1316.

Choi HS, Liu W, Misra P, Tanaka E, Zimmer JP, Ipe BI, Bawendi MG, Frangioni JV. 2007. Renal Clearance of Nanoparticles. *Nature Biotechnology*. 10: 1165-1170.

CMSE. Techniques . < <http://mit.edu/cmse/facilities/techniques.shtml> > Last accessed dated: 2012, January 3.

Demirel Kars M. 2008. Molecular Mechanisms of Vincristine and Paclitaxel Resistance in mcf-7 Cell Line. Ph.D. Thesis. Ankara: Middle East Technical University.

Demirel Kars M, Darcansoy İşeri Ö, Ural AU, Gündüz U. 2007. In Vitro Evaluation of Zoledronic Acid Resistance Developed in MCF-7 Cells. *Anticancer Research*. 27 (6B): 4031-4037.

Dobson J. 2006. Magnetic nanoparticles for drug delivery. *Drug Development Research*. 67: 55-60.

Ferrari M. 2005. Cancer Nanotechnology Opportunities and Challenges. *Nature Reviews Cancer*. 5: 161-171.

Finger LW, Hazen RM, Hofmeister AM. 1986. High-Pressure crystal chemistry of spinel ($MgAl_2O_4$) and magnetite (Fe_3O_4): Comparisons with silicate spinels. *Physics and Chemistry of Minerals*. 13 (4): 215-220.

Gang J, Park SB, Hyung W, Choi EH, Wen J, Kim HS, Shul YG, Haam S, Song SY. 2007. Magnetic poly ϵ -caprolactone nanoparticles containing Fe_3O_4 and gemcitabine enhance anti-tumor effect in pancreatic cancer xenograft mouse model. *Journal of Drug Targeting* 15 (6): 445-453.

Gottesman MM. 2002. Mechanisms of Cancer Drug Resistance. *Annual. Rev. Med.* 2002. 53: 615–27.

Gref R, Minamitake Y, Peracchia MT, Trubetskoy V, Torchilin V, Langer R. 1994. Biodegradable Long-circulating Polymeric Nanospheres. *Science* 263: 1600–1603.

Gupta AK, Wells S. 2004. Surface-Modified Superparamagnetic Nanoparticles for Drug Delivery: Preparation, Characterization, and Cytotoxicity Studies. *IEEE Transactions on Nanobioscience*. 3 (1): 66-73.

Gupta AK, Gupta M. 2005. Synthesis and surface engineering of iron oxide nanoparticles for biomedical applications. *Biomaterials*. 26 (18): 3995-4021.

Györfy B, Serra V, Jürchott K, Abdul-Ghani R, Garber M, Stein U, Petersen I, Lage H, Dietsch M, Schäfer R. 2005. Prediction of doxorubicin sensitivity in breast tumors based on gene expression profiles of drug-resistant cell lines correlates with patient survival. *Oncogene*. 24: 7542-7551.

Hai NH, Luong NH, Chau N, Tai NQ. 2009. Preparation of magnetic nanoparticles embedded in polystyrene microspheres. *Journal of Physics: Conference Series* 187: 012009.

Hang Y, Guo L, Roeske RW, Antony AC, Jayaram HN. 2004. Pteroyl- γ -glutamate-cysteine synthesis and its application in folate receptor-mediated cancer cell targeting using folate-tethered liposomes. *Analytical Biochemistry*. 332: 168-177.

Hoffman AS. 2008. The origins and evolution of “controlled” drug delivery systems. *Journal of Controlled Release*. 132 (3): 153-163

İşeri ÖD. 2009. Investigation of Docetaxel and Doxoubicin Resistance in MCF-7 Breast Carcinoma Cell Line. Ph.D. Thesis. Ankara: Middle East Technical University.

Jemal A, Bary F, Center MM, Ferlay J, Ward E, Forman D. 2011. Global Cancer Statistics. CA: A Cancer Journal for Clinicians 61: 69-80.

Karp G. 2005. Cell and Molecular Biology: Concepts and Experiments. NJ: John Wiley & Sons.

Kaul G, Amiji M. 2002. Long-Circulating Poly (Ethylene Glycol)-Modified Gelatin Nanoparticles for Intracellular Delivery. Pharmaceutical Research. 19 (7): 1061-1067.

Klug WS, Cummings MR, Spencer CA. 2006. Concepts of Genetic. NJ: Pearson.

Kohler N, Sun C, Wang J, Zhang M. 2005. Methotrexate-modified superparamagnetic nanoparticles and their intracellular uptake into human cancer cells. Langmuir. 21: 8858-8864.

Lan Q, Liu C, Yang F, Liu S, Xu J, Sun D. 2007. Synthesis of bilayer oleic acid coated Fe₃O₄ nanoparticles and their application in pH- responsive Pickering emulsions. *Journal of Colloidal and Interface Science*. 310: 260-269

Li XW, Lin XH, Zheng LQ, Yu Li, Lv Z, Zhang QQ, Liu WC. 2008. Effect of poly (ethylene glycol) stearate on the phase behavior of monopalmitate/ Tween80/ water system and characterization of poly(ethylene glycol) stearate modified solid lipid nanoparticles. *Colloids and Surfaces A: Physicochemical and Engineering Aspects*. 317: 3522-359.

Li W, Tan G, Ma Y, Li H, He G. 2011. Inhibition of α folate receptor resulting in a reversal of taxol resistance in nasopharyngeal carcinoma. *Otolaryngology Head and Neck Surgery*. 20 (10): 1-9.

Liu X, Kaminski M, Guan Y, Chen H, Liu H, Rosengart AJ. 2006. Preparation and characterization of hydrophobic superparamagnetic magnetite gel. *Journal of Magnetism and Magnetic Materials*. 306: 248- 253.

Lu Y, Low PS. 2002. Folate-Mediated Delivery of Macromolecular Anticancer Therapeutic Agents. *Advanced Drug Delivery Reviews*. 54 (5): 675-693

Lu Y, Low PS. 2003. Immunotherapy of Folate Receptor-Expressing Tumors: Review of Recent Advances and Future Prospects. *Journal of Controlled Release*. 91: 17-29

Lubbe AS, Bergemann C, Riess H, Schriever F, Reichardt P, Possinger K, Matthias M, Dorken B, Herrmann F, Gurtler R, Hohenberger P, Haas N, Sohr R, Sander B, Lemke AJ, Ohlendorf D, Huhnt W, Huhn D. 1996. Clinical experiences with magnetic drug targeting: A phase I study with 49-epidoxorubicin in 14 patients with advanced solid tumors. *Cancer Research*. 56: 4686.

McBain SC, Yiu HHP, Dobson J. 2008. Magnetic Nanoparticles for Gene and Drug Delivery. *International Journal of Nanomedicine*. 3 (2): 169-180.

Mohapatra S, Mallick SK, Maiti TK, Ghosh TK, Pramanik P. 2007. Synthesis of highly stable folic acid conjugated magnetite nanoparticles for targeting cancer cells. *Nanotechnology*. 18: 385102.

Mühlen A, Schwarz C, Mehnert W. 1998. Solid lipid nanoparticles (SLN) for controlled drug delivery- Drug release and release mechanism. *European Journal of Pharmaceutics and Biopharmaceutics*. 45 (2): 149-155.

National Cancer Institute. 2011. What is Cancer. <<http://www.cancer.gov/cancertopics/cancerlibrary/what-is-cancer>>. Last accessed date: 2012, January 3.

National Cancer Institute. 2011. What you need to know about cancer, risk factors. <[http://cancer.gov/cancertopics / wyntk/ cancer/page3](http://cancer.gov/cancertopics/wyntk/cancer/page3)> Last accessed date: 2012, January 3.

National Cancer Institute. 2010. Radiation Therapy for Cancer. <<http://www.cancer.gov/cancertopics/factsheet/Therapy/radiation>>. Last accessed date: 2012, January 3.

National Cancer Institute. 2007. Questions and answers about chemotherapy. <<http://www.cancer.gov/cancertopics/coping/chemotherapy-and-you/page2>>. Last accessed date: 2012, January 3.

NDT Resource Center. Diamagnetic, Paramagnetic, and Ferromagnetic Materials. <[http://www.ndt-ed.org/EducationResources/CommunityCollege/MagParticle/Physics/Magnetic Matls.htm](http://www.ndt-ed.org/EducationResources/CommunityCollege/MagParticle/Physics/MagneticMatls.htm)> Last accessed dated : 2012, January 3.

Okassa LN, Marchais H, Douziech-Eyrolles L, Herve K, Cohen-Jonathen S, Munnier E, Souce M, Linassier C, Dubois P, Chourpa I. 2007. Optimization of Iron Oxide Nanoparticles Encapsulation within Poly(d,l-lactide-co-glycolide) Sub-micron Particles. European Journal of Pharmaceutics and Biopharmaceutics. 67 (1): 31-38

O'Morgan D. 2007. *The Cell Cycle: Principles of Control*. New York: Oxford University Press.

Orive G, Hernandez RM, Gascon AR, Pedraz JL. 2005. Micro and Nano Drug Delivery Systems in Cancer Therapy. *Cancer Therapy*. 3: 131- 138

Orive G, Anitua E, Pedraz JL, Emerich DF. 2009. Biomaterials for Promoting Brain Protection, Repair and Regeneration. *Nature Reviews Neuroscience*. 10: 682-692.

Peer D, Karp JM, Hong S, Farokhzad OC, Margalit R, Langer R. 2007. Nanocarriers as an emerging platform for cancer therapy. *Nature Nanotechnology* 2: 751 – 760.

Purves WK, Sadava D, Orians GH, Heller HC. 2003. *Life: The Science of Biology* (7th Edition). Massachusetts: Sinauer Associates.

Ratman M, Hao H, Zheng H, Wang H, Qi H, Lee R, Pan X. 2003. Receptor induction and targeted drug delivery: a new antileukemia strategy. *Expert Opin. Biol Ther.* 3(4): 563-574.

Reddy JA, Low PS. 1998. Folate-mediated targeting of therapeutic and imaging agents to cancers. *Critical Reviews in Therapeutic Drug Carrier Systems*. 15 (6): 587-627.

Sahoo SK, Labhasetwar V. 2003. Nanotech Approaches to Drug Delivery and Imaging. *Drug Discovery Today*. 8: 1112-1120.

Senyei A, Widder K, Czerlinski C. 1978. Magnetic Guidance of Drug Carrying Microspheres. *Journal of Applied Physics*. 49: 3578-3583

Sonvico F, Mornet S, Vasseur S, Dubernet C, Jaillard D, Degrouard J, Hoebeke J, Duguet E, Colombo P, Couvreur P. 2005. Folate-Conjugated Iron Oxide Nanoparticles for Solid Tumor Targeting as Potential Specific Magnetic Hyperthermia Mediators: Synthesis, Physicochemical Characterization and in Vitro Experiments. *Bioconjugate Chemistry*. 16: 1181-1188.

Spaldin NA. 2011. *Magnetic Materials Fundamentals and applications*. Cambridge ; New York : Cambridge University Press.

Spinella MJ, Brigle KE et al. 1995. Distinguishing between Folate Receptor-mediated Transport and Reduced Folate Carrier-mediated Transport in L1210 Leukemia Cells. *Journal of Biological Chemistry*. 270: 7842-7849.

Strober W, Coligan JE, Kruisbeek A, Margulies D, Shevach EM. 1997. Current Protocols in Immunology, Vol. III, Trypan Blue Exclusion Test of Cell Viability, New York : Wiley. p. A.3B.1–A.3.B.2

Sun J, Shaobing Z, Hou P, Yang Y, Weng J, Li X, Li M. 2006. Synthesis and characterization of biocompatible Fe₃O₄ nanoparticles. Journal of Biomedical Materials Research. 80 (2): 333-341.

Sun C, Lee JSH, Zhang M. 2008. Magnetic Nanoparticles in MR Imaging and Drug Delivery. Advanced Drug Delivery Reviews. 60: 1252–1265.

TUIK. 2009. Ölüm nedeni istatistikleri. <<http://www.tuik.gov.tr/PreHaberBultenleri.do?id=10711>>. Last accessed date: 2012, January 3.

Varadan VK, Chen LF, Xie J. 2008. Nanomedicine: Design and Applications of Magnetic Nanomaterials, Nanosensors and Nanosystems. West Sussex: John Wiley & Sons.

Vlerken LEV, Amiji MM. 2006. Multi-functional polymeric nanoparticles for tumour-targeted drug delivery. Expert Opinions Drug Delivery. 3 (2): 205-216.

Widder KJ, Seneyl AE, Scarpelli GD. 1978. Magnetic Microspheres: A Model System of Site Specific Drug Delivery *in vivo*. Proceedings of the Society for Experimental Biology and Medicine. 158: 141- 146

Wilson MW, Kerlan RK, Fidelman NA, Venook AP, LaBerge JM, Koda J, Gordon RL. 2004. Hepatocellular Carcinoma: Regional Therapy with a Magnetic Targeted Carrier Bound to Doxorubicin in a Dual MR Imaging. Radiology. 2301: 287–293.

World Health Organization. 2012. Cancer. <<http://www.who.int/mediacentre/factsheets/fs297/en>>. Last accessed date: 2012, January 3.

World Health Organization. 2008. Cancer Incidence, Mortality and Prevalence Worldwide in 2008. Estimated number of cancer cases, all ages (total 12662,554) for both sexes. <http://globocan.iarc.fr/pie_pop.asp?selection=221900&title=World&sex=0&type=0&window=1&join=1&submit=%A0Execute%A0>. Last accessed date: 2012, January 3.

World Health Organization. 2008. Cancer Incidence, Mortality and Prevalence Worldwide in 2008. Estimated number of cancer cases, all ages (total 6044,710) for women. <http://globocan.iarc.fr/pie_pop.asp?selection=221900&title=World&sex=2&ty

pe=0&window=1&join=1&submit=%A0Execute%A0>. Last accessed date: 2012, January 3.

World Health Organization. 2008. Cancer Incidence, Mortality and Prevalence Worldwide in 2008. Estimated number of cancer cases, all ages (total 39,311) for women in Turkey. <http://globocan.iarc.fr/pie_pop.asp?selection=99792&title=%20Turkey&sex=2&type=0&window=1&join=1&submit=%A0Execute%A0>. Last accessed date: 2012, January 3.

Wu N, Lei F, Su M, Aslam M, Wong KC, Dravid VP. 2004. Interaction of Fatty Acid Monolayers with Cobalth Nanoparticles. *Nano Letters*. 4 (2) : 383-386

Xiong F, Li J, Wang H, Chen Y, Cheng Y, Zhu J. 2006. Synthesis, properties and application of a novel series of one-ended monooleate-modified poly (ethylene glycol) with active carboxylic terminal. *Polymer*. 47: 6636- 6641.

Yallapu MM, Foy SP, Jain TK, Labhasetwaar V. 2010. PEG-functionalized Magnetic Nanoparticles for Drug Delivery and Magnetic Resonance Imaging Applications. *Pharm Res*. 27: 2283-2295.

Yan F, Li J, Zhang J, Liu F, Yang W. 2009. Preparation of Fe₃O₄/polystyrene composite particles from monolayer oleic acid modified Fe₃O₄ nanoparticles

via miniemulsion polymerization. *Journal of Nanoparticle Research*. 11: 289-296.

Yuan F, Dellian M, Fukumura D et al. 1995. Vascular permeability in a human tumor xenograft: molecular size dependence and cut-off size. *Cancer Research*. 55: 3752-3756.

Zhang Y, Kohler N, Zhang MQ. 2002. Surface Modification of Superparamagnetic Magnetite Nanoparticles and Their Intracellular Uptake. *Biomaterials*. 23: 1553–1561.

Zhang L, He R, Gu HC. 2006. Oleic acid coating on the monodisperse magnetite nanoparticles. *Applied Surface Science*. 2531: 2611- 2617

Zhang J, Rana S, Sriavastava RS, Misra RDK. 2008. On the chemical synthesis and drug delivery response of folate receptor-activated, polyethylene glycol-functionalized magnetite nanoparticles. *Acta Biomaterialia*. 4: 40-48.

APPENDIX A

ATR AND FTIR SPECTRA

ATR spectra of pure oleic acid and PEG monooleate is given in Figure A

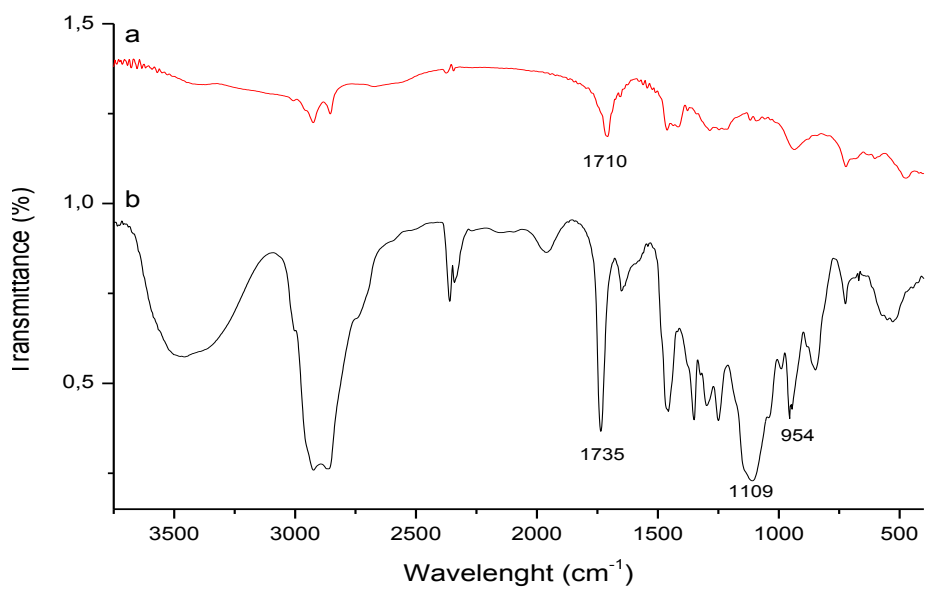


Figure A.1 ATR spectra of a) pure oleic acid and b) Polyethylene glycol monooleate.

Since PEG monooleate has an oleic acid part, it exhibited also vibration bands of oleic acid (Figure A.1). Specific bands of PEG were at 1109 and 954 cm^{-1} which are attributed to symmetric stretching vibrations of C-O-C and out of plane bending of C-H which are known as the fingerprint of PEG (Li 2008, Zhang *et al.* 2008). Peak at 1735 cm^{-1} belongs to vibration of C=O stretching (Xiong 2006).

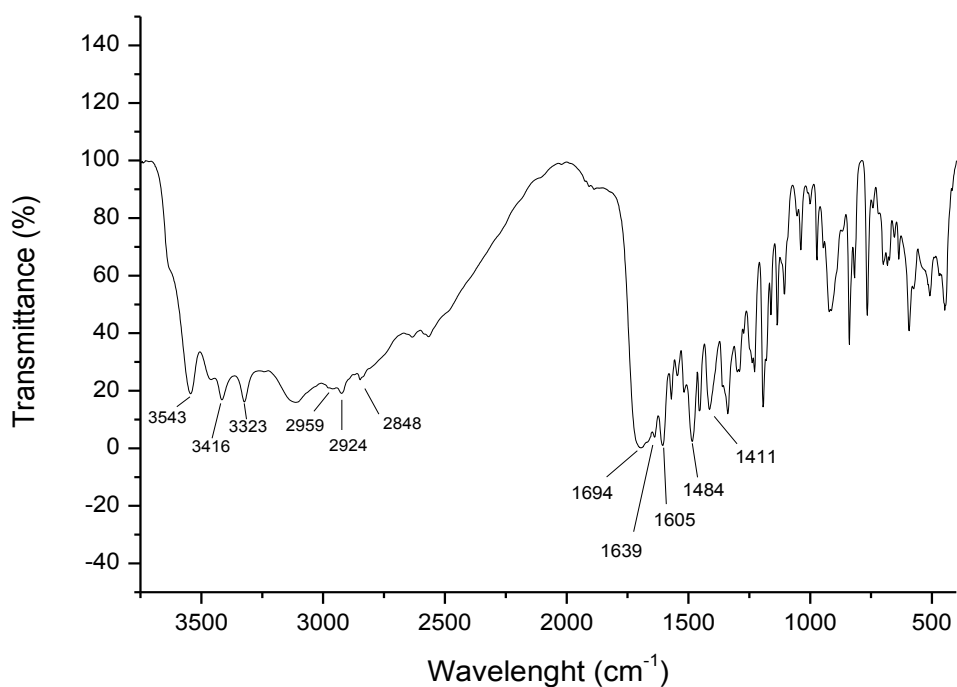


Figure A.2 FTIR Spectrum of pure folic acid

Characteristic bands of pure folic acid was observed at 3543, 3416, 3323 2959, 2924 2844 1694, 1639, 1605, 1484 and 1411 cm^{-1} in Fiture A.2. Peak at 3543

cm^{-1} was due to the $-\text{OH}$ stretching, while bands at 3416 and 3323 cm^{-1} were attributed to NH - stretching. Symmetric and asymmetric stretching vibrations of C-H of CH_2 were observed at 2959, 2924 and 2848 cm^{-1} , respectively. Peaks at 1694 and 1639 cm^{-1} were derived from C=O stretching of $-\text{COOH}$ and $-\text{CONH}_2$. Bending vibration of NH_2 was seen at 1605 cm^{-1} . The bands at 1484 and 1411 cm^{-1} were corresponded to the phenyl ring of folic acid and OH deformation of phenyl skeleton (Zhang *et al.* 2008, Mohapatra 2007).

APPENDIX B

HYSTERESIS LOOP CURVES

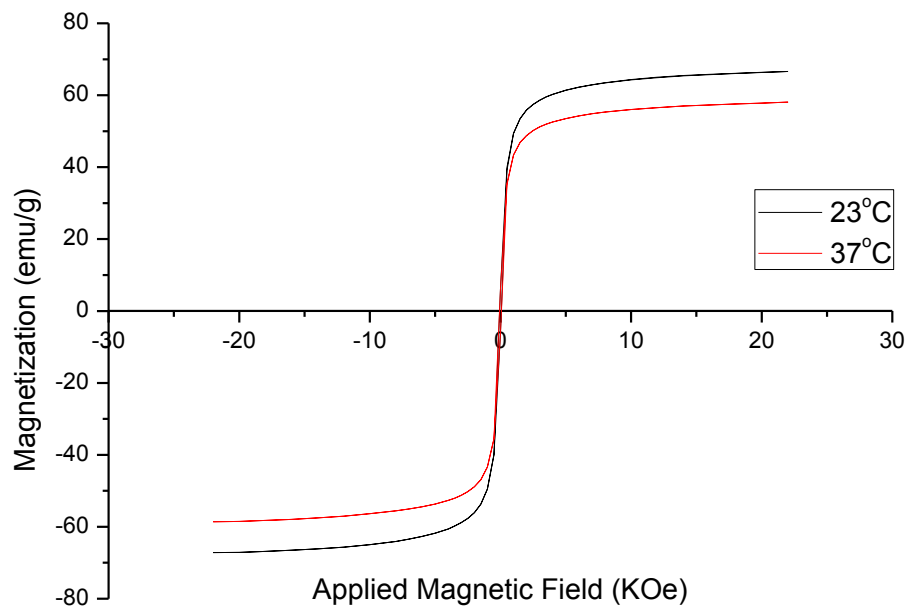


Figure B.1 Magnetization curve of N-MNP₃ at 23 °C and 37 °C

Table B.1 Magnetic Properties of N-MNP₃ (Ms: saturation magnetization, Mr: remanent magnetization, Mr/Ms: remanent squariness ratio, Hc: coercivity)

Temperature (°C)	Ms(emu/g)	Mr (emu/g)	(Mr/Ms)	Hc(KOe)
23 °C	66,89	6,53	0,09	0,07
37 °C	58,34	6,54	0,11	0,07

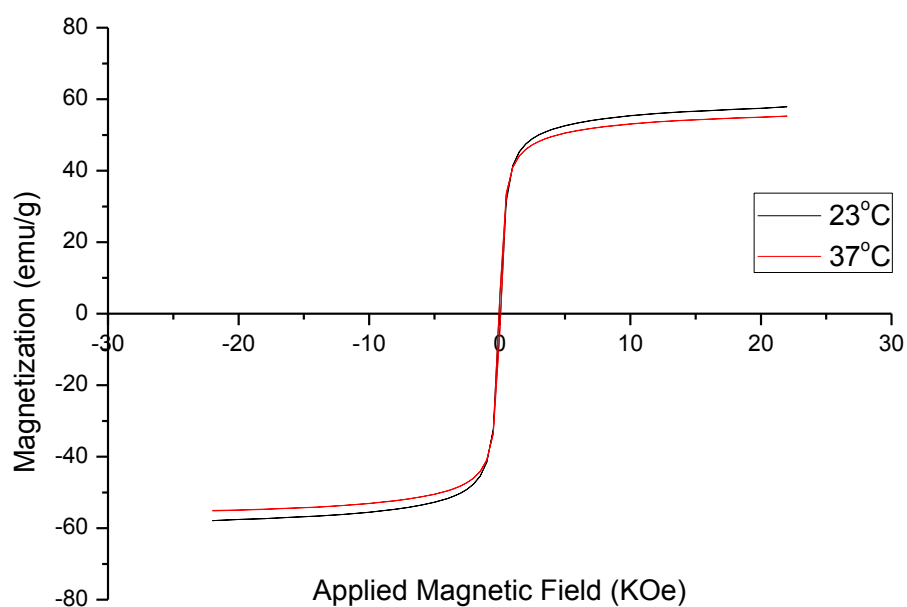


Figure B.2 Magnetization curve of OA- MNP₂

Table B.2 Magnetic Properties of OA- MNP₂

Temperature (°C)	Ms(emu/g)	Mr (emu/g)	(Mr/Ms)	Hc(KOe)
23 °C	57,87	4,73	0,08	0,06
37 °C	55,20	5,46	0,09	0,07

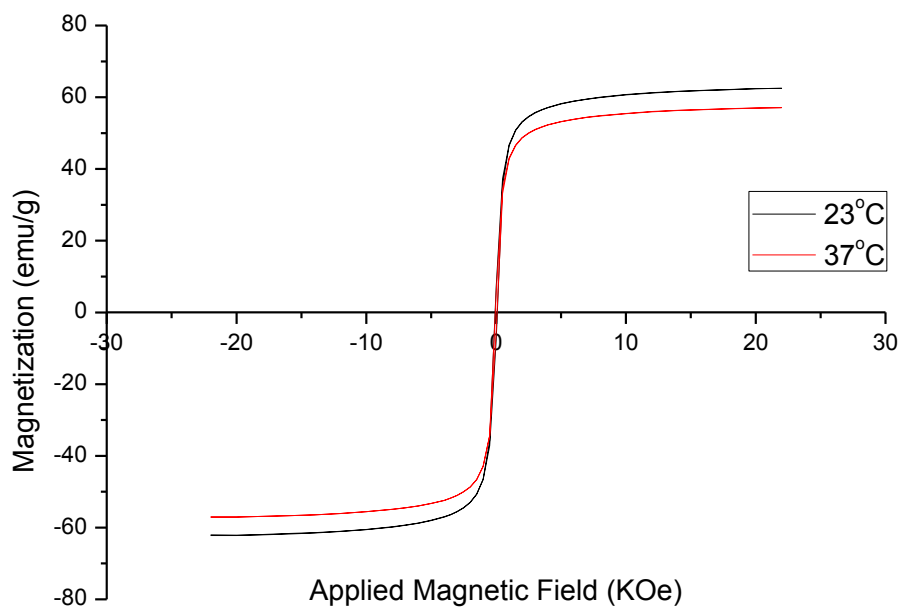


Figure B.3 Magnetization curve of PEG-MNP₂

Table B.3 Magnetic Properties of PEG-MNP₂

Temperature (°C)	Ms(emu/g)	Mr (emu/g)	(Mr/Ms)	Hc(KOe)
23 °C	62,38	7,27	0,11	0,08
37 °C	57,25	5,80	0,10	0,07

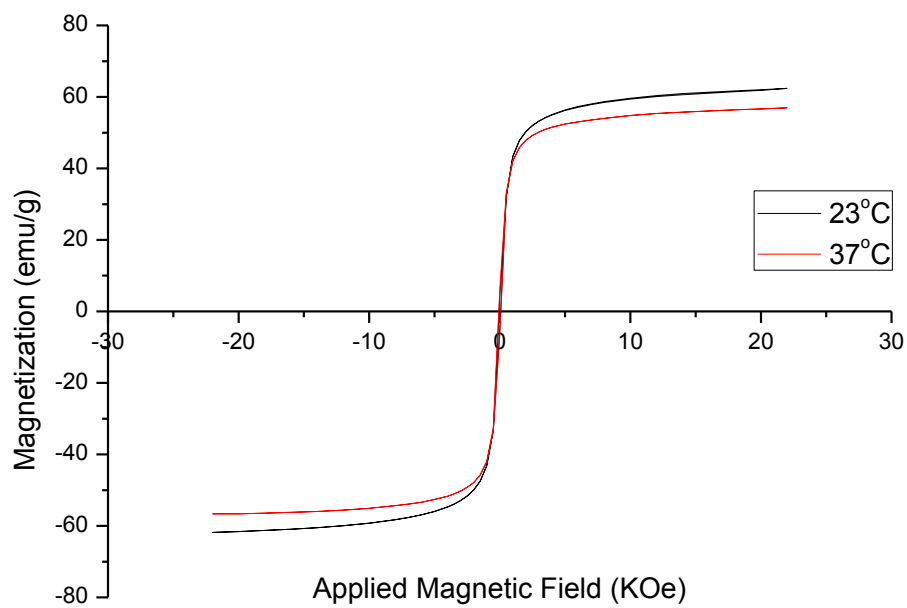


Figure B.4 Magnetization curve of FA-MNP₁

Table B.4 Magnetic Properties of FA-MNP₁

Temperature (°C)	Ms(emu/g)	Mr (emu/g)	(Mr/Ms)	Hc(KOe)
23 °C	62,32	4,31	0,06	0,05
37 °C	56,79	6,39	0,11	0,08

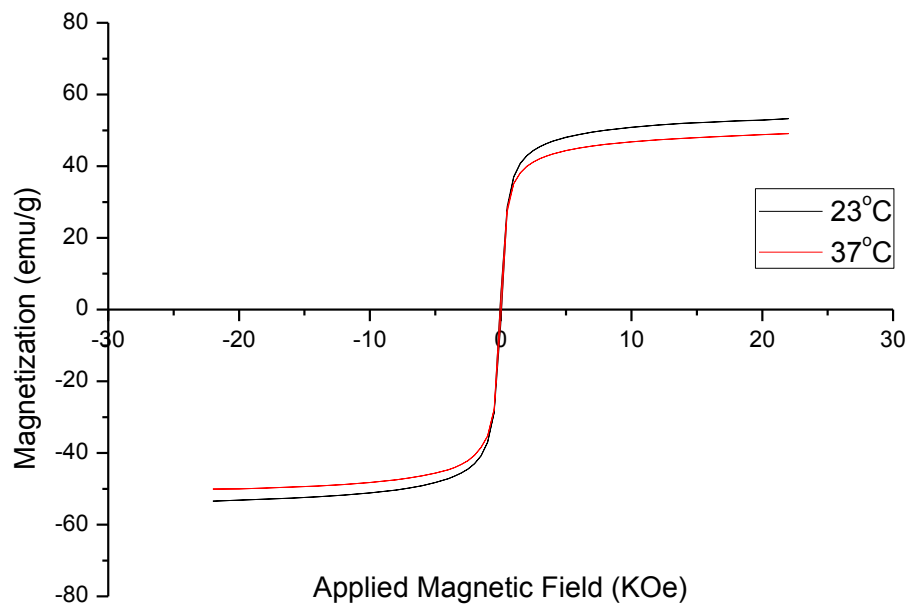


Figure B.5 Magnetization curve of FA-MNP₂

Table B.5 Magnetic Properties of FA-MNP₂

Temperature (°C)	Ms(emu/g)	Mr (emu/g)	(Mr/Ms)	Hc(KOe)
23 °C	53,33	4,12	0,07	0,06
37 °C	49,59	3,33	0,06	0,05